

DISS. ETH No. 16680

Tarsal kinematics

A dissertation submitted to the
SWISS FEDERAL INSTITUTE OF TECHNOLOGY ZURICH
for the degree of
Doctor of Sciences

presented by

PETER WOLF

MA Sports-Engineering, TU Chemnitz

born 19.01.1977

Citizen of Germany

Accepted on the recommendation of

Prof. Dr. Edgar Stüssi, examiner

Prof. Dr. David Howard, co-examiner

Prof. Dr. Robert Riener, co-examiner

2006

für meine Eltern und Schwestern

Table of contents

| | |
|--|------------|
| Table of contents | v |
| Summary | vii |
| Zusammenfassung | ix |
| Preface | xi |
| Chapter 1 Introduction | 1 |
| 1.1 Overview | 4 |
| Chapter 2 Literature | 5 |
| 2.1 Modelling of the passive mobility in human tarsal gears – implications from the literature | 7 |
| 2.1.1 Introduction | 7 |
| 2.1.2 Conventions | 9 |
| 2.1.3 Short summary of history of used methods | 10 |
| 2.1.4 Type of linkage between the rearfoot and lower leg | 10 |
| 2.1.5 Ligaments in tarsal gears | 18 |
| 2.1.6 Validation of tarsal gears | 20 |
| 2.1.7 Conclusions | 23 |
| 2.2 An alternative approach: Magnet resonance imaging | 25 |
| 2.3 Foot type classifications | 27 |
| 2.3.1 Methods to classify foot types | 27 |
| 2.3.2 Investigations of the dependence of foot function on foot morphology | 28 |
| 2.4 Purpose | 30 |
| Chapter 3 A non-invasive procedure to investigate tarsal kinematics | 31 |
| 3.1 Reliability of tarsal bone segmentation and its contribution to MR kinematic analyses methods | 33 |
| 3.1.1 Introduction | 33 |
| 3.1.2 Materials and methods | 34 |
| 3.1.3 Results | 38 |
| 3.1.4 Discussion | 42 |
| 3.1.5 Conclusion | 44 |
| 3.1.6 Supplement: Reproducibility of articulating surfaces | 44 |
| 3.2 Contribution of MR slice orientation on morphology and on methods enabling MR kinematic analyses of tarsal bones | 46 |
| 3.2.1 Introduction | 46 |
| 3.2.2 Method | 47 |
| 3.2.3 Results | 50 |
| 3.2.4 Discussion | 52 |
| 3.2.5 Conclusions | 55 |
| 3.3 A MR imaging procedure to measure tarsal bone positions in different foot excursions | 56 |
| 3.3.1 Introduction | 56 |
| 3.3.2 Methods | 57 |
| 3.3.3 Results | 60 |
| 3.3.4 Discussion and conclusions | 62 |
| 3.4 Tarsal bone positions in different foot excursions: MR imaging vs. intracortical pins | 65 |
| 3.4.1 Introduction | 65 |
| 3.4.2 Methods | 65 |
| 3.4.3 Results | 67 |
| 3.4.4 Discussion and conclusions | 68 |

| | |
|---|------------|
| Chapter 4 Tarsal joint kinematics and morphology of dynamically classified runners | 71 |
| 4.1 Quasi-static tarsal bone motion of dynamically classified runners | 73 |
| 4.1.1 Dynamic foot classification | 73 |
| 4.1.2 MR data acquisition and processing | 76 |
| 4.1.3 Results | 77 |
| 4.1.4 Discussion | 79 |
| 4.2 Transmission within the tarsal gearbox | 81 |
| 4.2.1 Introduction | 81 |
| 4.2.2 Methods | 81 |
| 4.2.3 Results | 82 |
| 4.2.4 Discussion and conclusions | 84 |
| 4.3 Tarsal joint curvature | 87 |
| 4.3.1 Method to analyse tarsal joint curvature | 87 |
| 4.3.2 Results of the tarsal joint curvature analysis | 91 |
| 4.3.3 Discussion of the tarsal joint curvatures | 93 |
| 4.4 Ligament properties: a discussion and an outlook | 95 |
| 4.4.1 Influence of initial ligament properties on calcaneal motion | 95 |
| 4.4.2 An approach to measure ligament lengths during the stance phase of gait | 97 |
| Chapter 5 Conclusions | 101 |
| 5.1 Most important contributions | 103 |
| 5.2 Outlook | 105 |
| References | 103 |
| Appendix A | 107 |
| Appendix B | 118 |
| Appendix C | 119 |
| Appendix D | 121 |
| Acknowledgements | 133 |
| Curriculum vitae | 135 |

Summary

The rationale of the present thesis is given by the common practise to predict foot motion based on foot morphology although knowledge about this vague deduction is limited: There is a lack of non-invasive methods which both quantify spatial foot bone kinematics and provide morphological parameters which monitor the three-dimensional nature of the foot joints. Appropriate methods would not only offer new insights into the still uncertain dependence of foot motion on foot morphology but also would have an impact on the demanding validation of current concepts representing tarsal kinematics (chapter 2).

This thesis established such a method quantifying tarsal joint rotations and tarsal bone morphology based on magnetic resonance (MR) imaging. Thereby, special emphasis was given to the core items of the such a procedure: First, it was found that semi-automatic segmentation of high-contrast and high-resolution images does not contribute to data processing; in particular, if tarsal kinematics were computed by an iterative fit of the closest points (ICP) describing different bone positions (chapter 3.1). After showing that the anisotropic spatial resolution of the MR images influences the accuracy of the ICP algorithm in the order of common video motion analyses (chapter 3.2), tarsal joint rotations in response to foot pronation and foot supination were registered by MR imaging. It became evident that the device providing the foot positions in combination with axial loading caused an explainable excursion of the calcaneus resulting in rotations in all tarsal joints. Finally, repeated measurements revealed that only a few degrees of rotation are necessary to distinguish between tarsal joint kinematics of different subjects (chapter 3.3). Thus, the presented procedure was found adequate to investigate spatial tarsal joint motion in combination with three-dimensional rearfoot morphology. Tarsal joint rotations acquired by MR imaging correlated significantly to those rotations at point in time of stance phase during running measured with intracortical pins (chapter 3.4). Therefore it was concluded that the MR procedure seems to be a promising approach to investigate foot kinematics which would otherwise only be available by the use of invasive methods.

By means of this established procedure the transmission between tarsal joint rotations were quantified to provide a basis to model the so called tarsal gearbox. The results show that tibio-calcaneal rotations correlated with tarsal joint rotations (chapter 4.2).

Next, the newly developed MR procedure was used to specify the dependence of foot motion on foot morphology. Initially, runners were classified based on calcaneal motion at the beginning of stance phase during running. Since an adequate classification was not achieved by their quasi-static tarsal joint rotations this detailed but quasi-static data (including joint axis orientations) did not improve the interpretation of the runners'

dynamic foot motion (chapter 4.1). Neither tarsal volumes and second moments of volume (chapter 4.1) nor tarsal joint curvatures (chapter 4.2) contributed to the magnitude of the calcaneal motion used for the runners' foot classification. It was concluded that morphological parameters of the tarsal bones are not feasible to predict rearfoot motion. In other words, predictions of the magnitude of rearfoot kinematics seem to be very limited based on morphological parameters or quasi-static joint motion, even when three-dimensionally and precisely measured. Thus, the results of this thesis do not support the above mentioned vague statement of the dependence of foot motion on its morphology.

Discussing the contribution of ligament properties on calcaneal kinematics revealed that the initial ligament properties may have been changed due to an previous injury resulting in more calcaneal motion. As exemplified on the posterior tibiotalar ligament, the presented MR procedure provides insights into ligament strains during quasi-static and, in combination with an adequate method, during dynamic foot motion (chapter 4.3).

Using the developed procedure and based on the presented results of this thesis future studies related to rearfoot kinematics should focus rather on other factors contributing to joint mechanics than bone and joint morphology; in particular on ligament properties.

Zusammenfassung

Die vorliegende Arbeit fusst auf der verbreiteten Praxis, Bewegungen des Fusses aufgrund seiner Morphologie abzuschätzen, obwohl diese vage Schlussfolgerung nicht erwiesen ist: Es mangelt nämlich an nicht-invasiven Verfahren, die sowohl das Quantifizieren der Fuss-Kinematik im Raum als auch das Erfassen morphologischer Parameter, welche den Aufbau der Fussgelenke widerspiegeln, ermöglichen. Entsprechende Verfahren brächten nicht nur neue Erkenntnisse hinsichtlich der undefinierten Abhängigkeit der Fuss-Bewegung von der Fuss-Morphologie, sondern wären auch bezüglich dem ausstehenden Überprüfen aktueller Modellansätze zur tarsalen Kinematik dienlich (Kapitel 2).

In dieser Arbeit wurde ein Verfahren entwickelt, welches das Quantifizieren der tarsalen Gelenksrotationen sowie der tarsalen Knochen-Morphologie mittels Magnet Resonanz Tomographie (MRT) ermöglicht. Besondere Beachtung fanden dabei die kritischen Merkmale eines solchen Verfahrens: Zunächst wurde festgestellt, dass die Datenverarbeitung nicht durch das halb-automatische Segmentieren der kontrastreichen und hoch aufgelösten Bilder beeinträchtigt wird; insbesondere gilt dies für die kinematische Auswertung basierend auf einem iterativen Annähern nächster Punkte (engl. iterative closest point fit (ICP)), welche verschiedene Knochenpositionen beschreiben (Kapitel 3.1). Nachdem gezeigt wurde, dass die anisotrope räumliche Auflösung der MRT Bilder diese Art des kinematische Auswertens in der selben Grössenordnung wie gewöhnliche Bewegungsanalysen beeinflusst (Kapitel 3.2), wurden tarsale Gelenksrotationen in Folge einer Pro- und Supination des Fusses mittels MRT erfasst. Es wurde deutlich, dass die Apparatur, welche ein Positionieren sowie axiale Belasten des Fusses ermöglicht, ein sinnvolles Auslenken des Calcaneus verursachte, was wiederum Rotationen in allen tarsalen Gelenken nach sich zog. Letztlich zeigte sich in wiederholten Messungen, dass nur wenige Grad an Rotation notwendig sind, um zwischen tarsaler Gelenks-Kinematik verschiedener Probanden zu unterscheiden (Kapitel 3.3). Daher ist das entwickelte Verfahren im Stande, räumliche tarsale Gelenksbewegungen nebst dreidimensionaler Morphologie des Rückfusses zu erfassen. Derart ermittelte Gelenksrotationen stimmten signifikant mit Rotationsausmassen zu einem Zeitpunkt der Standphase im Laufen überein - gemessen mit intrakortikalen Schrauben. Folglich bildet das MRT Verfahren ebenfalls eine viel versprechende Methode zum Erfassen der Fuss-Kinematik, welche sonst nur anhand invasiver Verfahren erfassbar wäre.

Die Übertragungsverhältnisse innerhalb der tarsalen Gelenke wurden anhand des entwickelten Verfahrens quantifiziert, um so einen Ansatz des Modellierens des so genannten tarsalen Getriebes bereitzustellen. Die Ergebnisse zeigten, dass tibio-calcaneale Rotationen mit tarsalen Gelenksrotationen korrelierten (Kapitel 4.2).

Unter Anwendung des neu entwickelten MRT Verfahrens wurde weiterhin die Abhängigkeit der Fussbewegung von der Fuss-Morphologie präzisiert. Dazu wurden Läufer zunächst aufgrund der Calcanealen Bewegung zu Beginn der Standphase klassifiziert. Da ein vergleichbares Klassifizieren nicht anhand quasi-statischer Rotationen der tarsalen Gelenke gelang, trugen diese detaillierten wenn auch quasi-statische Daten (inklusive Lage der Gelenksachsen) nicht zur Interpretation der dynamischen Fussbewegung der Läufer bei (Kapitel 4.1). Das Ausmass der Calcanealen Bewegung, welches zum Klassifizieren der Läufer genutzt wurde, konnte weder anhand der tarsalen Volumina und Trägheitsmomente (Kapitel 4.1) noch anhand tarsaler Gelenkskrümmungen (Kapitel 4.2) erklärt werden. Daraus wurde gefolgert, dass es nicht gelingt die Rückfussbewegung mittels morphologischer Parameter der tarsalen Knochen abzuschätzen. Mit anderen Worten, Vorhersagen des Ausmasses der Rückfuss-Kinematik können kaum basierend auf morphologischer oder statischer Gelenksbewegungen gemacht werden, selbst wenn jene dreidimensional und präzise vorliegen. Daher sprechen die Resultate der vorliegenden Arbeit gegen die oben erwähnte vage Aussage bezüglich der Abhängigkeit der Fussbewegungen von seiner Morphologie.

Die Diskussion des Einflusses der Bänderigenschaften auf die calcaneale Kinematik offenbarte, dass initiale Bänderigenschaften möglicherweise durch eine Verletzung beeinträchtigt wurden, wodurch es zu einem Mehr an Calcanealer Beweglichkeit kam. Anhand des Ligamentum tibiotalaris posterior wurde beispielhaft aufgeführt, dass das vorgestellte MRT Verfahren zum Erfassen beliebiger Fusspositionen und Belastungen ebenfalls Erkenntnisse hinsichtlich Dehnungen der Bänder liefert, und dies sowohl in quasi-statischen als auch, in Kombination mit einer geeigneten Methode, in dynamischen Fussbewegungen (Kapitel 4.3).

Unter Nutzung des entwickelten Verfahren sowie anhand der vorgestellten Ergebnisse dieser Arbeit sollten sich zukünftige Studien betreffend der Rückfuss-Kinematik weniger auf die Knochen- und Gelenksmorphologie als auf andere Einflussfaktoren der Gelenksmechanik konzentrieren, insbesondere auf die Bänder und deren Eigenschaften.

Preface

The magnetic resonance imaging was performed at the Institute for Biomedical Engineering, University and ETH Zurich, Switzerland. The study including intracortical pins was conducted at the Department of Orthopaedics, Karolinska Institute at the Huddinge University Hospital, Stockholm, Sweden, in collaboration with the Centre for Rehabilitation and Human Performance Research, University of Salford, United Kingdom. The remaining parts of the thesis were performed at the Institute for Biomechanics, ETH Zurich, Switzerland.

Chapter 2.1, 3.1, 3.3, 3.4, and 4.2 are based on the following manuscripts:

Wolf P, Stacoff A, Stuessi E. Modelling of the passive mobility in human tarsal gears - implications from the literature. *The Foot*, 2004, 14: 23-34.

Wolf P, Luechinger R, Stacoff A, Boesiger P, Stuessi E. Reliability of tarsal bone segmentation and its contribution to MR kinematic analyses methods. Submitted to *Computerized Medical Imaging and Graphics*.

Wolf P, Luechinger R, Boesiger P, Stuessi E, Stacoff A. A MR imaging procedure to measure tarsal bone positions in different foot excursions. Submitted to *Journal of Biomechanical Engineering*.

Wolf P, Stacoff A, Liu A, Nester C, Arndt A, Lundberg A, Stuessi E. Tarsal bone positions in different foot excursions: MR imaging vs. intracortical pins. Submitted to Submitted to *Journal of Biomechanics*.

Wolf P, Luechinger R, Boesiger P, Stuessi E, Stacoff A. Transmission within the tarsal gearbox. Submitted to *Journal of the American Podiatric Medical Association*.

Because these stand-alone papers constituted chapters in this thesis, these chapters contain occasionally redundant information in the 'methods' section.

Chapter 1

Introduction

Common opinion is that foot morphology and foot function are dependent on each other (Inman, 1976; Root et al., 1977). In combination with clinical studies reporting the predestination of certain foot morphologies for typical running injuries (Clement et al., 1981; Franco, 1987; Heil, 1992), this vague statement results in a common practise: Orthotists, podiatric physicians and shoe manufactures classify foot morphologies to predict foot function hoping that an effective prevention or treatment can be achieved (Rothstein, 1985; Scharfbillig et al., 2004).

However, the current literature does not confirm the mentioned dependence: Several authors have found that variability of calcaneal motion can not be explained by predefined foot classifications based on morphological parameters (Cornwall and McPoil, 2004; Hunt et al., 2000; Hunt and Smith, 2004; Kernozek and Ricard, 1990; Knutzen and Price, 1994; McPoil and Cornwall, 1996ab). But these studies - and thus their conclusions - were limited: Since morphological variables were derived from radiographic evaluation, anthropometric measurements or foot prints, no detailed three-dimensional information about the mechanical basis of the foot joints was available. Further, the overall foot motion is performed by many joints within the foot which are hardly detectable by the common registration of skin markers. Hence, neither morphological parameters with direct influence on foot motion were measured nor rotations of single foot joints could be quantified.

These limitations of previous studies demonstrate the lack of methods monitoring foot joint rotations preferably in combination with relevant morphology. Thus, the first main purpose of this thesis was the development of a non-invasive procedure providing insights into three-dimensional foot kinematics and morphology. Thereby, it was focused on tarsal joint rotations due to the particular demand of validating procedures of current concepts of rearfoot modelling (Wolf et al., 2004).

Interestingly, the dependence of foot function on foot morphology was always investigated based on morphological classifications. However, clinicians and shoe manufactures are interested in functional differences. Therefore, it seems more appropriate to classify subjects firstly based on their foot motion and then seek after morphological differences. Thus, the second main purpose of this thesis was the investigation of tarsal bone morphology - in particular joint curvature - of dynamically classified runners.

Hence, the impact of the thesis is to provide new non-invasive insights into tarsal joint kinematics and to specify the dependence of foot function on foot morphology. A short overview of the presented work is given in the chapter below.

1.1 Overview

Chapter 2 addresses the review of the literature. Past and current concepts of tarsal kinematics are discussed, methods to investigate tarsal joint motion are presented, and foot type classifications are reported. Thereby, the lack of methods quantifying tarsal joint rotations non-invasively as well as the demand of new approaches to verify the dependence of foot motion on foot morphology are elaborated. Based on that, the purposes of this thesis are formulated at the end of chapter 2.

Chapter 3 deals with the first main purpose of this thesis, the establishment of a magnetic resonance (MR) imaging procedure monitoring tarsal bone rotations under considerable load. At first, the influence of semi-automatic segmentation and of MR slice orientation on further data processing is determined. Thereafter, a device enabling arbitrary foot positioning and loading in the MR is presented. For the first time, tarsal joint rotations are measured non-invasively during foot pronation and supination under a load simulating standing. The required rotational degrees to distinguish between different tarsal kinematics are estimated. Finally, the tarsal joint rotations observed during lying supine in the MR are compared with tarsal joint rotations which were opto-electrically measured during relaxed standing and during the stance phase of running.

Chapter 4 is related to the second main purpose of this thesis, the investigation of tarsal bone morphology of subjects classified based on their calcaneal motion during the beginning of stance phase of running. The first part of this chapter describes the classification of runners into two groups (reduced and enhanced calcaneal motion during heel strike). By using the developed MR imaging procedure, subtalar joint axis orientations are computed and discussed with regard to the dynamical classification. Then, based on the now available pool of tarsal joint rotations, transmissions within the tarsal joints are quantified providing a basis to model the tarsal gearbox. Thereafter, tarsal joint curvatures of the classified runners are calculated and their contribution to tarsal kinematics is elaborated. Finally, the influence of ligament properties on calcaneal motion is discussed, and an outlook how to evaluate ligament lengths during running is given.

Chapter 5 summarises the most important contributions of this thesis.

Chapter 2

Literature

The literature review is divided into three sections, covering the modelling of tarsal gears, an alternative approach to investigate tarsal kinematics, and current foot type classifications attempting to monitor tarsal kinematics. Based on the conclusions drawn from the different parts of the literature review, the final chapter addresses the purpose of the thesis.

2.1 Modelling of the passive mobility in human tarsal gears – implications from the literature

2.1.1 Introduction

Knowledge about gears¹ in the tarsus and adjacent bones is of great importance in biomechanics and orthopaedics. Generally, gears describe a functional relationship between their elements. In a human tarsus, gears are comprised of bones and ligaments (passive elements). Gears are driven by internal and external forces or more precisely, muscles, joint forces, and ground reaction forces (driving elements). Regarding the lower extremities the functional relationship within gears is often called movement coupling.

In the tarsus and adjacent bones movement coupling enables three basic dynamic functions required for human mobility:

- (1) Absorbing impact forces by certain movements of foot and shank bones; i.e. damping (Bogdan et al., 1978; James et al., 1978; Harris, 1991);
- (2) Providing an optimal support area for the whole body while walking or running by i.e. allowing the foot to accommodate to uneven ground or avoiding uncompensated swings in the body's centre of mass; i.e. stabilisation (Olerud and Rosendahl, 1987; Saltzman and Nawoczenski, 1995);
- (3) Creating a rigid lever for push-off; i.e. propulsion (James et al., 1978; Morris, 1977).

When movement coupling is disturbed by i.e. degenerative diseases, congenital deformities or overuse, the walking pattern is changed (Sammerco et al., 1973; Perry, 1992). Normally these changes are compensated by functional adaptations (Debrunner 1998), but if they are not compensated, they may cause restrictions to the mobility of the subject who is affected.

The orthopaedic surgeon tries to prevent decreasing mobility with various interventions, in severe cases with arthrodesis or endoprosthesis. Both kind of operations may be successful in restoring a pain free mobility (Mazur et al., 1979). However, these interventions require compensatory mechanisms or adaptations by the patient which may be observed in a change of movement coupling between the foot and shank (Lundberg, 1988; Mazur et al.,

¹ The term gear is used after Leardini and coworkers (1999a) instead of the term kinematic chain. Normally, a kinematic chain consists of bones only which is insufficient with regards to the present topic.

1979). Therefore, knowledge about physiological movement coupling arising from human tarsal gears is essential in orthopaedics (Hintermann et al., 1994a; Leardini and O'Connor, 2002; Michelson et al., 2000; Siegler et al., 1988a).

Movement coupling is not only important for activities of daily living but also for recreational activities, especially running. It has been estimated that between one third and more than the half of all runners suffer at least one injury per year (Hintermann et al., 1994a; Subotnick, 1977; van Mechelen, 1992). Among the most typical running injuries are Achilles tendon pain, shin splints and patellofemoral pain syndrome (PFPS) (Stacoff, 1998). During the 1970s and 1980s, high impact forces and excessive foot pronation were thought to increase running injuries but no direct relationship could be established in a correct way (Nigg et al., 1995; Stergiou, 1996). Currently, among the main contributing factors towards the aetiology of many injuries are thought to be a disturbed muscle control and an unphysiological movement coupling between calcaneal eversion and tibial internal rotation. However, the importance of these factors has not been demonstrated yet. As a consequence, well determined knowledge about the actual effects of treatments like orthoses or physiotherapy is still lacking (Ball and Afheldt, 2002ab). Hence, manufacturers of shoes and orthoses and shoe orthotists need more than ever a fundamental understanding of physiological movement coupling of human tarsal gears (Hintermann et al., 1994a; Nawoczenski et al., 1998).

The purpose of this chapter is to review the literature concerning the passive mobility in human tarsal gears and the resulting movement coupling between the tarsus and adjacent bones, respectively. The review puts especial emphasis on investigations that deal with passive factors influencing movement coupling. The aim is to provide a basis for biomechanical models which describe the functionality of the tarsus and adjacent bones. Furthermore, the relevant literature is reviewed to provide an idea of how tarsal models may be validated and of how to discuss the results of movement coupling gained in previous investigations.

Not reviewed are problems related to single tarsal joint kinematics (see van Langelaan, 1983), to the anatomy of bones of interest (see Chan and Rudins, 1994), to pressure distribution and joint forces (see Debrunner, 1998) and to muscle activity (Perry, 1992).

After a short chapter of conventions the relevant literature is divided in the following way: history of method, type of linkage, influence of ligaments, validation. Overlay may occur, but is attempted to be minimised.

2.1.2 Conventions

A number of different terms have been used to describe rotations between the lower leg and foot complex (McDonald and Tavener, 1999). In order to avoid misinterpretations all terms of the reviewed literature were adapted to the conventions provided by the International Society of Biomechanics (Wu et al., 2002): The tarsus consists of the talus, calcaneus, navicular and cuboid (see Fig. 2-1). Therefore, tarsal joints are the talo-crural joint (synonymous with ankle joint), the talo-calcaneal joint (synonymous with subtalar joint), the talo-navicular, calcaneo-cuboid and navicular-cuboid joint. Rotations at these joints are defined as follows: dorsi-/plantarflexion (DF/PF) in the sagittal plane about the medio-lateral axis, eversion and inversion (EV/INV) in the frontal plane about the anterior-posterior axis and ab-/adduction (ABD/ADD) in the transverse plane about the vertical axis (see Fig. 2-1). If motion occurs in all three planes and DF, EV and ABD are coupled, pronation (PRO) is the term used. If PF, INV and AD are coupled it is termed supination (SUP) (Wright, et al., 1964). Internal and external rotations (IntRot/ExRot) are expressions used to describe relative rotations of tibia and fibula against the foot in the transverse plane about the vertical axis (Wu et al., 2002).

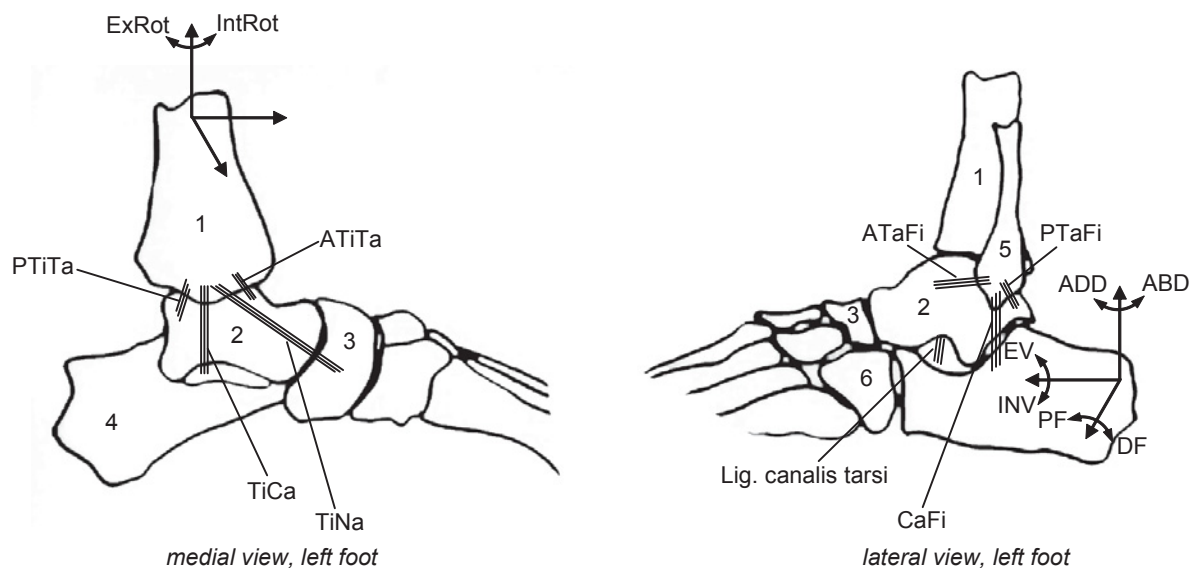


Fig. 2-1 Bones and ligaments in the rearfoot: tibia (1), talus (2), navicular (3), calcaneus (4), fibula (5), cuboid (6). Ligament abbreviations are listed in Tab. 2-1.

2.1.3 Short summary of history of used methods

Biomechanical research on movement coupling in the lower leg and foot complex began in the last decades of the 19th century. Lovett et al. (1898) verified that foot pronation consists of coupled movements of the tarsal and adjacent bones based on their in vivo X-ray as well as in vitro intracortical pin study.

Lovett et al. (1898) formulated that pronation consists “of the horizontal rotation of the astragalus (talus) with the sinking of its head, the rotation in valgus of the calcis (calcaneus) beneath it, and the rotation in valgus and abduction of the front foot as a whole, occurring between astragalus and scaphoid (navicular), calcis and cuboid”. Over a number of years several wooden models were developed to describe the movement of the whole foot in relation to the shank and vice versa (Hicks, 1953; Inman, 1969; Inman, 1976; Jones, 1945; Rubin, 1971). In the 1980s different elaborated test jigs were built to evaluate the coupling mechanisms between the foot and shank in vitro (Engsberg, 1987; Olerud, 1985; van Langelaan, 1983). Using specifically developed or modified test jigs in vivo (static) kinematic investigations with high accuracy became also possible by marking the bones of interest with radiographic absorbing materials (Benink, 1985; Lundberg, 1988). In the 1990s, movement coupling in the tarsus and adjacent bones was evaluated during locomotion using skin markers (Cornwall and McPoil, 1995; McClay and Manal, 1997; Nigg et al., 1992) and by intracortical pins (Stacoff, 1998). Recently, a dynamic cadaver measurement device was developed (Sharkey and Hamel, 1998) to evaluate movement coupling between foot bones under certain muscle forces introduced by actuators. Newer methods like resonance imaging and electromagnetic tracking devices have also been used to investigate movement coupling in the tarsal joints non-invasively and with improved accuracy (Cornwall and McPoil, 1999; Longatti, 2003; Stindel et al., 2001, Woodburn et al., 2002).

In summary, movement coupling in the lower leg and foot complex has been investigated for more than hundred years with different methods. Despite all efforts to understand the function of the tarsus during gait, uncertainties remain up to the present time (see chapter 2.1.1). Thus, movement coupling in the lower leg and foot complex remains a topic that still needs more investigations, maybe even new methods.

2.1.4 Type of linkage between the rearfoot and lower leg

Modelling of movement coupling arising from human gears in the tarsus and adjacent bones request answers concerning the number of degrees of freedom within the studied bones. For that purpose, this chapter is divided into three parts: Firstly, the literature is reviewed concerning the assumption that specific joints can be defined between tarsal

bones. Secondly, studies are summarised which simulate movement coupling between the tarsus and lower leg by one single joint. Thirdly, publications are summarised which discuss the tarsus as a kinematic chain or gear.

Joints in the tarsus

Ankle and subtalar joint

Concerning modelling of the ankle and subtalar joint the investigations of Isman and Inman (Inman, 1976; Isman and Inman, 1969) are often cited. To determine whether these two joints behave as single axis joints and if so what orientation they have, Isman and Inman (1969) investigated 46 specimens in a special test jig. The axes were determined by those lateral and medial points, respectively, which showed the least amount of displacement while moving the relevant bones against each other. Isman and Inman (1969) found a moving axis for both joints but they stated that the ankle and subtalar joint can be simplified as single axis joints for certain purposes. In a subsequent consideration, Inman (1969) mentioned that the subtalar joint is anatomically complicated but acts functionally as a simple hinge joint. He developed a wooden model with an inclined axis representing an average of those he found in the anatomical studies to explain the mechanism of horizontal leg rotation upon a fixed foot (1969). Later Inman extended this work to a final number of 107 specimens including the old cases (1976). Once again it was found that a single rigid axis neither for the ankle nor the subtalar joint could be established through the whole possible motion arc in these joints. While knowing these facts, Inman (1976) repeated the earlier made statement that for all practical purposes, motion about the ankle and subtalar joints can be considered to be each about a single rigid axis. This consideration complies with several anatomical studies of the first decades of the 20th century, e.g. Cunningham (1902), Strasser (1917) and Braus (1921), and also later with in vitro investigations (Singh et al., 1992).

These single rigid axes approach for the ankle and subtalar joint was used in several biomechanical models to examine kinematics and kinetics of the rearfoot. Stauffer and coworkers (1977) proposed a two dimensional foot model with one single rigid axis to predict ankle joint forces. Likewise Salathe and coworkers (1986) started their kinetic examination with a two dimensional hinge joint model, the latest three dimensional version of their model being published recently (Salathe and Arangio, 2002). Further three dimensional rearfoot models using rigid hinges for the ankle and subtalar joint in accordance with the work of Inman are known from literature (Burdett, 1982; Dul and Johnson, 1985; Gauffin et al., 1993; Procter and Paul, 1982; van den Bogert et al., 1994).

Scott and Winter (1991) intended a validation of the assumed fixed hinge joints. The individual axes of rotation of the ankle and subtalar joint were found by manual manipulation and identification of locations with the least motion on the skin of three

different subjects. The authors used the concept that for validation the excursions of certain skin markers during motion should produce circles if the line of sight is coinciding with the axis of the assumed hinge joint. Scott and Winter (1991) mentioned that during the foot flat phase of walking Inman's proposed assumption of fixed hinge joints is warranted. But during heel strike and toe off the deviations from a circular arc were within five to ten percent of the radius for all subjects. Hence, Scott and Winter (1991) concluded that during walking the general assumption of fixed ankle and subtalar hinge joints is questionable. Recently, Leardini and O'Connor (2002) confirmed this conclusion. They investigated the lever arms of the main flexor and extensor muscles of the ankle by a mathematical model and reported that the displacement of the centre of rotation significantly affects the muscle lever arm lengths. They concluded that ankle models with a fixed centre of rotation are only acceptable in exercises with a limited range of motion near the neutral position.

Once again it has to be noted, that Inman (1976) found no single rigid axis for movements at ankle and subtalar joint in his experiments. This was also stated quite earlier by Fick (1911) for the subtalar joint. Barnett and Napier (1952) investigated more than 150 foot specimens and reported that the changing axis of the ankle joint is due to the medial profile of the talus with two different arcs and radii, respectively. They showed that in PF, the axis of the ankle joint is inclined downwards and medially in the frontal plane, but it is inclined downwards and laterally during DF. This has been confirmed later by studies regarding the ankle and/or subtalar axis in vitro (Bottlang et al., 1999; Hicks, 1953; Leardini, 2001; Michelson et al., 2000; Siegler et al., 1988a; Thoma et al., 1993; van Langelaan et al., 1974) and in vivo (Sammerco et al., 1973).

Lundberg and coworkers (1989a) investigated in vivo the resulting tibial rotations in the transverse plane due to calcaneal PF/DF. They used the moving ankle axis to explain the change of tibial IntRot to tibial ExRot towards maximal calcaneal DF. With an input movement of tibial ExRot the deviation and inclination of helical axes describing movements between lower leg and rearfoot bones varied. This result was previously shown in vitro (Engsberg, 1987; van Langelaan, 1983) and in vivo (Benink, 1985). All of these studies confirmed that neither the ankle nor the subtalar joint have a single rigid axis during the entire range of motion.

Distally located tarsal joints

In contrast to the above regarded ankle and subtalar joints less attention has been devoted to the more distal tarsal joints. The contribution in walking of other rear- and midfoot joints than the ankle and subtalar has been adequately manifested over the last 15 years (Astion et al., 1997; Lundberg et al., 1989a; Nester et al., 2000).

The talo-navicular joint is regarded by all authors as ball-and-socket joint with firm ligaments preventing multiaxial movement (Lovett and Cotton, 1898; Shepard, 1951).

Hicks (1953) highlighted that the talonavicular articulation is part of two joints: on the one hand it forms the talo-calcaneal-navicular joint complex, on the other hand it forms together with this complex and the calcaneal-cuboid articulation the Chopart or midtarsal joint. The spherical shape of the head of the talus is required to enable the hinge type movements in these two joints to take place. Huson (1961) also stated that the talo-navicular ball-and-socket joint is necessary to combine movements occurring in adjacent bones. This statement points out that certain tarsal joint movements seem to interact with each other in a distinct way, a fact that will be reviewed in the next but one subchapter.

In the relevant literature motion in the Chopart or midtarsal joint is controversially discussed. The midtarsal joint motion is thought to take place simultaneously at two hinge axes: at an oblique and at a longitudinal axis (Manter, 1941). Manter's (1941) remarks are based on an *in vitro* foot study in which motion in the tarsal joints was produced manually. Manter's results and opinion of simultaneously midtarsal movements about different hinge joints have not seriously been questioned until Nester and coworkers (Nester et al., 2001). They pointed out that the simultaneous movement of midtarsal joint pronation (about one axis) combined with midtarsal joint supination (about the other axis) could occur according to Manter (1941). However, since the members of the midtarsal joint would have to move in two opposite directions at the same time, there is obviously a contradiction. Nester and coworkers (2002) investigated three-dimensional kinematics of the fore- and rearfoot during Int/ExRot *in vivo*. They calculated one axis for midtarsal motion which has been shown to change remarkably through stance phase (Nester et al., 2001).

It is generally accepted that navicular and cuboid act as a unit and perform motion at the midtarsal joint (Elftman, 1960; Huson, 1961; Manter, 1941; Shepard, 1951). Ambagtsheer (1978) measured only 2° and 6° relative rotation in the frontal plane between the navicular and cuboid during 35° and 50° of ExRot. Van Langelaan (1983) used a specially built test jig and performed ExRot to ten foot specimens. He reported that the bundles of helical axes found for calcaneo-cuboid and naviculo-calcaneal movements lay closely together. Hence, motion between the navicular and cuboid is negligible.

In summary, the first part of this chapter manifests that the ankle and subtalar joint can generally be modelled as hinge joints, but that the orientation of these joint axes must be adjusted depending on the investigated point in time or phase of the gait cycle. Based on the reviewed literature, the second part of this chapter reveals that an explicit modelling of the midtarsal joint is controversially discussed. However, if better understanding of tarsal

gears is attempted further structures besides the bones may have to be included into the model. This point will be picked up in chapter 2.1.5.

Simulation of movement coupling by one single joint

In the first section of chapter proposed mechanisms of single tarsal joints were reviewed. In this section, literature is summarised assuming one joint mechanism at the rearfoot complex to explain movement coupling.

Making the assumption of a hinge joint to understand movement coupling between the lower leg and rearfoot has the longest tradition. In 1917, Strasser mentioned that Int/ExRot of the tibia is only possible at the subtalar joint and as a consequence of rotation of the foot about its longitudinal axis. Later years, it was gradually believed that Int/ExRot takes place as a result of the oblique to all cardinal planes orientation of the subtalar axis. Jones (1945) explained by means of a wooden model that “on account of the obliquity of the axis of the subtalar joint a lateral torque in the tibia produces a component of force which acts to invert the foot”. Hicks (1953) reported that the double movement, leg rotation and foot pronation, is a simple hinge joint movement at the subtalar joint. He developed another wooden model to demonstrate that “when the foot tends to supinate (...), the leg rotates laterally, and when the foot tends to pronate, the leg rotates medially”. Rubin (1971) also developed a wooden model and confirmed the results of Hicks (1953). Inman (1976) modified his 1969 developed wooden model (see above) to show that lower leg and foot rotations depend on different orientations of the subtalar joint. The linear relationship within lower leg and foot rotations depending on the hinge axis orientation (1976) was investigated in vitro by Hintermann and Nigg (1993). They reported an almost linear relationship between calcaneal EV and tibial IntRot with an averaged movement coupling ratio of 0.46 (quotient IntRot/EV). The relationship between calcaneal INV and tibial ExRot was found to be linear, too, the averaged movement coupling ratio (quotient ExRot/INV) about 0.74 was higher, however (1993). This agrees with Inman’s (1976) above discussed theory.

Instead of using a hinge joint to explain movement coupling between the foot and lower leg Lapidus (1963), and more explicitly Wright and coworkers (1964), proposed the model of a universal joint. Wright and coworkers (1964) mentioned the foot as one member of the joint, the leg as the other; the interposed axes reflecting the ankle and subtalar joint axis. Wright and coworkers (1964) remarked that contrary to the axes of a universal joint, the ankle and subtalar axis neither intersect nor are they mutually perpendicular. But Wright and coworkers (1964) were able to explain the experimentally observed tibia rotation during foot flexion on the basis of a universal joint: Foot flexion occurred not in a plane perpendicular to the ankle axis, hence rotation about both universal joint axes is necessary and consequently, the tibia rotates about its long axis (Wright et al., 1964).

Olerud and Rosendahl (1986, 1987) revived the idea of a universal joint within the foot and lower leg. They mentioned that the mortise and the trochlea tali may be regarded as one fork, the talus acting as the centre piece and that calcaneus, cuboid and navicular works as another fork. Olerud and Rosendahl (1986, 1987) investigated ten specimens in a test jig allowing EV/INV, PF/DF and Int/ExRot, and found a nearly linear relationship within foot INV and tibial ExRot: Per degree inversion an averaged external rotation of 0.44° occurred. The distal fork constituted a three segment linked system (cuboid-calcaneus, calcaneus-talus, talus-navicular) with varying geometrical properties during the range of motion. This was used as explanation for the also observed torsion-transmitting changes and did not contradict the proposed universal joint approach.

The assumption of a universal joint acting within lower leg and rearfoot was also integrated in several mathematical models (Apkarian et al., 1989; Salathe and Arangio, 2002). Both hinge and universal joint approaches implies that the movement coupling ratio in one direction is inversely proportional to that in the opposite direction. Hintermann and coworkers (1993, 1994a) evaluated this fact in vitro. They used a modified test jig of Engsborg (1987) which allowed among other features tibial rotation about its longitudinal axis and foot EV/INV. Hintermann and coworkers (1993, 1994a) reported that the movement coupling ratio induced by a foot excursion was not identical to the opposite case where motion is induced by tibial rotation. In particular, every degree of calcaneal EV resulted in average 0.46° of tibial IntRot; but, every degree of tibial IntRot excursion resulted in only average 0.08° of calcaneal EV. This demonstrates that the movement coupling of calcaneus and tibia for a given input movement depends in the direction of transfer. The dependence can neither be simulated by a hinge nor by a universal joint (Hintermann and Nigg, 1993; Hintermann et al., 1994a).

Stacoff and coworkers (2000ab) investigated movement coupling between calcaneus and tibia in vivo. The results of five subjects running with intracortical pins with reflective marker triads show that the average movement coupling ratio between calcaneal frontal and tibial transverse plane motion changes during stance: Between heel strike and midstance every degree of calcaneal EV was coupled with 0.58° of tibial IntRot, between midstance and take-off every degree of calcaneal INV was followed by 0.46° of tibial ExRot. Hence, the authors concluded that the movement coupling between foot and lower leg is far more complex than a hinge or universal joint (Stacoff et al., 2000ab).

In summary, this subchapter clarifies that neither a single rigid hinge nor a universal joint can simulate movement coupling between the lower leg and rearfoot during the whole stance phase. But, it remains to be seen whether a hinge or universal joint may be applied for a selected duration of the stance phase, which would require an adapted definition of these axes. However, since movement coupling between tibia and calcaneus seems to be

dependent on the direction of transfer, the one segment which causes the other to move has to be determined.

Tarsal kinematic chain or tarsal gears

The preceding subchapter reveals that the explanation of movement coupling between the lower leg and foot as a single joint is somewhat unsatisfactory. In this subchapter the literature is reviewed in which the interaction of all tarsal joints is described by a kinematic chain or tarsal gear instead of by the single joint approach to explain movement coupling.

Huson (1961) assumed in his thesis that the movement of the talus causes a prescribed motion of both calcaneus and navicular/cuboid; the latter two are mentioned to move together as a block. Furthermore, this closed kinematic chain was thought to be invertible and talar transverse rotation to be equal to tibial Ex/IntRot. Huson (1961) confirmed his closed kinematic chain assumption by an in vitro investigation of fourteen specimens. By manually exposing Huson (1961) showed that “movement of each tarsal bone involves a shift such that it must be followed (or better accompanied) by a shift of the neighbouring bones”. Hence, Huson (1961) concluded that motion in the subtalar joint is as prescribed followed by talo-navicular and then calcaneo-cuboid joint motion and vice versa. The mobility of this closed kinematic chain becomes reduced almost completely after fusing one of the tarsal bones; therefore, there is only one degree of freedom for the whole tarsal mechanism. Huson (1961) emphasised two other conceptions related to the closed tarsal kinematic chain: tarsal joints are poly-axial and ligaments control the tarsal movements. Huson and coworkers (1977) could confirm both conceptions later by a roentgen-photogrammetry study: They found that tarsal joints function in a reproducible manner about axes whose orientations change continuously during motion. While changing the motion direction the viscoelastic ligament properties became evident (Huson et al., 1977). In 1986, Huson and coworkers (1986) stated that the closed tarsal kinematic chain can be driven by lower leg rotation but there was a remarkable delay between the tibial and talar rotations. This tibio-talar delay was thought to be caused by the initially insufficient tension of horizontal tibiotalar ligaments, especially the anterior talofibular ligament (ATaFi); only after tension has built up the talus followed tibial motion (Huson et al., 1986).

Ambagtsheer (1978) investigated tarsal movements with intracortical pins in every tarsal bone. The observed results led to the conclusion that the tarsal bones constitute a closed kinematic chain independent of input movement and influenced by ligaments. This is in agreement with Huson (1961).

Nester (1997) is associated with the closed tarsal kinematic chain approach in his literature review concerning the rearfoot complex. But he also stated that up to that point in time the literature lacked a specific description of a functional model for the tarsus. Nester (1997)

remarked that the ankle joint mainly provides DF/PF, the subtalar joint EV/INV and the midtarsal EV/INV as well as AB/AD and that the combined movements PRO/SUP are realised at a “rearfoot complex axis”. The orientation of this rearfoot complex axis is thought to be influenced by all three joint axis orientations what involves a great individual variation in rearfoot axis orientation. Nester (1997) proposed to categorise patients in terms of the orientation of their rearfoot complex axis and to develop a functional model for each category. However, Nester and co-workers have not published concrete model realisations to date.

An adequate consideration of the guiding function of ligaments in tarsal modelling has been proposed only ten years ago. At first, DF/PF at the ankle joint was modelled as a four bar linkage (Thoma et al., 1993). This ankle gear consists of the tibia and talus and is controlled by the anterior talofibular (ATaFi) which was already proposed by Huson (1961) and the calcaneofibular (CaFi) ligament. This ankle gear allows a rotary and gliding component of the tibia against the trochlea tali. Thoma and coworkers (1993) confirmed their four bar linkage by an in vitro x-ray investigation of six foot specimens.

Leardini and coworkers (1999a) built a test jig to move six rearfoot specimens through their range of DF/PF while applying only the minimum necessary load to drive passive flexion. The rearfoot complex was constrained only by the passive structures of the joints. Leardini and coworkers (1999a) evaluated that the path of calcaneal motion with respect to the tibia during DF was virtually the same as in PF. Most of the motion occurred at the ankle, less at the subtalar joint. It was also shown that the calcaneofibular (CaFi) and the tibio calcaneal (TiCa) ligaments remain nearly isometric. Leardini and coworkers (1999b) extended their work and concluded that the entire rearfoot complex can be regarded as a single degree of unrestricted freedom mechanism. They modelled this mechanism as a four bar linkage consisting of the shank bones, the hind foot bones and the two isometric CaFi and TiCa ligaments. This gear with one degree of unrestricted freedom was mentioned to describe the rearfoot complex during DF/PF in an unloaded condition (Leardini et al., 1999). Subsequently, retinacula and muscle units were implemented in this two dimensional model; furthermore, the model was proved under the conditions of ankle joint prostheses (Leardini, 2001; Leardini and Moschella, 2002).

In summary, the closed tarsal kinematic chain approach with one degree of freedom is well accepted in literature. However, the evaluation of passive and driving elements of tarsal gears to explain certain tarsal movements is still in the beginning. The consideration of guiding ligaments may provide a better basis for modelling complex movement behaviours between tarsal bones than for modelling based on bony structures and ligaments limiting the range of motion only.

2.1.5 Ligaments in tarsal gears

The generally accepted role of the tarsal ligaments is to prevent multiaxial movements and to limit the range of motion at tarsal joints. However, more recent publications distinguish explicitly between two different strain behaviours and thus, two different roles of the tarsal ligaments. One behaviour is described with an increasing or decreasing ligament length during a particular motion. Hence, such ligament behaviour would limit the particular motion. The other behaviour is based on the observation that ligaments may be maximally strained by $\pm 3\%$; a behaviour which is devoted as 'isometric' (Leardini et al., 1999a). Hence, such isometric ligament behaviour could guide a motion. The distinction of these two behaviours is important when attempting to model the human tarsus, because limiting ligaments act somehow like a rope in contrast to guiding ligaments which act rather like a bar. Leardini and coworkers (1999a) developed their four bar linkage model exactly from this point of view (see previous chapter): Two of the bars were represented by the CaFi and TiCa ligament due to their isometric behaviour during DF/PF. To provide further similar justified tarsal gears, a literature summary about the qualitative strain behaviour of the main rearfoot ligaments during certain foot motions is given in Tab. 2-1. Note that e.g., the ATaFi ligament may be regarded as a guiding link during foot EV/INV, however, that has to be proved in future tarsal gear models. Among others, Luo and coworkers (1997) provide information on ligament geometry, Attarian and coworkers (1985) and Siegler and coworkers (1988b) on material properties of ligaments.

The behaviour of tarsal ligaments was also investigated by (sequentially) cutting ligaments and measuring the changes in the range of motion in certain tarsal joints (Hintermann et al., 1995; Hollis et al., 1995; Rasmussen, 1985; Stephens and Sammarco, 1992) or in movement coupling between calcaneus and tibia (Sommer et al., 1996). But based on the results of these investigations no decision can be made whether a ligament guides or limits a motion: Both guiding and limiting ligaments are under stress; hence, cutting either ligament enlarges the range of motion.

In summary, one can conclude that future tarsal investigations should evaluate whether the explicit distinction of guiding and limiting behaviour of ligaments and their effects on tarsal gears may help to improve the understanding of movement coupling at the tarsus.

Tab. 2-1 Summary of reported rearfoot ligaments, the motion in which they become strained, and the type of strain behaviour. For ligament positions see Fig. 2-1.

| Ligament | Motion | Strain behaviour | Literature | |
|-------------------------------|------------------------------|--------------------------------------|--|---|
| Calcaneofibular (CaFi) | foot DF / PF | isometric in DF / PF | Renstrom et al. (1988) Bruns and Rehder (1993) Leardini et al. (1999b) | |
| | | isometric in PF | Luo et al. (1997) | |
| | | increased in max. DF | Colville et al. (1990) Nigg et al. (1990) Cawley and France (1991) Luo et al. (1997) Parenteau et al. (1998) | |
| | foot EV / INV | isometric in EV | Luo et al. (1997) | |
| | | increased in INV, decreased in EV | Renstrom et al. (1988) Colville et al. (1990) Nigg et al. (1990) Luo et al. (1997) Parenteau et al. (1998) | |
| | | increased in ABD | Renstrom et al. (1988) Colville et al. (1990) Nigg et al. (1990) | |
| | Anterior talofibular (ATaFi) | foot DF / PF | increased in PF | Renstrom et al. (1988) Nigg et al. (1990) Cawley and France (1991) Luo et al. (1997) |
| | | | decreased in DF | Colville et al. (1990) Leardini et al. (1999) Bruns and Rehder (1993) |
| | | | isometric in EV / INV | Renstrom et al. (1988) Nigg et al. (1990) Luo et al. (1997) |
| foot EV / INV | | increased in max. EV | Cawley and France (1991) | |
| | | increased in AB | Colville et al. (1990) Nigg et al. (1990) Cawley and France (1991) | |
| | | increased in DF / PF | Luo et al. (1997) | |
| Posterior talofibular (PTaFi) | foot EV / INV | isometric in EV / INV | Luo et al. (1997) | |
| | foot ABD/ADD | increased in ADD | Colville et al. (1990) | |
| | foot DF / PF | increased in PF | Luo et al. (1997) | |
| Anterior tibiotalar (ATiTa) | foot EV / INV | isometric in EV / INV | Luo et al. (1997) | |
| | foot DF / PF | increased in DF, decreased in PF | Bruns and Rehder (1993) Luo et al. (1997) | |
| Posterior tibiotalar (PTiTa) | foot EV / INV | increased in EV / INV | Luo et al. (1997) | |
| | foot DF / PF | isometric | Bruns and Rehder (1993) Leardini et al. (1999b) | |
| Tibiocalcaneal (TiCa) | foot EV / INV | increased in max. DF | Luo et al. (1997) | |
| | foot EV / INV | increased in EV, decreased in INV | Luo et al. (1997) | |
| Tibionavicular (TiNa) | foot DF / PF | increased in PF, decreased in DF | Luo et al. (1997) | |
| | foot EV / INV | increased in EV, decreased in INV | Luo et al. (1997) | |
| Lig. canalis tarsi | foot DF / PF | increased in PF, decreased in DF | Luo et al. (1997) | |
| | foot EV / INV | isometric in EV / INV | Luo et al. (1997) | |

2.1.6 Validation of tarsal gears

After modelling the tarsus (see chapter 2.1.4 and 2.1.5) it is reasonable to validate these models. Thus, this chapter summarises *in vitro* and *in vivo* investigations which concentrate on validation procedures. Additionally, a comparison of static versus dynamic investigations is provided and the effect of tibial load on the biomechanics of the tarsal bones is reviewed.

In vitro studies

There are a number of *in vitro* studies focussing on the relative tarsal joint movements and axes orientations (Benink, 1985; Bottlang et al., 1999; Engsborg, 1987; Hicks, 1953; Leardini et al., 2001; Manter, 1941; Siegler et al., 1988a; van Langelaan, 1983), but only a few *in vitro* studies looking closely at movement coupling between the rearfoot and lower leg (Hintermann et al., 1994a; Hintermann and Nigg, 1995; Olerud, 1985; Olerud and Rosendahl, 1987;). The more recent studies were already described in chapter 2.1.4. As mentioned above, movement coupling between calcaneal EV/INV and tibial IntRot/ExRot may affect typical running injuries (see chapter 2.1.1). Because movement coupling may be discussed in view of the movement coupling ratio, studies which focussed on this quotient will be reviewed here. For the benefit of better comparison the corresponding evaluated movement coupling ratios are listed in Tab. 2-2.

Tab. 2-2 shows various differences between investigations, i.e. Olerud and Rosendahl (1987) found lower movement coupling ratios than Hintermann and Nigg (1993). A major reason for these differences may be the construction of the two used test jigs: The test jig of Olerud and Rosendahl (1987) allowed three degrees of freedom in contrast to the six degrees of freedom measurement device of Hintermann and Nigg (1993). Furthermore, Hintermann and Nigg (1993) fixed the calcaneus on a foot plate; hence, motion of the foot plate represents calcaneal motion. However, Olerud and Rosendahl (1987) fixed the fore foot on a plate; since no load was applied to the tibia / foot, it can be assumed that the calcaneus could move relative to the foot plate. However, the plate was mentioned to represent calcaneal motion by Olerud and Rosendahl (1987).

Loads applied to the tibia / foot used for foot fixation are only of minor importance. The primary purpose of applying loads to the tibia / foot during *in vitro* investigations is to provide a more realistic simulation of *in vivo* situations. Some studies suggest that relative tarsal joint movements are not load dependent (Benink, 1985; Michelson et al., 1996), others suggest the opposite (Fraser and Ahmend, 1983; Hintermann and Nigg, 1995; Liu et al., 2000). In particular, Hintermann and coworkers (1994a) and Sommer and coworkers (1996) compared the movement coupling ratios between calcaneal EV/INV and tibial IntRot/ExRot with and without applying a load in the longitudinal direction of the tibia.

Tab. 2-2 Summary of reported coupling movement ratios between calcaneal EV (INV) range of motion and tibial ExRot (IntRot) range of motion.

| condition | Δ Tib. IntRot / Δ Cal. EV | Δ Tib. ExRot / Δ Cal. INV | literature |
|-----------------------------------|---|---|-----------------------------|
| in vitro ^a , no load | 0.42 ^b | 0.46 | Olerud and Rosendahl (1987) |
| | 0.46 | 0.74 | Hintermann and Nigg (1993) |
| | 0.40 | 0.7 | Sommer et al. (1996) |
| in vitro ^a , with load | 0.29, 600 N load | 0.62, 600 N load | Hintermann et al. (1994) |
| | 0.28, 600 N load | 0.35, 600 N load | Sommer et al. (1996) |
| in vivo ^a , static | | 0.2 ^c , Body weight load | Lundberg et al. (1989b) |
| in vivo, running ^d | 0.62, low arch | | Nigg et al. (1992) |
| | 0.68, normal arch | | |
| | 0.96, high arch | | |
| | 0.92, barefoot | | Kim et al. (1995) |
| | 0.98, shod | | |
| | 0.55, low arch, sandals | | Nawoczenski et al. (1995) |
| | 1.00, high arch, sandals | | |
| | 0.65, normals | | McClay and Manal (1997) |
| | 0.81, pronators | | |
| | 0.56, low arch, sandals | | Nawoczenski et al. (1998) |
| in vivo, running ^e | 0.90, high arch, sandals | | |
| | 0.66, barefoot | | Stacoff et al. (2000a) |
| | 0.58, shod | 0.46, shod | Stacoff et al. (2000b) |
| | 0.35 ^f tibia / shoe | 0.38 ^d tibia / shoe | |

^a Exposing movement at calcaneus.

^b Movement from EV to neutral position.

^c Ratio between whole foot (foot plate) and tibia.

^d Range of motion between heel strike and maximal shoe eversion, skin and shoe/sandal markers.

^e Bone pins in calcaneus and tibia.

^f Ratio between shoe motion and tibia.

The results are summarised in Tab. 2-2. Since decreased movement coupling ratios were found with tibial load, it becomes evident that these ratios and thus movement coupling between the rearfoot and lower leg is in fact load dependent.

Reasons may be that tibial load increases the articulating surfaces (McCullough and Burge, 1980; Stormont et al., 1985) and influences ligament forces and strains (Bahr et al., 1998; Cawley and France, 1991).

Hintermann and coworkers (1994a) extended their study and determined that the movement coupling ratios between calcaneal EV/INV and tibial IntRot/ExRot depends on the dorsi - plantarflexion position of the foot, too.

In spite of the measuring complexity the above reviewed in vitro investigations could not take into account the influences of muscle activity and of dynamic foot motion. Recently, Sharkey and Hamel (1998) presented a dynamic cadaver measurement device to evaluate relative movements within foot bones: The device reproduces the sagittal kinematics of the tibia while applying assumed physiological muscle forces of the major extrinsic muscles. In

2002, Michelson and coworkers provided first results using this dynamic cadaver measurement device when investigating the kinematic behaviour of the ankle following malleolar fractures and medial ligaments disruption.

In summary, *in vitro* studies have determined movement coupling ratios between calcaneal EV (INV) and tibial IntRot (ExRot) between 0.29 (0.35) and 0.46 (0.75). The reason for these discrepancies may be both the different test jigs and the dependence of movement coupling ratios on tibial load and foot flexion or other unknowns.

In vivo studies

Lundberg and coworkers (1989abc) investigated rearfoot complex kinematics *in vivo*. Radiopaque markers were introduced into the tarsal and adjacent bones and the tests were performed under full body load. In addition to the evaluation of the effect of foot flexion or tibial rotation, the effect of tilting a foot plate in the frontal plane on the three dimensional tarsal kinematics was investigated. Lundberg and coworkers (1989b) reported a mean movement coupling ratio between foot INV and tibial ExRot of 0.2. However, in this testing procedure the calcaneus did not move more than 2.5° during the input arc of 20° foot plate inversion; thus, this ratio can not be compared to the others listed in Tab. 2-2. But Lundberg and coworkers (1989b) mentioned higher movement coupling ratios during INV than in EV what agrees with *in vitro* findings (see Tab. 2-2).

Lundberg and coworkers (1989abc) used a roentgen stereophotogrammetry method which allows to provide results with high accuracy; however, the investigation was performed under static conditions. Since the axes of tarsal joints show different orientations during static and dynamic measurements (Nester et al., 2001) it is debatable to transfer the results of Lundberg and coworkers (1989abc) to more dynamic conditions such as walking and running.

Inman (1976) showed that the more the subtalar joint axis is inclined in the sagittal plane the more the tibial Ex/IntRot is following foot INV/EV. Investigations related to movement coupling during locomotion often used the subject's arch height as an indicator of subtalar axis orientation. In general, higher movement coupling ratios (see Tab. 2-2) were found for the high arched feet compared to normal or low arched feet (Nawoczenski et al., 1995; Nawoczenski et al., 1998; Nigg et al., 1992), confirming Inman's (1976) theory. However, arch classification and the non-invasive method have two major points of criticism: Firstly, the investigations were performed with skin markers which are regarded to overestimate the movement amplitudes due to the non-rigid attachment of the skin to the bone and by muscle contractions underneath the skin (Reinschmidt et al., 1997abc). Secondly, arch classifications are typically performed by static measurements which are regarded as ineffective (Hamill et al., 1989; Mathieson et al., 1999, McPoil and Cornwall, 1996a) or

insufficient (Nigg et al., 1993) taking into account the observed variability in dynamic variables. Kim and coworkers (1995) reported that arch height did not influence movement coupling ratios between EV and tibial IntRot, neither in shod nor in barefoot condition. Furthermore, Tab. 2-2 shows that the movement coupling ratio in shod and in barefoot condition were nearly the same (Kim et al., 1995).

McClay and Manal (1997) also used skin and shoe markers but assigned their subjects to a pronator and a normal group based on the subject's EV peak. For the first group a mean movement coupling ratio of 0.81 and for the latter of 0.65 was found. This was mainly caused by the significant greater tibial IntRot found in the pronator group (McClay and Manal, 1997).

Stacoff and coworkers (2000ab) investigated movement coupling ratios in vivo with intracortical pins to avoid above mentioned skin marker problems (see subchapter 2.1.4). Stacoff and coworkers (2000a) reported in agreement with Kim and coworkers (1995) nearly the same mean movement coupling ratio between calcaneal EV and tibial IntRot for barefoot (0.66) and shod running (0.58). Stacoff and coworkers (2000b) also provided movement coupling ratios between the shoe and the tibia which are remarkably lower compared to earlier in vivo studies (see Tab. 2-2). Contrary to in vitro studies, Stacoff and coworkers (2000ab) determined a higher movement coupling ratio between calcaneal EV and tibial IntRot compared to the ratio between calcaneal INV and tibial ExRot (see Tab. 2-2).

In summary, in vivo studies have determined movement coupling ratios between calcaneal/shoe EV and tibial IntRot between 0.35 and 1.00. These discrepancies are only insufficiently explained by subject classification based on anatomical foot structure. It is possible that skin movement artefacts further increase inaccuracies and thus contributes to these discrepancies. Thus, these large differences in movement coupling ratios do not allow to characterise human tarsal function to an acceptable degree. For further investigations, e.g. modelling of the rearfoot, an improvement, or if possible, validation seems necessary.

2.1.7 Conclusions

The biomechanics of the human tarsus has attracted researchers for more than hundred years. Generally, the relevant literature has increased since the 1970s, especially to improve the knowledge on the aetiology of typical running injuries.

However, the type of linkage at the tarsus which represents movement coupling between the rearfoot and lower leg is controversially discussed: In older literature a single rigid hinge joint as well as a universal joint are suggested. In the more recent literature, neither of these two joints are accepted to represent movement coupling during the whole stance

phase. This is because movement coupling ratios between the calcaneus and tibia have been reported to change continuously during the stance phase; it remains open whether a hinge or universal joint may be applied for a selected duration of the stance phase.

A further important part of the literature focuses on the closed kinematic chain approach of the tarsus. Traditionally, bony structures and ligaments limiting the range of motion are considered in kinematic chains. But, several recent papers suggest distinguishing between limiting (strained) and guiding (isometric) ligaments. The consideration of guiding ligaments in models of tarsal gears has already been shown to improve the simulation of tarsal movements in the sagittal plane.

Lastly, the large discrepancies of the reported movement coupling ratios indicate that there is presently no validation available which allows to characterise human tarsal function to an acceptable degree. Hence, future studies should improve the validation procedures of human tarsal models. Beyond, to improve the knowledge on movement coupling between the calcaneus and the tibia, e.g. three-dimensional, additional tarsal gears need to be established.

2.2 An alternative approach: Magnet resonance imaging

In the previous chapter it was indicated that for the current modelling of human tarsal gears procedures are missing which characterise tarsal kinematics to an acceptable degree. In the past, tarsal kinematics have been examined by two- and three-dimensional X-ray stereophotogrammetry (Benink, 1985; van Langelaan, 1983; Lundberg et al., 1989abc) or intracortical pins (Arndt, 2004; Reinschmidt et al., 1997ac; Stacoff et al., 2000abc) (for more details see chapter 2.1.6). However, these methods were all invasive or ionising and thus, they cannot be established as a routine tool in living subjects. Although skin markers enable non-invasive investigations without harmful radiation, tarsal kinematics are hardly detectable by the use of them: Most of the foot bones are too small to place three markers on them. Furthermore, the motion of the bones relative to the skin limits the validity of skin markers (Maslen and Ackland, 1994; Tranberg and Karlsson, 1998; Westblad et al., 2002).

Magnetic resonance (MR) imaging is yet another approach. It overcomes the above mentioned limitations and since bone volumes can be accurately measured in the MR (Boutry et al., 2004; Cohen et al., 1999), it can provide insights into discrete tarsal bone positions of different foot excursions. In the following paragraph studies using MR imaging in combination with foot positioning devices to investigate tarsal kinematics are summarised.

In the late 1990s, Stindel, Udupa and coworkers were the first to present a MR compatible foot positioning device (Stindel et al., 1998; Udupa et al., 1998). This device allowed to place the foot into a defined pronation and supination, respectively, about an axis specified by the subtalar joint axis orientation reported by Inman (1976). Therewith, it was possible to distinguish quasi-static kinematic behaviour of fused joints from healthy joints. Unfortunately, the results of these studies are limited since the foot positioning device does not allow to bear any load. The same is true for a more recently presented device providing defined foot positions in the sagittal plane (Mattingly et al., 2006). From previous studies it is evident that load does in fact alter tarsal joint kinematics (Fraser and Ahmend, 1983; Hintermann et al., 1994a; Michelson et al., 1990). Thus, a foot positioning device should feature a load bearing system which, for instance, should simulate upright standing. With such a device, tarsal kinematics evaluated in the lying posture of MR imaging may be comparable with results gained with X-ray stereophotogrammetry and test jigs featuring quasi-static motion in an upright posture as presented by i.a. Benink (1985) and Lundberg (1989a).

Recently, a more complex MR compatible foot positioning device has been presented enabling to rotate the foot in all cardinal body planes (Ringleb et al., 2005; Siegler et al., 2005). Being intended as a clinical diagnostic tool for ligament injuries, the foot was moved

by an inversion moment (3.4 Nm) or an anterior drawer force (150 N), the resulting foot position was fixed and imaging of the tarsal bones was performed (Ringleb et al., 2005; Siegler et al., 2005). However, it must be stated that this approach provided only limited new knowledge of fundamental tarsal bone kinematics because (i) only seven subjects have been measured in vivo so far, (ii) the device features no axial load, and (iii) motion of the cuboid and navicular has not been monitored. Thus, to profit from MR imaging to investigate fundamental tarsal kinematics non-invasively and without harmful radiation further adequate foot positioning and loading devices are needed.

Further, it has to be noted that tarsal kinematics results from the whole tarsal mechanics which is influenced by external load and muscle forces, ligament behaviour, and bone morphology. Now, three-dimensional tarsal bone morphology, particularly the joint curvature, is assessable by MR imaging. Hence, MR imaging seems to be a promising approach to describe tarsal kinematics and joint curvatures. It should be interesting to see the potential of this approach to gain new insights into tarsal joint mechanics.

2.3 Foot type classifications

Common opinion is that foot function depends on foot morphology (Inman, 1976; Root et al., 1977). And, clinical evidence suggests that certain foot morphologies are predestined for typical running injuries (Clement et al., 1981; Franco, 1987; Heil, 1992).

Furthermore, it is common practise that orthotists, physical therapists and shoe manufacturers classify foot morphologies to predict foot function hoping that an effective treatment can be based on their decision (Rothstein, 1985; Scharfbillig et al., 2004).

The purpose of this chapter is to review methods classifying foot types based on morphology at first. Thereafter, results of studies investigating the dependence of foot function on foot classification are summarised.

2.3.1 Methods to classify foot types

Foot types are usually classified based on morphological parameters derived from *a) radiographic evaluations* (i.a. Gentili et al., 1996), *b) anthropometric measurements* (i.a. McPoil and Cornwall, 1996b), *c) footprints* (Mathieson et al., 1999), and *d) visual non-quantitative assessments* (i.a. Dahle et al., 1991). These different methods are discussed in the following paragraphs.

a) Radiographic evaluations: Foot morphology classifications based on radiographic and video-fluoroscopic approaches are characterised by a high reliability of the quantification of two-dimensional (2D) parameters, i.e. talo-calcaneal or talo-navicular angle (Saltzman et al., 1995; Wearing et al., 1998). However, it is difficult to draw conclusions from 2D parameters on three-dimensional (3D) foot function (Stindel et al., 2001). Furthermore, the complexity and the harmful radiation are disadvantageous. Consequently, radiographic evaluations can not be preferred as a clinical standard.

b) Anthropometric measurements: Anthropometric measurements are easily to perform: arch height, neutral rearfoot position, and passive range of motion (ROM_{passive}) are assessable with ruler and goniometer, respectively. However, there are some limitations: First, the arch height can not provide 3D information about the underlying bone positions or the nature of tarsal joints (Stindel et al., 1999ab). Second, the determination of the neutral rearfoot position is not trivial because foot care specialists have shown a large variability of ± 3 degrees related to the subtalar neutral position (Pierrynowski et al., 1996). The low reliability of the neutral rearfoot position is also confirmed by Elveru and coworkers (1988) and Menz (1995). In a more general sense, the usability of neutral rearfoot position gained without load (Allinger and Engsborg, 1993; Debrunner and Hepp, 1994; Hlavac, 1967; Milgrom et al., 1985) has been criticised (Ball and Afheldt, 2002ab). Lastly, the passive rearfoot motion is influenced by the foot position (Milgrom et al., 1985)

which makes the comparison of the passive range of motion of several studies using another standardised foot positions each difficult (Menz, 1995). Considering all the mentioned limitations, the feasibility of anthropometric measurements to classify foot morphologies is questionable.

c) Foot prints: Foot print parameters are often employed in gait analysis as an indirect measure of arch height, and, as such, have been used to classify foot morphology (Hogan and Staheli, 2002; Rosenbaum et al., 1994; Staheli et al., 1987). Beside the before mentioned questionable classification based on arch heights, the validity of employing foot prints as an indirect measure of arch height is controversial: In contrast to smaller studies showing moderate correlations (Chu et al., 1995; Shiang et al., 1998), larger studies have not identified a significant correlation between footprint-based estimations of the arch height and corresponding clinical measurements (Hawes et al., 1992; McPoil and Cornwall, 2000). Apparently, the variability of tissue thickness beneath the foot invalidates the use of foot prints as an estimation of the arch height and in consequence, as a parameter to classify foot morphology.

d) Visual assessment: The visual non-quantitative assessment of foot morphologies is influenced by subjective assessments and experience resulting in large variability (Hawes et al., 1992) or low reliability (Cowan et al., 1994). Therefore, this approach seems also useless to classify foot morphology.

In summary, the above mentioned methods have not provided a feasible classification of foot morphologies since none of them provide detailed 3D information about the nature of the foot joints in general and tarsal joints in particular.

An alternative approach is magnet resonance imaging (MRI) offering non-ionising insights into 3D bone morphology. Spatial positions of the centre of gravity and principal moments of geometry of the tarsal bones measured by MRI were used to classify foot morphology first in the late 1990s (Stindel et al., 1998; Stindel et al., 1999ab). Further morphological parameters like joint curvatures are also acquirable by MRI but have not been investigated so far. However, joint mechanics are in fact directly influenced by joint curvatures and thus, curvatures might provide a more appropriate basis to classify foot morphology than centroid and second moments of volume.

2.3.2 Investigations of the dependence of foot function on foot morphology

The literature provides only few investigations concerning the relationship between foot morphology and foot function. In these studies, foot types have usually been classified based on morphological parameters derived from radiographic evaluation, anthropometric measurements or footprints (Razeghi and Batt, 2002). These foot classifications were then

used to explain the variability of dynamic parameters associated with lower extremity injuries. However, several authors have found that variations of the calcaneal motion (maximum, point in time of maximum, range of motion) can not be explained by the predefined foot classifications based on static parameters or ROM_{passive} of the foot (Cornwall and McPoil, 2004; Hunt et al., 2000; Hunt and Smith, 2004; Kernozek and Ricard, 1990; Knutzen and Price, 1994; McPoil and Cornwall, 1996ab).

Further, movement coupling between the lower leg and rearfoot which is presently associated with typical running injuries (McClay, 2000; Stergiou, 1996) has shown only a slight correlation with foot arch height (Nawoczinski et al., 1998; Nigg et al., 1993).

Under the assumption that foot function does in fact mainly depend on foot morphology, the results of the cited studies indicate that the foot classifications based on static parameters or ROM_{passive} were insufficient to characterise foot morphology. The classification parameters were not able to monitor the 3D nature of the foot joints and thus, dynamic foot function was not predictable.

However, it has been shown that even 3D morphology parameters like the spatial positions of the centroid and second moments of volume of the tarsal bones measured by MRI do not correlate with quasi-static tarsal joint rotations (Stindel et al., 1999b). This leads to the conclusion that either foot function depends less on foot morphology than previously assumed or the used morphology parameters have a minor influence on joint mechanics.

It is interesting to note that all studies investigating the dependence of foot function on foot morphology started from morphological classifications. But, it is the functional difference that is of original interest for clinicians and shoe manufacturers. Therefore, it seems appropriate to investigate foot morphology by the use of dynamical foot classifications. Thereby, it should be focused on parameters which are obviously linked with joint mechanics such as the joint curvature which is thought to influence kinematics, in particular during quasi-static motion (Benink, 1985; Leardini et al., 1999c; Lundberg et al., 1989b; van Langelaan, 1983). This approach might give new insights into the still uncertain relationship between foot morphology and foot function (Cornwall and McPoil, 2004; Hunt and Smith, 2004; Razeghi and Batt, 2002) which is important in view of an effective prevention and treatment of foot injuries (Rothstein, 1985; Scharfbillig et al., 2004).

2.4 Purpose

Today, knowledge of three-dimensional (3D) tarsal bone mechanics is still limited despite the ongoing research. It has been shown that concepts such as the hinge or universal joint representing tarsal kinematics are outdated and are proven to be insufficient. More complex models of the tarsus, so called tarsal gears, are about to be developed whereby validation procedures are the main problem of today: Standard video motion analyses do not provide insights into tarsal kinematics due to the hidden nature of tarsal anatomy; and more elaborated procedures such as X-ray stereophotogrammetry implicate harmful radiation. An alternative approach to investigate tarsal kinematics is based on magnetic resonance imaging (MRI) featuring 3D information of the tarsal bone morphology, in particular, the joint curvatures of the tarsal bones with considerable implications on tarsal joint kinematics.

In order to gain a better fundamental knowledge of the relationship of foot function and foot morphology which is important in view of an effective prevention and treatment of foot injuries new approaches have to be elaborated. One such approach could be to investigate dynamically classified subjects by a MR procedure enabling defined foot positions and loads.

Thus, there are two main purposes that will be addressed in this thesis:

1. The development of a magnetic resonance imaging procedure enabling investigations of quasi-static tarsal bone motion and morphology;
2. The application of the newly developed MRI procedure to investigate tarsal bone morphology of dynamically classified subjects.

Chapter 3
A non-invasive procedure
to investigate tarsal kinematics

In view of the first main purpose of the thesis, this chapter is related to the development of a magnetic resonance (MR) imaging procedure providing unique insights into quasi-static tarsal bone motion and morphology. The chapter is divided into four sections, each covering one crucial point of image acquisition and processing: First, the reliability of semi-automatic image segmentation is examined; second, the influence of different slice orientation is determined; third, a foot positioning and loading device is presented; and fourth, the newly developed non-invasive method is compared to the invasive state-of-the-art (video motion analysis with intracortical pins).

3.1 Reliability of tarsal bone segmentation and its contribution to MR kinematic analyses methods

3.1.1 Introduction

Currently, magnet resonance (MR) imaging is increasingly used in the research of foot biomechanics. Thereby, the process to achieve precise three-dimensional (3D) reconstructions of the bones of interest is of main importance, because the reconstructed bony surfaces provide the morphological basis of present finite element models of the foot (Bandak et al., 2001; Camacho et al., 2002; Cheung et al., 2005). Furthermore, the volumes of foot bones enable to constitute a principal axes coordinate system which can be used to analyse foot kinematics with MR imaging (Ringleb et al., 2005; Udupa et al., 1998). In contrast to common stereophotogrammetry, such an approach - in combination with recently developed MR compatible foot positioning and loading devices - provides new insights into tarsal bone kinematics (Mattingly et al., 2006; Siegler et al., 2005). In this way, MR imaging is superior to any other image based procedure because of its non-invasive character without harmful radiation (Siegler et al., 2005; Udupa et al., 1998).

The 3D reconstruction of the tarsal bones is based on segmented bony parts in the respective MR images. If this image data processing involves operator interaction, precision errors are to be expected (Eckstein et al., 2002). The reliability of in-house reconstruction solutions has frequently been reported in the publication of such a method (Barra and Boire, 2002; Stagni et al., 2004; Stammberger et al., 1999; Stindel et al., 1999a). The reliability of common commercial 3D reconstruction software - in many clinical and scientific environments the only choice - has mostly been investigated in the case of brain tissue volumetry (Agartz et al., 2001; Bartlett et al., 1994; Okugawa et al., 2003), but has not been reported for morphological parameters of tarsal bones so far.

Furthermore, if principal axes or surface point clouds providing MR kinematic analyses are based on semi-automatic segmentation, the accuracy of these analyses methods will be

affected by the operator performing the segmentation. However, it is currently not known to which degree this accuracy is influenced by using commercially available software.

Thus, the purpose of this study was to evaluate the intra- and interoperator reproducibility of tarsal bone segmentation performed with a commercially available software (AMIRA, Mercury Computer Systems, Berlin, Germany). In doing so, the following morphological parameters of the calcaneus, talus, navicular, and cuboid were investigated: volume, moments of inertia and the orientation of their principal axes, respectively. Lastly, the influence of repeated segmentations on a MR kinematic analyses method which is based on principal axes was determined and compared to another MR kinematic analyses method based on surface point clouds.

3.1.2 Materials and methods

Subjects

Five volunteers without signs of musculoskeletal diseases participated in this study (two female, three male). The different foot and shoe sizes (EUR 36, 38, 43, 46, 49) were not only chosen to reflect the bandwidth of tarsal bone size but also to estimate the precision of the segmentation in general (Gluer et al., 1995). Informed written consent in accordance to the local research ethics committee was obtained from all subjects.

Data acquisition

Imaging was performed on a 3 Tesla whole-body MR unit (Intera 3T, Philips Medical Systems, Best, The Netherlands) equipped with a Quasar Dual gradient system (gradient strength up to 80 mT/m and gradient slew rate up to 200 mT/m/ms). The right lower leg and rearfoot were placed on a 12 element synergy spine coil (Philips Medical Systems) in neutral position and fixed by sandbags. A 3D T1 weighted gradient echo sequence with water selective excitation and second order shimming was used to obtain fat suppressed, high-contrast and high-resolution images of the tarsal bones. Sequence parameters were as follows: repetition time 16 ms, echo time 4 ms, and flip angle 11°; 200 mm field of view; a 288 x 273 acquisition matrix; Fourier interpolated to 512 x 512 pixels; 1.4 mm thick overcontinuous slices with 50% slice overlapping. Thus, the measured spatial resolution was 0.69 x 0.73 x 1.4 mm³ and the resolution of the reconstructed images was 0.39 x 0.39 x 0.7 mm³. For each subject 100 sagittal slices were acquired during 7 min (Fig. 3-1).

The signal intensities of tarsal bones, cartilage (ankle, subtalar and talonavicular joints), fatty tissues (border of heel fat pad), muscles (m. quadratus plantae) and tendons (Achilles), and background noise were measured for all subjects. Contrast-to-noise ratios (CNR) were calculated as the difference between the mean signal intensities of no-bone tissues (SI_i) and the signal intensity of bone tissue (SI_{bone}) divided by the standard deviation (SD) of the noise $[(SI_i - SI_{bone}) / SD_{noise}]$. The standard deviation of noise was estimated by the mean signal intensity of air (Kaufmann et al., 1989). Contrast-to-noise ratio between bone and cartilage (fatty tissues, muscles, tendons) was found to be 55.0 ± 11.3 (54.6 ± 12.6 , 50.7 ± 9.3 , 4.5 ± 4.1). These ratios outline the high-contrast quality of the images.

Data processing

The 3D reconstruction of the tarsal bones was performed with AMIRA. The appropriate image pixels were assigned to the specific tarsal bones using an intensity threshold function. This was done slice by slice in the acquisition plane first. Thereafter, the result was controlled in the other two perpendicular planes. Since vessels and tendons exhibited similar intensities as the tarsal bones (see also CNR) the operators' duty was to check whether these non-bony tissues were erroneously segmented and if necessary, to correct this. In this manner, the operators were able to segment a complete tarsal bone in 20 to 40 min depending on experience and bone size.

The image data sets of the five subjects were set anonymous, each replicated five times, and set in a random order. This ensured that the segmentation conditions (i.e. threshold) had to be set by the operators for each data set individually. Based on these 25 image data sets operator A as well as B (C as well as D) segmented the calcaneus and cuboid (the navicular and talus). Therefore, each bone was segmented a total of 50 times. Each operator segmented 2-3 datasets a week. Thus, the overall time to complete the whole segmentation of all image data sets was about 3 month.

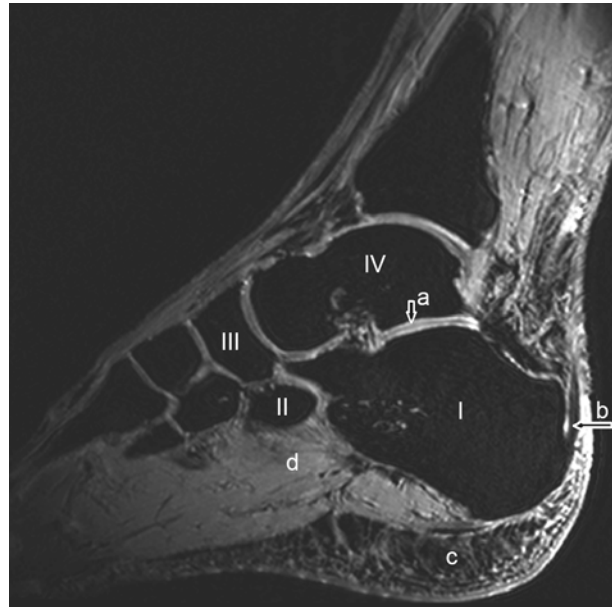


Fig. 3-1 Sagittal MR image of tarsal bones. Fat suppressed 3D T1 weighted gradient echo sequence with selective water excitation. Calcaneus (I), cuboid (II), navicular (III), talus (IV), and cartilage (a), Achilles tendon (b), heel fat pad (c), musculus quadratus plantae (d).

Morphological parameters

After using a built-in function of AMIRA to smooth by subvoxel-weights, volume and surface area of reconstructed bones were calculated. Then, a surface point cloud of each bone was read in MatLab (MathWorks, Massachusetts). Cubes with same density (1 g/cm^3) and side length of 0.7 mm were placed inside the surface point cloud. Second moments of volume and related principal axes were calculated (Fig. 3-2) whereby cubes on the surface were weighted by factor 0.5.

The moments of volume were normalised

by the arbitrary defined density. The angles (direction cosine) between the resulting first two principal axes and the axes of the MR coordinate system were later used to evaluate the reliability of such a principal axes coordinate system defining the orientation of the bones in space. This user written routine was checked with ellipsoids similar to the talar bones: Hereby, the numerical error of the second moments was found to be less than 1% and of the axes orientation was less than 0.005° .

Intraoperator reproducibility

Based on the described morphological parameters the intraoperator reproducibility was determined using the intraclass correlation coefficient ($\text{ICC}_{3,1}$) described by Shrout and Fleiss (1979). Since repeated segmentations have to be taken into account the calculation of the coefficient was modified as recommended by Eliasziw and coworkers (1994) (see appendix A, eq. A-1).

Interoperator reproducibility

The interoperator reproducibility was estimated by the intraclass correlation coefficient ($\text{ICC}_{2,1}$) as suggested by Shrout and Fleiss (1979). To consider repeated measurements and random operator effects the calculation of the intraclass correlation coefficient was modified as recommended by Eliasziw and coworkers (1994) (see appendix A, eq. A-2). The advantage of this reproducibility estimation is that the results can be generalised to other operators and thus, provide the precision of further studies.

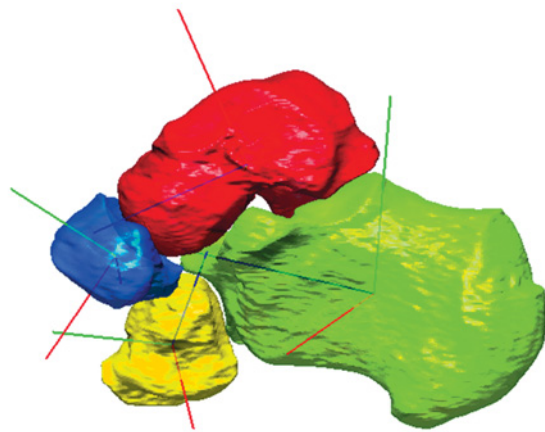


Fig. 3-2 Tarsal bones with principal axes intersecting the centroid each. Calcaneus (green), cuboid (yellow), navicular (blue), talus (red). Each red principal axis is related to the biggest, each blue axis to the smallest second moment of inertia.

Influence of segmentation on two methods of MR kinematic analyses

Method I: The principal axes coordinate systems approach

Rotations of the principal axes coordinate system of each tarsal bone in different excursions have been used to investigate tarsal bone kinematics measured by MR imaging (Ringleb et al., 2005; Udupa et al., 1998). If the principal axes system attached to the centroid of each tarsal bone is independent of repeated segmentations, the matrix multiplication of the inverse of a reference principal axes system T_{ref} with any principal axes system T_{jk} of the operator j and his k^{th} repeated segmentation has to be a unit matrix E :

$$\text{inv}(T_{ref}) \times T_{jk} = E \quad (\text{eq. 3-1})$$

Therefore, the finite helical axis rotation β between a reference and the principal axes system out of another segmentation has to be zero. If equation 3-1 is not fulfilled the described matrix multiplication of the investigated principal axes systems provides the finite helical axis rotation β which aligns the two systems. Thus, the value of β can be used to determine the influence of repeated segmentations on the accuracy of the principal axes approach.

For each operator the k^{th} principal axes system linked with the median volume out of all repeated segmentations was selected as the reference. Therewith, the intraoperator influence of repeated segmentations on the accuracy was evaluated. To determine the interoperator influence, the bones which were repeatedly segmented by two operators were accordingly pooled. Again, the median volume was determined and its embedded principal axes system was chosen as the reference.

Method II: The registration of surface point clouds

A further approach to evaluate tarsal bone kinematics measured by MR imaging is based on the surface point cloud of each bone and each excursion. Rotations and translations are derived from the registration of the point clouds out of two points in time and excursions, respectively, provided by an iterative closest point algorithm ICP (Besl and McKay, 1992). Briefly, the description of the ICP can be summarised as follows: First, the matching points on a surface of an excursion and of a reference are computed based on the minimum distance; second, the corresponding points are registered by a least square singular value decomposition; third, the resulting transformation is applied to the reference point cloud. This iteration is terminated when the change of the mean square error of the distances between the reference point cloud and the point cloud of the excursion falls below a defined threshold.

Again, for operator j the surface point cloud linked with the median volume out of all segmentations was selected as the reference to determine the intraoperator influence of repeated segmentations on the accuracy of this method. To determine the interoperator

influence, the corresponding bones out of all segmentations and operators were pooled, the median volume was calculated and its corresponding surface point cloud was chosen as the reference. Therefore, the same segmentations were chosen to evaluate intra- and inter-operator reproducibility effects on the accuracy of method I and II.

3.1.3 Results

The mean volumes of each tarsal bone of the repeated segmentations are presented in Tab. 3-1 for each operator and for each of the five subjects. Interestingly, bigger shoe size did not come along with bigger bones since subject 3 with EUR 43 exhibited bigger bones than subject 4 with EUR 46. The volume related reproducibilities in terms of an interclass correlation coefficient (ICC) was at least 0.998 or better whereas the worst confidence interval limit (CI 95%) was determined for the cuboid (operator A, 0.994).

Tab. 3-1 Mean volumes \pm standard deviation (SD) [cm³] of all subjects of shoe size EUR 36 to 49. Related to these volumes, the intraoperator reproducibility in terms of an interclass correlation coefficient ICC_{2,1} with the lower 95% confidence interval limit (CI 95%) as well as the interoperator reproducibility ICC_{3,1} are given for the corresponding operators (op), too.

| bone | op | subject 1 | subject 2 | subject 3 | subject 4 | subject 5 | intraoperator | interoperator |
|-----------|----|--------------------------------|--------------------------------|--------------------------------|--------------------------------|--------------------------------|-----------------------------|-----------------------------|
| | | (EUR 36) | (EUR 38) | (EUR 43) | (EUR 46) | (EUR 49) | reproducibility | reproducibility |
| | | <i>mean \pmSD</i> | <i>mean \pmSD</i> | <i>mean \pmSD</i> | <i>mean \pmSD</i> | <i>mean \pmSD</i> | ICC _{2,1} (CI 95%) | ICC _{3,1} (CI 95%) |
| calcaneus | A | 47.1 \pm 0.6 | 62.0 \pm 0.6 | 88.5 \pm 0.3 | 87.3 \pm 0.1 | 96.9 \pm 1.0 | 0.999 (0.998) | 0.999 (0.998) |
| | B | 46.8 \pm 0.1 | 62.0 \pm 0.3 | 87.8 \pm 0.3 | 86.6 \pm 0.2 | 96.7 \pm 0.1 | 0.999 (0.999) | |
| cuboid | A | 8.5 \pm 0.2 | 10.9 \pm 0.1 | 15.9 \pm 0.2 | 12.3 \pm 0.1 | 18.8 \pm 0.3 | 0.998 (0.994) | 0.999 (0.996) |
| | B | 8.6 \pm 0.0 | 10.9 \pm 0.1 | 15.7 \pm 0.1 | 12.2 \pm 0.0 | 18.7 \pm 0.1 | 0.999 (0.999) | |
| navicular | C | 7.3 \pm 0.1 | 8.4 \pm 0.0 | 15.0 \pm 0.2 | 11.5 \pm 0.1 | 18.7 \pm 0.0 | 0.999 (0.999) | 0.999 (0.999) |
| | D | 7.3 \pm 0.1 | 8.5 \pm 0.1 | 15.1 \pm 0.1 | 11.4 \pm 0.1 | 18.7 \pm 0.1 | 0.999 (0.999) | |
| talus | C | 23.9 \pm 0.0 | 31.3 \pm 0.1 | 52.1 \pm 0.2 | 41.3 \pm 0.1 | 50.4 \pm 0.2 | 0.999 (0.999) | 0.999 (0.998) |
| | D | 24.1 \pm 0.1 | 31.4 \pm 0.2 | 52.1 \pm 0.2 | 41.2 \pm 0.1 | 50.6 \pm 0.2 | 0.999 (0.999) | |

In the same manner, the mean second moments of volume of repeated segmentations and the related ICC, respectively, were shown in the following tables: In Tab. 3-2 the moments about the most anterior-posterior principal axis are listed, in Tab. 3-3 the moments about the most medial-lateral axis, and in Tab. 3-4 the moments about the most superior-inferior axis. Again, all related ICCs were at least 0.998 and those of the cuboid were the worst. Tab. 3-5 shows the intra- and Tab. 3-6 the interoperator reproducibility related to the orientation of the first two principal axes with respect to the MR coordinate system. In general, these ICCs were at least 0.997. Only the orientation of principal axes of the cuboid was less reproducible whereas the worst ICC (0.967) was found for the angle of the first axis with respect to the y-axis of the MR coordinate system.

Tab. 3-2 Mean 2nd moments of volume normalised by density \pm their standard deviation (SD) [cm⁵] about the most anterior-posterior principal axis of the bones out of five segmentations each. Related to these moments, the intraoperator reproducibility in terms of an interclass correlation coefficient ICC_{2,1} with the lower 95% confidence interval limit (CI 95%) as well as the interoperator reproducibility ICC_{3,1} are given for the corresponding operators (op), too.

| bone | op | subject 1 (EUR 36) | subject 2 (EUR 38) | subject 3 (EUR 43) | subject 4 (EUR 46) | subject 5 (EUR 49) | intraoperator reproducibility | interoperator reproducibility |
|-----------|----|--------------------------------|--------------------------------|--------------------------------|--------------------------------|--------------------------------|----------------------------------|----------------------------------|
| | | <i>mean \pmSD</i> | <i>mean \pmSD</i> | <i>mean \pmSD</i> | <i>mean \pmSD</i> | <i>mean \pmSD</i> | <i>ICC_{2,1}(CI 95%)</i> | <i>ICC_{3,1}(CI 95%)</i> |
| calcaneus | A | 69.0 \pm 0.4 | 111.2 \pm 1.1 | 196.5 \pm 0.6 | 190.7 \pm 0.4 | 222.5 \pm 4.4 | 0.999 (0.997) | 0.999 (0.997) |
| | B | 69.1 \pm 0.7 | 110.3 \pm 0.7 | 196.7 \pm 1.7 | 188.6 \pm 0.2 | 219.4 \pm 0.8 | 0.999 (0.999) | |
| cuboid | A | 7.1 \pm 0.2 | 10.1 \pm 0.1 | 18.7 \pm 0.3 | 12.3 \pm 0.1 | 26.1 \pm 0.7 | 0.998 (0.994) | 0.998 (0.995) |
| | B | 7.0 \pm 0.0 | 10.2 \pm 0.1 | 18.4 \pm 0.2 | 12.2 \pm 0.0 | 25.4 \pm 0.2 | 0.999 (0.999) | |
| navicular | C | 7.1 \pm 0.1 | 10.5 \pm 0.1 | 26.2 \pm 0.4 | 16.5 \pm 0.1 | 34.5 \pm 0.4 | 0.999 (0.999) | 0.999 (0.998) |
| | D | 7.2 \pm 0.2 | 10.5 \pm 0.0 | 26.6 \pm 0.3 | 16.2 \pm 0.2 | 34.8 \pm 0.2 | 0.999 (0.999) | |
| talus | C | 26.1 \pm 0.1 | 39.0 \pm 0.3 | 92.0 \pm 0.7 | 62.4 \pm 0.3 | 86.7 \pm 0.6 | 0.999 (0.999) | 0.999 (0.999) |
| | D | 26.3 \pm 0.3 | 39.0 \pm 0.3 | 91.8 \pm 0.6 | 62.6 \pm 0.3 | 87.1 \pm 0.5 | 0.999 (0.999) | |

Tab. 3-3 Mean 2nd moments of volume normalised by density \pm their standard deviation (SD) [cm⁵] about the most medial-lateral axis of the bones out of five segmentations each. Related to these moments, the intraoperator reproducibility in terms of an interclass correlation coefficient ICC_{2,1} with the lower 95% confidence interval limit (CI 95%) as well as the interoperator reproducibility ICC_{3,1} are given for the corresponding operators (op), too.

| bone | op | subject 1 (EUR 36) | subject 2 (EUR 38) | subject 3 (EUR 43) | subject 4 (EUR 46) | subject 5 (EUR 49) | intraoperator reproducibility | interoperator reproducibility |
|-----------|----|--------------------------------|--------------------------------|--------------------------------|--------------------------------|--------------------------------|----------------------------------|----------------------------------|
| | | <i>mean \pmSD</i> | <i>mean \pmSD</i> | <i>mean \pmSD</i> | <i>mean \pmSD</i> | <i>mean \pmSD</i> | <i>ICC_{2,1}(CI 95%)</i> | <i>ICC_{3,1}(CI 95%)</i> |
| calcaneus | A | 196.1 \pm 1.1 | 288.1 \pm 2.2 | 543.6 \pm 2.3 | 498.6 \pm 0.7 | 717.5 \pm 14 | 0.999 (0.998) | 0.999 (0.998) |
| | B | 196.3 \pm 2.1 | 286.4 \pm 1.9 | 545.1 \pm 4.4 | 490.9 \pm 2.3 | 707.4 \pm 1.4 | 0.999 (0.999) | |
| cuboid | A | 7.8 \pm 0.2 | 11.0 \pm 0.0 | 21.2 \pm 0.3 | 12.5 \pm 0.1 | 26.5 \pm 0.6 | 0.999 (0.999) | 0.998 (0.994) |
| | B | 7.6 \pm 0.0 | 11.0 \pm 0.1 | 20.9 \pm 0.3 | 12.3 \pm 0.3 | 26.0 \pm 0.2 | 0.999 (0.999) | |
| navicular | C | 3.1 \pm 0.0 | 4.6 \pm 0.0 | 10.2 \pm 0.2 | 7.1 \pm 0.0 | 14.6 \pm 0.1 | 0.999 (0.999) | 0.999 (0.999) |
| | D | 3.1 \pm 0.1 | 4.6 \pm 0.0 | 10.4 \pm 0.1 | 7.0 \pm 0.1 | 14.7 \pm 0.1 | 0.999 (0.999) | |
| talus | C | 45.9 \pm 1.1 | 73.7 \pm 0.3 | 166.2 \pm 0.6 | 111.4 \pm 0.4 | 154.6 \pm 1.0 | 0.999 (0.999) | 0.999 (0.998) |
| | D | 46.3 \pm 0.3 | 74.6 \pm 0.5 | 166.9 \pm 1.0 | 112.1 \pm 0.2 | 156.3 \pm 0.8 | 0.999 (0.999) | |

Tab. 3-4 Mean 2nd moments of volume normalised by density [cm⁵] about the most inferior-superior axis.

| bone | op | subject 1 (EUR 36) | subject 2 (EUR 38) | subject 3 (EUR 43) | subject 4 (EUR 46) | subject 5 (EUR 49) | intraoperator reproducibility | interoperator reproducibility |
|-----------|----|-----------------------|-----------------------|-----------------------|-----------------------|-----------------------|----------------------------------|----------------------------------|
| | | <i>mean ±SD</i> | <i>mean ±SD</i> | <i>mean ±SD</i> | <i>mean ±SD</i> | <i>mean ±SD</i> | <i>ICC_{2,1}(CI 95%)</i> | <i>ICC_{3,1}(CI 95%)</i> |
| calcaneus | A | 178.4 ±1.1 | 261.9 ±2.1 | 493.7 ±2.0 | 453.6 ±0.6 | 651.4 ±11 | 0.999 (0.998) | 0.999 (0.998) |
| | B | 178.3 ±2.0 | 260.7 ±2.0 | 495.2 ±4.0 | 446.0 ±2.2 | 643.0 ±1.4 | 0.999 (0.999) | |
| cuboid | A | 4.7 ±0.1 | 7.0 ±0.1 | 13.4 ±0.3 | 8.6 ±0.1 | 17.8 ±0.5 | 0.998 (0.992) | 0.998 (0.994) |
| | B | 4.7 ±0.0 | 7.0 ±0.1 | 13.1±0.2 | 8.6 ±0.0 | 17.3 ±0.2 | 0.998 (0.998) | |
| navicular | C | 6.4 ±0.1 | 8.3 ±0.1 | 23.1 ±0.6 | 13.6 ±0.1 | 32.1 ±0.4 | 0.999 (0.997) | 0.999 (0.997) |
| | D | 6.4 ±0.2 | 8.3 ±0.1 | 23.6 ±0.2 | 13.4 ±0.2 | 32.4 ±0.2 | 0.999 (0.999) | |
| talus | C | 53.0 ±0.1 | 85.0 ±0.4 | 185.9 ±1.0 | 125.4 ±0.4 | 172.9 ±1.1 | 0.999 (0.999) | 0.999 (0.999) |
| | D | 53.4 ±0.4 | 85.8 ±0.6 | 181.4 ±5.4 | 125.7 ±0.2 | 174.2 ±0.7 | 0.999 (0.999) | |

Tab. 3-5 Intraoperator reproducibilities related to the orientation of the first two principal axes. The intraclass correlation coefficient $ICC_{2,1}$ and the lower 95% confidence interval limit (CI 95%) are given for the angles between each axis and the axes of the MR coordinate system (angle_MRx, angle_MRy, angle_MRz).

| bone | op | first axis | | | second axis | | |
|-----------|----|----------------------------------|----------------------------------|----------------------------------|----------------------------------|----------------------------------|----------------------------------|
| | | angle_MRx | angle_MRy | angle_MRz | angle_Wx | angle_Wy | angle_Wz |
| | | <i>ICC_{2,1}(CI 95%)</i> | <i>ICC_{2,1}(CI 95%)</i> | <i>ICC_{2,1}(CI 95%)</i> | <i>ICC_{2,1}(CI 95%)</i> | <i>ICC_{2,1}(CI 95%)</i> | <i>ICC_{2,1}(CI 95%)</i> |
| calcaneus | A | 0.999 (0.999) | 0.999 (0.994) | 0.999 (0.999) | 0.999 (0.999) | 0.999 (0.995) | 0.999 (0.999) |
| | B | 0.999 (0.999) | 0.999 (0.999) | 0.999 (0.999) | 0.999 (0.999) | 0.999 (0.999) | 0.999 (0.999) |
| cuboid | A | 0.998 (0.994) | 0.978 (0.919) | 0.978 (0.911) | 0.999 (0.999) | 0.999 (0.998) | 0.982 (0.934) |
| | B | 0.999 (0.999) | 0.978 (0.958) | 0.978 (0.966) | 0.999 (0.999) | 0.999 (0.999) | 0.982 (0.963) |
| navicular | C | 0.999 (0.999) | 0.999 (0.999) | 0.999 (0.999) | 0.999 (0.999) | 0.999 (0.999) | 0.999 (0.999) |
| | D | 0.999 (0.999) | 0.999 (0.999) | 0.999 (0.999) | 0.999 (0.999) | 0.999 (0.999) | 0.999 (0.999) |
| talus | C | 0.999 (0.999) | 0.999 (0.999) | 0.999 (0.997) | 0.999 (0.999) | 0.999 (0.986) | 0.999 (0.999) |
| | D | 0.999 (0.998) | 0.999 (0.999) | 0.999 (0.999) | 0.999 (0.999) | 0.999 (0.997) | 0.999 (0.999) |

Tab. 3-6 Interoperator reproducibilities related to the orientation of the first two principal axes.

| bone | op | first axis | | | second axis | | |
|-----------|-----|----------------------------------|----------------------------------|----------------------------------|----------------------------------|----------------------------------|----------------------------------|
| | | angle_Wx | angle_Wy | angle_Wz | angle_Wx | angle_Wy | angle_Wz |
| | | <i>ICC_{3,1}(CI 95%)</i> | <i>ICC_{3,1}(CI 95%)</i> | <i>ICC_{3,1}(CI 95%)</i> | <i>ICC_{3,1}(CI 95%)</i> | <i>ICC_{3,1}(CI 95%)</i> | <i>ICC_{3,1}(CI 95%)</i> |
| calcaneus | A&B | 0.999 (0.999) | 0.999 (0.999) | 0.999 (0.999) | 0.999 (0.999) | 0.999 (0.997) | 0.999 (0.999) |
| cuboid | A&B | 0.998 (0.994) | 0.967 (0.904) | 0.979 (0.946) | 0.999 (0.997) | 0.999 (0.998) | 0.976 (0.932) |
| navicular | C&D | 0.999 (0.999) | 0.999 (0.999) | 0.999 (0.999) | 0.999 (0.999) | 0.999 (0.999) | 0.999 (0.998) |
| talus | C&D | 0.998 (0.991) | 0.999 (0.999) | 0.999 (0.998) | 0.999 (0.999) | 0.997 (0.988) | 0.999 (0.999) |

Tab. 3-7 Mean helical axis rotation \pm standard deviation (SD) [°] to align principal axes systems out of repeated segmentations with a reference. The rotations are shown for each operator (A, B, C, D) as well as for a pool of principal axes systems provided by two operators (A&B, C&D).

| bone | op | subject 1 (EUR 36) | subject 2 (EUR 38) | subject 3 (EUR 43) | subject 4 (EUR 46) | subject 5 (EUR 49) |
|-----------|-----|--------------------------------|--------------------------------|--------------------------------|--------------------------------|--------------------------------|
| | | <i>mean \pmSD</i> | <i>mean \pmSD</i> | <i>mean \pmSD</i> | <i>mean \pmSD</i> | <i>mean \pmSD</i> |
| calcaneus | A | 0.19 \pm 0.1 | 0.47 \pm 0.3 | 0.22 \pm 0.1 | 0.27 \pm 0.1 | 0.83 \pm 1.2 |
| | B | 0.15 \pm 0.1 | 0.29 \pm 0.2 | 0.14 \pm 0.0 | 0.08 \pm 0.0 | 0.15 \pm 0.1 |
| | A&B | 0.20 \pm 0.1 | 0.54 \pm 0.3 | 0.25 \pm 0.1 | 0.21 \pm 0.1 | 0.19 \pm 0.1 |
| cuboid | A | 3.36 \pm 1.5 | 2.35 \pm 0.8 | 1.31 \pm 0.4 | 5.82 \pm 3.5 | 6.71 \pm 5.5 |
| | B | 1.01 \pm 0.9 | 0.50 \pm 0.2 | 0.50 \pm 0.2 | 2.35 \pm 1.5 | 4.59 \pm 1.6 |
| | A&B | 1.91 \pm 1.1 | 1.20 \pm 1.0 | 0.68 \pm 0.4 | 4.53 \pm 2.9 | 3.48 \pm 2.4 |
| navicular | C | 0.39 \pm 0.3 | 0.19 \pm 0.1 | 0.21 \pm 0.2 | 0.22 \pm 0.2 | 0.54 \pm 0.1 |
| | D | 0.68 \pm 0.4 | 0.41 \pm 0.3 | 0.54 \pm 0.2 | 0.32 \pm 0.1 | 0.83 \pm 0.2 |
| | C&D | 0.85 \pm 0.3 | 0.29 \pm 0.2 | 0.63 \pm 0.2 | 0.24 \pm 0.1 | 0.62 \pm 0.3 |
| talus | C | 0.30 \pm 0.1 | 0.16 \pm 0.1 | 0.25 \pm 0.1 | 0.14 \pm 0.1 | 0.32 \pm 0.3 |
| | D | 0.18 \pm 0.1 | 0.12 \pm 0.0 | 0.26 \pm 0.1 | 0.32 \pm 0.2 | 0.14 \pm 0.1 |
| | C&D | 0.20 \pm 0.1 | 0.27 \pm 0.2 | 0.41 \pm 0.2 | 0.30 \pm 0.2 | 0.25 \pm 0.1 |

Tab. 3-8 Mean helical axis rotation \pm standard deviation (SD) [°] to align surface point clouds out of repeated segmentations with a reference. The rotations are shown for each operator (A, B, C, D) as well as for a pool of surface point clouds provided by two operators (A&B, C&D).

| bone | op | subject 1 (EUR 36) | subject 2 (EUR 38) | subject 3 (EUR 43) | subject 4 (EUR 46) | subject 5 (EUR 49) |
|-----------|-----|--------------------------------|--------------------------------|--------------------------------|--------------------------------|--------------------------------|
| | | <i>mean \pmSD</i> | <i>mean \pmSD</i> | <i>mean \pmSD</i> | <i>mean \pmSD</i> | <i>mean \pmSD</i> |
| calcaneus | A | 0.02 \pm 0.0 | 0.02 \pm 0.0 | 0.02 \pm 0.0 | 0.04 \pm 0.0 | 0.02 \pm 0.0 |
| | B | 0.02 \pm 0.0 | 0.02 \pm 0.0 | 0.01 \pm 0.0 | 0.01 \pm 0.0 | 0.03 \pm 0.0 |
| | A&B | 0.03 \pm 0.0 | 0.03 \pm 0.0 | 0.04 \pm 0.0 | 0.02 \pm 0.0 | 0.03 \pm 0.0 |
| cuboid | A | 0.14 \pm 0.0 | 0.02 \pm 0.0 | 0.04 \pm 0.0 | 0.07 \pm 0.0 | 0.14 \pm 0.1 |
| | B | 0.04 \pm 0.1 | 0.02 \pm 0.0 | 0.01 \pm 0.0 | 0.02 \pm 0.0 | 0.04 \pm 0.0 |
| | A&B | 0.24 \pm 0.4 | 0.04 \pm 0.0 | 0.03 \pm 0.0 | 0.04 \pm 0.0 | 0.06 \pm 0.0 |
| navicular | C | 0.02 \pm 0.0 | 0.02 \pm 0.0 | 0.02 \pm 0.0 | 0.02 \pm 0.0 | 0.01 \pm 0.0 |
| | D | 0.09 \pm 0.1 | 0.03 \pm 0.0 | 0.03 \pm 0.0 | 0.03 \pm 0.0 | 0.01 \pm 0.0 |
| | C&D | 0.08 \pm 0.0 | 0.02 \pm 0.0 | 0.03 \pm 0.0 | 0.03 \pm 0.0 | 0.01 \pm 0.0 |
| talus | C | 0.01 \pm 0.0 | 0.02 \pm 0.0 | 0.01 \pm 0.0 | 0.01 \pm 0.0 | 0.01 \pm 0.0 |
| | D | 0.02 \pm 0.0 | 0.02 \pm 0.0 | 0.01 \pm 0.0 | 0.01 \pm 0.0 | 0.01 \pm 0.0 |
| | C&D | 0.01 \pm 0.0 | 0.03 \pm 0.0 | 0.01 \pm 0.0 | 0.02 \pm 0.0 | 0.02 \pm 0.0 |

The influence of repeated segmentations on the accuracy of the MR kinematic analyses method based on principal axes is listed in Tab. 3-7. The orientation of the cuboid based on a principal axes coordinate system was affected up to 6.7° while the orientation of other bones was only affected up to 0.8°.

Finally, Tab. 3-8 shows the influence of repeated segmentations on the accuracy of the MR kinematic analyses method based on surface point clouds. In general, no orientation was affected by more than 0.1°.

3.1.4 Discussion

Due to the increasing biomechanical use of 3D reconstructed tarsal bones the present study focused on the reproducibility of their segmentation using a commercially available software and on its consequences on kinematic analyses methods.

Reproducibility of tarsal bone morphology

The evaluation of the intra- and interoperator reproducibility was based on the segmentation of four tarsal bones (calcaneus, cuboid, navicular, talus) of five subjects performed by two operators five times each. The calculated intraclass correlation coefficients $ICC_{2,1}$ as well as $ICC_{3,1}$ related to the volume and second moments were all higher or equal to 0.998 (see Table 3-1 to 3-4). These results outline the excellent reliability of the tarsal bone morphology segmented semi-automatically with a commercially available software. Since all operators were new to image processing, the good outcome show that threshold segmentation in combination with certain freehand tools can be regarded as an appropriate approach for inexperienced operators without much influence on reliability.

Recently, Siegler and coworkers (2005) evaluated the reproducibility of the volume and geometrical moments of inertia (mm^4) related to the calcaneus and talus. In contrast to the current study, not only their segmentation with an in-house developed software (Udupa et al., 1994) was repeated, but also the whole MR procedure was performed several times. This extension of possible influences on reproducibility might explain the slightly worse ICCs of 0.942 to 0.997 reported by Siegler and coworkers (2005) compared to the ICCs of at least 0.998 shown in Tab. 3-1 to 3-4. The influence of repeated MR acquisitions in combination with the semi-automatic segmentation described in the present study will be a goal of future studies (see chapter 3.3).

Prior to the above mentioned study, another work out of their collaboration was more explicitly dedicated to the reproducibility of tarsal bone segmentation: Stindel and coworkers (2005) calculated correlation coefficients of twice repeated segmentations done with their in-house developed software (Udupa et al., 1994). These coefficients can not be directly compared to the ICC shown in the present study. However, Stindel and coworkers

(2005) reported that the worst correlation coefficient of the tarsal bone volumes is the one for the cuboid which is in agreement with the present study based on the tarsal bone volumes where the worst lower confidence interval limit (CI 95%) of the ICCs was determined for the cuboid as well.

A further request of the present study was the reliability of orientation of the bones in space evaluated by the angles between the first two principal axes and the axes of the MR coordinate system. Both the intra- and interoperator reproducibility was found to be excellent since no ICC was lower than 0.967. Once more, the repetition of the segmentation influenced mostly the cuboid: The ICCs related to the orientation of the other tarsal bones were in the range of 0.997 and higher whereas some angles calculated for the cuboid principal axes showed lowered ICCs to 0.967 (see Tab. 3-5 and 3-6). These results are again in agreement with the work of Stindel and coworkers (2005) where the principal axes orientation showed the worst correlation coefficients for the cuboid in comparison to the other tarsal bones. However, Stindel and coworkers (2005) did not report to which degree their range of correlation coefficients (0.85 to 0.99) from repeated segmentations influence MR kinematic analyses methods based on principal axes systems. However, such an estimation was done in the present study, and the results are discussed in the following subchapter.

Influence on MR kinematic analyses methods

The influence of repeated segmentations on two MR kinematic analyses methods was estimated by defining a principal axes coordinate system (method I; method II: surface point cloud) as a reference and by determining the helical axis rotation to align the reference with a coordinate system (surface point cloud) out of another segmentation. Tab. 3-7 shows that the principal axes approach used for the calcaneus, navicular, and talus was only affected by 0.1° to 0.9° . However, the repetition of the segmentation influenced this MR kinematic analyses method for the cuboid up to 6.7° (operator A, subject 5) with a mean value of 2.4° (operators A&B, all subjects). This can be explained by the nearly identical second moment of volume about the most medial-lateral and the most anterior-posterior axis (see Tab. 3-2 and 3-3) which was typical for the cuboid compared to the other tarsal bones. Thus, even small segmentation errors remarkably contribute to the computation of the principal axes and consequently, to the orientation of a coordinate system based on these axes. Note that compared to the other bones, the ICCs calculated for the orientation of the first two principal axes of the cuboid were only up to 0.021 lower (see Tab. 3-6). However, these small differences have a great effect on the precision of the MR kinematic analyses method I as mentioned before.

The influence of repeated segmentations on MR kinematic analyses with method II was considerably smaller: Related to the calcaneus, navicular and talus, this method was

affected by less than 0.1° due to repeated semi-automatic segmentations done by different operators (see Tab. 3-8). Even the orientation of the cuboid was only influenced up to 0.2° (operators A&B, subject 1) with a mean value of 0.1° (operators A&B, all subjects).

Now, these large differences between the estimated influence of repeated segmentations on the accuracy of two different MR kinematic analyses methods can be easily explained: Slight segmentation variations of the outer border of a bone will affect the moments of inertia, and therewith the principal axes, more than the general shape of the surface point cloud. This is particularly true for the cuboid with two nearly identical moments of inertia: Here, the surface point clouds in combination with an ICP algorithm was superior to the principal axes since any irregular contour warranted the use of the ICP.

3.1.5 Conclusion

In the present study the reliability of tarsal bones segmentation based on high-contrast and high-resolution MR images and the use of commercially available software AMIRA was investigated. Both intra- and interoperator reproducibility of the volume and the second moments of all tarsal bones were excellent. Related to this morphological parameters it can be stated that under the described conditions the presented tarsal bone segmentation is reliable and that even inexperienced operators are in fact interchangeable.

Furthermore, it was shown that a MR kinematic analyses method which is based on surface point clouds is considerably less influenced by repeated segmentation (cuboid: up to 0.2° , other tarsal bones up to 0.1°) compared to a method which is based on principal axes of inertia (cuboid up to 6.7° , other tarsal bones up to 0.8°). Thus, tarsal surface point clouds in combination with an ICP algorithm are recommended for investigations of tarsal bone kinematics using MR imaging.

3.1.6 Supplement: Reproducibility of articulating surfaces

The above presented study was completed with the quantification of the differences in articulating surfaces of the tarsal bones caused by repeated segmentations. This evaluation included the tarsal bones of the subject with median shoe size (EUR 43). After each bone was segmented five times by two operators (see chapter 3.1.2) those two were chosen which showed the greatest difference of bony volumes within both operators. This was assumed to be the worst case of repeated segmentation. Then, the percentage of identically segmented border voxels being part of the articulating surface was determined for every tarsal bone.

Differences of segmented voxels in the assumed worst case of repetition were visualised with 3D reconstructed volumes in Fig. 3-3. The higher the difference between segmented voxels the darker the part of the surface. It became apparent that bony parts where

ligaments and tendons are attached to the bone show the highest differences in segmentation.

Overall, 98.8% and 99.7% of all articulating surface voxels of calcaneus and talus, respectively, were identically segmented. Further, 98.9% and 98.3% of the posterior articulating surface voxels of navicular and cuboid, respectively, were identically segmented, too. It is concluded that the semi-automatic segmentation does not influence the processing of articulating surfaces of the tarsal bones such as the computation of the tarsal joint curvatures.

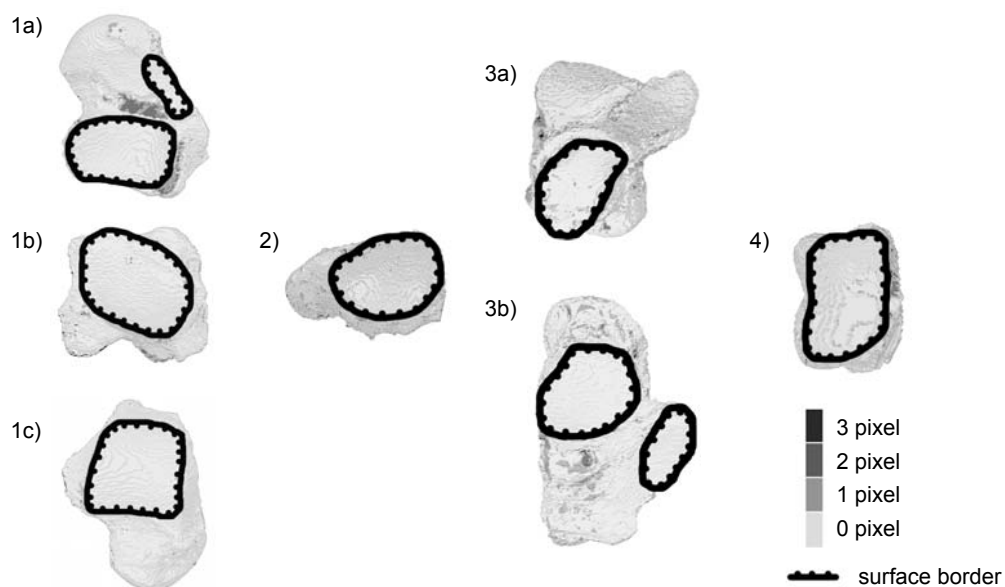


Fig. 3-3 Comparison of two 3D reconstructed tarsal bones (worst case segmentation). Talus seen from (1a) inferior view, (1b) anterior view, and (1c) superior view. Navicular seen from (2) posterior view. Calcaneus seen from (3a) anterior and (3b) superior view. Cuboid seen from (4) posterior view. Differences in segmented voxels are given by grey scale. Articulating surface borders are emphasised.

3.2 Contribution of MR slice orientation on morphology and on methods enabling MR kinematic analyses of tarsal bones

3.2.1 Introduction

Magnet resonance (MR) imaging is increasingly important in the present research of foot biomechanics. It facilitates the precise three-dimensional reconstruction of bones and thus, provides the morphological basis of finite element models of the foot (e.g. Bandak et al., 2001; Camacho et al., 2002; Cheung et al., 2005). Furthermore, morphological parameters, e.g. the centroid and principal axes, even make it possible to analyse bone kinematics with MR imaging (Ringleb et al., 2005; Udupa et al., 1998). In contrast to common stereophotogrammetry, MR imaging in combination with recently developed MR compatible foot positioning and loading devices enables insights into tarsal bone kinematics (Mattingly et al., 2006; Siegler et al., 2005). Thereby, MR imaging is superior to any other image based procedures because it is non-invasive and without harmful radiation (Siegler et al., 2005; Udupa et al., 1998).

The accuracy of bone reconstruction is influenced by the usually anisotropic spatial resolution during MR imaging whereby the slice thickness is substantially larger than the in-plane resolution. Considering the irregular shape of the tarsal bones and a finite spatial resolution, these volume effects vary due to different MR slice orientations. In spite of the broad applications of tarsal bone morphology derived from MR imaging no study has addressed to this circumstance. Therefore, it remains unclear to which degree the tarsal bone morphology is influenced by different slice orientations under a given imaging resolution.

The MR slice orientation will hardly affect comparisons of tarsal bone morphology of different subjects as long as the slice orientation relative to the bones of each subject is kept constant. However, when MR procedures are used to investigate kinematics, the MR slice orientation relative to the bones will change in each excursion (the general MR slice orientation is kept constant). Therefore, partial volume effects vary and as a consequence, morphological parameters change, too. Because the morphology builds the basis for MR kinematic analyses methods the accuracy thereof is mainly affected by the relative change of slice orientations. However, it is currently not known to which degree the accuracy is influenced.

Thus, the purpose of this study was to determine the influence of MR slice orientation on volume, surface, and second moments of volume of the tarsal bones, and on two methods enabling MR kinematic analyses of these bones.

3.2.2 Method

Data acquisition

One volunteer without signs of musculoskeletal diseases participated in this study (28 years, 70 kg, 1.80 m, shoe size EUR 46). Informed written consent in accordance to the local research ethics committee was obtained. Imaging was performed on a 3 Tesla whole-body MR unit (Intera 3T, Philips Medical Systems). The right lower leg and rearfoot were placed on a 12 element synergy spine coil (Philips Medical Systems) in neutral position and fixed with sandbags. A 3D T1 weighted gradient echo sequence with following parameters was used: TR/TE = 16 ms / 4 ms, FA 11°, 200 mm FOV, 288 x 275 acquisition matrix, Fourier interpolated to 512 x 512 pixels, and 1.4 mm thick overcontinuous slices with 50% slice overlapping resulting in a reconstructed spatial resolution of 0.39 x 0.39 x 0.70 mm³. Contrast-to-noise ratios of bone to cartilage, fatty tissues, and muscles, respectively, were considerably higher than 20 outlining the high-contrast quality of the images (see Fig. 3-4). In order to investigate the influence of MR slice orientation on tarsal bone morphology four different orientations were chosen: sagittal (100 slices), transversal (140 slices), transversal rotated about 45° at coronal axis (orientation A, 120 slices), and transversal rotated about -45° at coronal axis (orientation B, 150 slices), see Fig. 3-5. Each scan of the acquisition took 7 to 10 minutes.

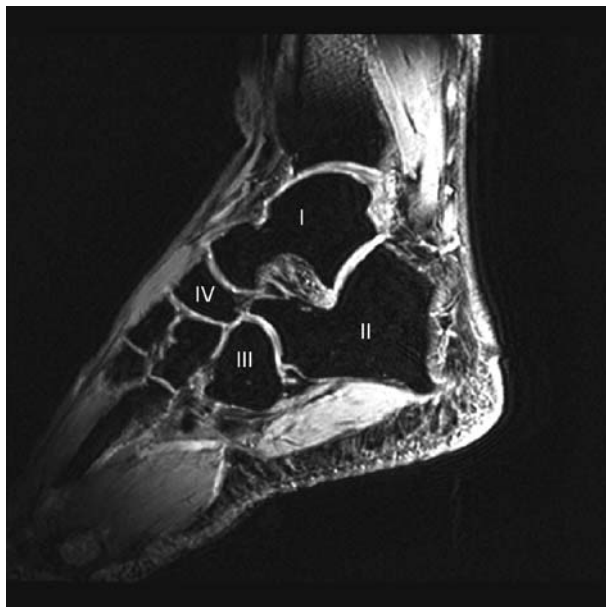


Fig. 3-4 Sagittal MR image of tarsal bones: (I) talus, (II) calcaneus, (III) cuboid, (IV) navicular.

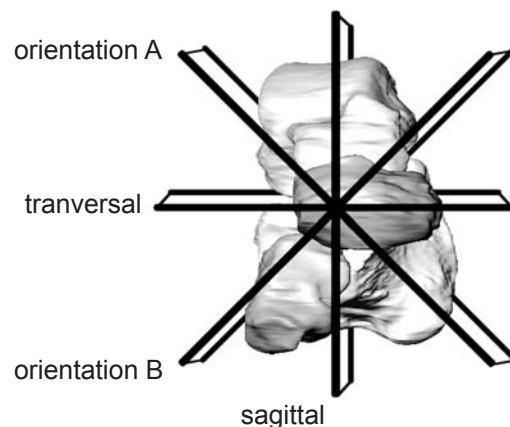


Fig. 3-5 Anterior view of tarsal bones. The bones were reconstructed out of four different slice orientations: orientation A, B, sagittal, and transversal.

Data processing

The segmentation and the 3D reconstruction of the tarsal bones were performed with AMIRA (Mercury Computer Systems, Berlin) by two operators. Tarsal bones were semi-automatically segmented five times for each orientation with one exception: The cuboid was only reconstructed for the sagittal slices and slice orientation B since the other orientations did not contain the whole cuboid. After smoothing by subvoxel-weights, tarsal volumes and surface areas were read out. And like for all calculated morphological parameters, one-way ANOVAs were performed to determine the influence of MR slice orientation.

In a previous study (see chapter 3.1), intraclass correlation coefficients ($ICC_{2,1}$) (Eliasziw et al., 1994; Shrout and Fleiss, 1979) of tarsal bone morphology out of repeated segmentations were found to be higher than 0.98 warranting the interoperator reproducibility of the image processing. Furthermore, it had been verified in another pilot study that tarsal bone morphologies are more likely to be influenced by different slice orientations than by completely repeated MR measurements: For instance, the results related to the tarsal volume (tarsal second moment about medial-lateral axis) showed for the slice orientation as source of variation a p-value of 0.002 (0.001) whereas repeated MR measurement as source of variation showed a p-value of 0.418 (0.949).

The surface points were read in MatLab (MathWorks, Massachusetts). Cubes with same density (1 g/cm^3) and side length (0.7 mm) were placed inside the surface point cloud. Therewith, second moments of volume and resulting principal axes were calculated whereas border cubes were weighted by factor 0.5. The second moments of volume were normalised by the arbitrary defined density of 1 g/cm^3 . This user written routine was checked with ellipsoids similar to the talar bones: The numerical error of the second moments of inertia was found to be less than 1% and of the axes orientation was less than 0.005° .

Influence on two methods of MR kinematic analyses

Methods of MR kinematic analyses are based on morphological parameters which are likely to be affected by slice orientation on their part considering an anisotropy finite spatial resolution. Therefore, the following approach was chosen to estimate this influence on such kinematic analyses methods: The tarsal bones were held in their position and the general MR slice orientation was changed. Thereby, a defined change of the MR slice orientation from A to transversal, for instance, was equal to a tarsal excursion of 45° about an anterior-posterior foot axis (see Fig. 3-5). Thus, keeping the tarsal bones in place and changing the MR slice orientation reflected not only large excursions of the tarsal bones but also large changes in the slice orientation relative to the bones. Consequentially, partial volume

effects vary resulting in differences within the morphology and thus, affecting the MR kinematic analyses methods. Two kinematic methods and the estimation of the influence of different slice orientation on them are described in the following subchapters.

Method I: The principal axes coordinate systems approach

Rotations of the principal axes coordinate system of each tarsal bone in different excursions have been used to investigate tarsal bone kinematics measured by MR imaging (Udupa et al., 1998; Ringleb et al., 2005). If the principal axes system attached to the centroid for each tarsal bone is independent of the slice orientation, the matrix multiplication of the inverse of a reference principal axes system T_{ref} with any principal axes system out of the i^{th} slice orientation and k^{th} repeated segmentation T_{ik} has to be a unit matrix E :

$$\text{inv}(T_{ref}) \times T_{ik} = E \quad (\text{eq. 3-2})$$

Therefore, the finite helical axis rotation β between a reference and the principal axes system out of another slice orientation has to be zero. If the equation 3-2 is not fulfilled the described matrix multiplication of the investigated principal axes systems provides the finite helical axis rotation β which aligns the two systems. Thus, the value of β can be used to investigate the influence of slice orientation on principal axes systems and to estimate the accuracy of this kinematic analyses method.

Out of the four segmented slice orientations the transversal orientation (140 slices) was chosen as the reference because in this orientation most slices can be expected to cut the tarsal bone surface almost perpendicular which does best avoid partial volume effects. Due to the above mentioned circumstance that the cuboid was not completely available in the transversal orientation, sagittal slices were chosen as reference orientation for this bone.

Out of the reference orientation each median volume was selected out of the five repeated segmentations.

MR kinematic analyses method II: The registration of surface point clouds

The second approach to evaluate tarsal bone kinematics measured by MR imaging is based on the surface point cloud of each bone and each excursion. Rotations and translations are derived from the registration of the point clouds of two excursions by an iterative closest point algorithm ICP (Besl and McKay, 1992). In brief, related to all surface points of a reference the matching points on a surface of an excursion of the same bone are computed based on the minimum distance at first; thereafter, the corresponding points are registered by a least square singular value decomposition; finally, the resulting transformation is applied to the reference point cloud. This iteration is terminated when the change of the mean square error of the distances between the reference point cloud and the point cloud of the excursion falls below a defined threshold.

Once more, out of the overall registration of each bone and each excursion the finite helical axis rotation β was computed to estimate the accuracy of the proposed kinematic analyses method.

Again, in the current approach the transversal slices (calcaneus, navicular, talus) and sagittal (cuboid) slices, respectively, were chosen as reference orientation with the same repetition of segmentation as used for method I. Note, that method I is 600 times faster than method II (for instance: calcaneus, computation of one excursions took 1 min vs. 10 h).

3.2.3 Results

Tab. 3-9 to 3-11 show the mean and the standard deviation (SD) of the calculated morphological parameters over the repeated segmentations of the four different MR slice orientations. Tarsal bone volumes and surface areas are significantly influenced by the slice orientation as well as the second moments of volume about all axis ($p < 0.05$): Tarsal volumes were influenced up to 3.5%, tarsal surface areas up to 3.2%, and tarsal second moments up to 8.5%. Overall, bigger bones were less affected than smaller bones.

Tab. 3-12 and 3-13 show the finite helical axis rotation β to fit the principal axes systems and the surface point clouds, respectively. Corresponding finite helical axis rotations were found to be half for the latter approach ($0.2\text{-}2.6^\circ$) compared to the former one ($0.5\text{-}9.0^\circ$).

Tab. 3-9 Mean volumes and SD [cm^3] of tarsal bones which were five times reconstructed out of each MR slice orientation A, B, sagittal, and transversal. The influence of the slice orientation is reflected by the p-value out of an one-way ANOVA and by the difference [%] between the maximal and minimal volume.

| orientation | | calcaneus | cuboid* | navicular | talus |
|-------------|------|-----------|---------|-----------|--------|
| A | mean | 85.7 | | 11.6 | 41.7 |
| | SD | 0.1 | | 0.1 | 0.3 |
| B | mean | 84.6 | 12.4 | 11.2 | 40.8 |
| | SD | 0.2 | 0.1 | 0.0 | 0.1 |
| sag | mean | 86.2 | 12.1 | 11.6 | 41.4 |
| | SD | 0.2 | 0.0 | 0.1 | 0.1 |
| trans | mean | 85.2 | | 11.3 | 41.2 |
| | SD | 0.3 | | 0.1 | 0.2 |
| p | | <0.001 | 0.003 | <0.001 | <0.001 |
| max-min [%] | | 1.9 | 2.5 | 3.5 | 2.2 |

*) Only slice orientations were considered containing the whole bone.

Tab. 3-10 Mean surface areas and SD [cm^2] of tarsal bones which were five times reconstructed out of each MR slice orientation A, B, sagittal, and transversal. The influence of the slice orientation is reflected by the p-value out of an one-way ANOVA.

| orientation | | calcaneus | cuboid* | navicular | talus |
|-------------|------|-----------|---------|-----------|--------|
| A | mean | 123.8 | | 31.8 | 75.7 |
| | SD | 0.3 | | 0.2 | 0.3 |
| B | mean | 123.5 | 30.5 | 31.1 | 75.0 |
| | SD | 0.2 | 0.2 | 0.2 | 0.1 |
| sag | mean | 124.4 | 30.2 | 32.1 | 75.0 |
| | SD | 0.1 | 0.1 | 0.2 | 0.1 |
| trans | mean | 123.7 | | 31.4 | 75.2 |
| | SD | 0.5 | | 0.2 | 0.1 |
| p | | <0.001 | 0.019 | <0.001 | <0.001 |
| max-min [%] | | 0.6 | 1.0 | 3.2 | 0.9 |

*) Only slice orientations were considered containing the whole bone.

Tab. 3-11a Mean 2nd moments of volume and SD normalised by density [cm⁵] of the calcaneus reconstructed out of MR slice orientation A, B, sagittal, and transversal. The influence of the slice orientation is reflected by the p-value out of an one-way ANOVA.

| orientation | | medial-lateral | anterior-posterior | superior-inferior |
|-------------|-------------|----------------|--------------------|-------------------|
| A | <i>mean</i> | 498.1 | 187.5 | 453.4 |
| | <i>SD</i> | 1.1 | 0.2 | 1.3 |
| B | <i>mean</i> | 485.8 | 183.6 | 442.3 |
| | <i>SD</i> | 1.0 | 0.3 | 1.3 |
| sagittal | <i>mean</i> | 492.3 | 188.8 | 447.5 |
| | <i>SD</i> | 1.7 | 0.7 | 1.7 |
| transversal | <i>mean</i> | 490.0 | 184.1 | 446.9 |
| | <i>SD</i> | 5.3 | 1.9 | 4.9 |
| p | | <0.001 | <0.001 | <0.001 |
| max-min [%] | | 2.5 | 2.6 | 2.5 |

Tab. 3-11c Mean 2nd moments of volume and SD of the navicular [cm⁵].

| orientation | | medial-lateral | anterior-posterior | superior-inferior |
|-------------|-------------|----------------|--------------------|-------------------|
| A | <i>mean</i> | 7.5 | 16.5 | 13.7 |
| | <i>SD</i> | 0.1 | 0.2 | 0.1 |
| B | <i>mean</i> | 7.1 | 15.5 | 12.9 |
| | <i>SD</i> | 0.1 | 0.1 | 0.0 |
| sagittal | <i>mean</i> | 7.4 | 16.9 | 14.0 |
| | <i>SD</i> | 0.1 | 0.3 | 0.3 |
| transversal | <i>mean</i> | 7.2 | 15.9 | 13.2 |
| | <i>SD</i> | 0.1 | 0.2 | 0.2 |
| p | | <0.001 | <0.001 | <0.001 |
| max-min [%] | | 5.6 | 6.4 | 8.5 |

Tab. 3-12 Mean finite helical axis rotation β and SD [°] to align principal axes systems of tarsal bones which were five times reconstructed out of each MR slice orientation.

| orientation | | calcaneus | cuboid* | navicular | talus |
|-------------|-------------|-----------|---------|-----------|-------|
| A | <i>mean</i> | 0.51 | | 0.90 | 0.77 |
| | <i>SD</i> | 0.08 | | 0.85 | 0.14 |
| B | <i>mean</i> | 0.97 | 9.01 | 0.50 | 0.66 |
| | <i>SD</i> | 0.13 | 1.03 | 0.26 | 0.18 |
| sag | <i>mean</i> | 2.64 | 3.88 | 3.68 | 3.70 |
| | <i>SD</i> | 0.14 | 1.93 | 0.55 | 0.07 |
| trans | <i>mean</i> | 0.43 | | 0.68 | 0.58 |
| | <i>SD</i> | 0.14 | | 0.35 | 0.42 |

*) Only slice orientations were considered containing the whole bone.

Tab. 3-11b Mean 2nd moments of volume and SD normalised by density [cm⁵] of the cuboid reconstructed out of MR slice orientation B and sagittal. The influence of the slice orientation is reflected by the p-value out of an one-way ANOVA.

| orientation* | | medial-lateral | anterior-posterior | superior-inferior |
|--------------|-------------|----------------|--------------------|-------------------|
| B | <i>mean</i> | 13.2 | 9.2 | 12.7 |
| | <i>SD</i> | 0.3 | 0.1 | 0.1 |
| sagittal | <i>mean</i> | 12.5 | 8.7 | 12.4 |
| | <i>SD</i> | 0.0 | 0.0 | 0.1 |
| p | | 0.006 | <0.001 | 0.046 |
| max-min [%] | | 5.6 | 5.8 | 2.4 |

Tab. 3-11d Mean 2nd moments of volume and SD of the talus [cm⁵].

| orientation | | medial-lateral | anterior-posterior | superior-inferior |
|-------------|-------------|----------------|--------------------|-------------------|
| A | <i>mean</i> | 113.8 | 64.7 | 128.0 |
| | <i>SD</i> | 1.0 | 0.7 | 1.1 |
| B | <i>mean</i> | 111.2 | 62.2 | 125.5 |
| | <i>SD</i> | 0.3 | 0.2 | 0.3 |
| sagittal | <i>mean</i> | 113.3 | 63.7 | 127.6 |
| | <i>SD</i> | 0.4 | 0.4 | 0.5 |
| transversal | <i>mean</i> | 112.5 | 63.4 | 126.9 |
| | <i>SD</i> | 0.5 | 0.2 | 0.5 |
| p | | <0.001 | <0.001 | <0.001 |
| max-min [%] | | 2.3 | 4.0 | 2.0 |

Tab. 3-13 Mean finite helical axis rotation β and SD [°] to fit point clouds of tarsal bones which were five times reconstructed out of each MR slice orientation.

| orientation | | calcaneus | cuboid* | navicular | talus |
|-------------|-------------|-----------|---------|-----------|-------|
| A | <i>mean</i> | 0.20 | | 0.62 | 0.16 |
| | <i>SD</i> | 0.07 | | 0.60 | 0.01 |
| B | <i>mean</i> | 0.23 | 2.56 | 0.35 | 0.35 |
| | <i>SD</i> | 0.03 | 0.06 | 0.07 | 0.10 |
| sag | <i>mean</i> | 0.84 | 0.04 | 1.81 | 0.81 |
| | <i>SD</i> | 0.04 | 0.01 | 0.03 | 0.01 |
| trans | <i>mean</i> | 0.05 | | 0.06 | 0.03 |
| | <i>SD</i> | 0.03 | | 0.02 | 0.01 |

*) Only slice orientations were considered containing the whole bone.

3.2.4 Discussion

Effects on tarsal bone morphology

The purpose of concern was to determine the influence of MR slice orientation on tarsal bone morphology. For that purpose, a pilot study under comparable conditions revealed that tarsal bone morphology is more likely to be influenced by slice orientation than by repeated MR measurements. The results (see Tab. 3-9 to 3-11) clearly demonstrate that MR slice orientation affects all computed morphological parameters ($p < 0.05$): volume (surface area, second moments of volume) were up to 3.5% (3.2%, 8.5%) different between different slice orientations. The two smaller tarsal bones, cuboid and navicular, showed always about 2% higher differences compared to the bigger bones, talus and calcaneus. Therefore, considering the same resolution, future MR studies comparing tarsal bone morphology of different subjects have to consider that differences in morphological parameters up to 8% are likely to be introduced by different slice orientations. This can be reduced with a better spatial resolution or by keeping the MR slice orientation relative to the tarsal bones constant.

Comparable studies on tarsal bones are not available in the relevant literature.

Effects on MR kinematic analyses methods

In general, physiological movements of the tarsal bones can be expected to be of the order of up to 20° (van Langelaan, 1983). But in the present study, rotations of 45° and 90° are considered. Thus, smaller changes of MR slice orientation relative to the tarsal bones will occur when physiological tarsal bone kinematics are investigated with a constant MR slice orientation. Therefore, morphological parameters may be considerably less affected by the relative MR slice orientation. Consequently, the presented accuracies of the two methods enabling MR kinematic analyses are at the upper limit.

The principal axes coordinate systems approach

The first method which based on principal axes coordinate systems of each bone in each excursion was found to have an accuracy of $0.5\text{-}3.7^\circ$ with the exception of the cuboid (discussed later in this subchapter). Without this exception the accuracy of the principal axes approach were in the range of common stereophotogrammetry systems usually used to investigate kinematics (Chiara et al., 2005) whereas MR imaging in combination with certain foot excursions is the only approach to investigate tarsal bone kinematics in vivo, non-invasively and without harmful radiation (Udupa et al., 1998).

The principal axes systems out of the sagittal slices had to be aligned to the corresponding transversal systems with three to five times higher finite helical axis rotations β compared to the other orientations (see Tab. 3-12). This is not unexpected because the projected dimension of the foot is largest in the sagittal plane. Therefore, 20 to 50 less slices were

needed to image the rearfoot in the sagittal plane compared to the other orientations resulting in considerably more partial volume effects. Furthermore, the sagittal and transversal slices are perpendicular to each other reflecting the biggest possible excursion of the tarsal bones relative to a constant MR slice orientation (90° , see Fig. 3-5). This will also result in variations of the outer border of the bones and thus, end in considerably different principal axes systems out of the sagittal slices. Note, if the sagittal slices are not considered due to the arguments above the accuracy depended more on repeated segmentations than on slice orientation: This is indicated by the order of the alignment within the transversal reference orientation ($0.4\text{-}0.7^\circ$) which is similar to the alignment of principal axes systems out of section orientation A and B with the reference orientation ($0.5\text{-}0.9^\circ$ and $0.5\text{-}1.0^\circ$, respectively; see Tab. 3-12).

Stindel and coworkers (2001) estimated the precision of their principal axes approach evaluating tarsal bone kinematics by MR imaging to be of the order $1\text{-}2^\circ$. In the present study, the precision of the principal axes approach to investigate tarsal bone kinematics is slightly better ($0.5\text{-}1^\circ$) if rotations of 45° about the anterior posterior axis are considered (see Table 3-12). The spatial resolution of MR images of $0.55 \times 0.55 \times 1.5 \text{ mm}^3$ processed by Stindel and coworkers (2001) is worse than the one used in the present study ($0.39 \times 0.39 \times 0.7 \text{ mm}^3$) resulting in more spatial volume effects which may explain their decreased precision.

Recently, Mattingly and coworkers (2006) used the same approach as provided by Stindel and coworkers (2001) to investigate rearfoot bone motion with MR imaging; they mentioned an precision of 0.3° . Unfortunately, the motion used by Mattingly and coworkers (2006) to evaluate their kinematic approach is neither given in the mentioned paper nor in further references using their principal axes coordinate systems to evaluate tarsal bone kinematics. Therefore, values provided by Mattingly and coworkers (2006) can not directly be compared to the present study.

The registration of surface point clouds

An iterative closest point algorithm (ICP) provides another approach to evaluate tarsal bone kinematics in different foot excursion. Under the same presented conditions, this approach is two times less affected ($0.2\text{-}1.8^\circ$, see Tab. 3-13) than the principal axes approach ($0.5\text{-}3.7^\circ$, see Tab. 3-12) (with the exception of the cuboid).

These large discrepancies between the accuracy of the two different MR kinematic analyses methods show the different influence of the MR slice orientation on each of these analyses: On the one hand slight variations of the outer border of the bone due to variations of partial volume effect will result in considerable different second moments of volume between different MR slice orientations (see Tab. 3-11). Thus, a few degrees of finite helical axes

rotation β ($0.5-3.7^\circ$) are needed to align principal axes coordinate systems between different slice orientations (see Tab. 3-12). On the other hand, however, (excepting sagittal slices and large rotations, respectively) the general shape of the bone is only effected negligibly and therefore, smaller rotations ($0.2-1.8^\circ$) fit the point clouds out of different slice orientations with the ICP (see Tab. 3-13). Note, if only translations occur in the tarsal bones, both methods should have been affected in the same manner. Although the principal axes approach is slightly less precision it provides at least a very good initial registration of surface point clouds. This reduced the used time consuming ICP by factor 1.5.

The cuboid

The cuboid was more challenging to investigate. It was not completely acquirable in transversal slices as well as in slice orientation A. Therefore, sagittal slices were chosen as reference to evaluate both kinematic approaches.

Overall, the highest finite helical axis rotations β were determined for the alignment of the principal axes of the cuboid. This was not unexpected since the second moments of volume about the most medio-lateral and the most anterior posterior axis were almost equal (see Tab. 3-11). Thus, even small segmentations errors contributed to a deviation of the orientation of a principal axes coordinate system. This is confirmed by the considerably higher finite helical axis rotations β calculated for the alignment within the reference slice orientation of the cuboid compared to the other tarsal bones (3.9° vs $0.4-0.7^\circ$, see Tab. 3-12). Thus, a remarkable error propagation affected the alignment of the principal axes of the cuboid out of different slice orientations. Hence, MR kinematic analyses based on principal axes systems are limited to bones with considerable different second moments such as the calcaneus, the navicular, and the talus; but not the cuboid.

On the other hand, the ICP algorithm is not affected by similar second moments as long as no perfect symmetry is given: Any irregular contour warranted the use of the ICP. Therefore, the registration of surface point cloud should be preferred if the kinematics of bones with nearly equal moments are of interest.

Limitations

In the present study, a very basic approach was chosen to evaluate the precision of two MR kinematic analyses methods. In contrast to Siegler and coworkers (2005) neither the tarsal bones were moved nor the MR analysis was directly compared to other kinematic evaluations. Siegler and coworkers (2005) found differences of $1-6^\circ$ between an opto-electric kinematic measuring system and a MR analysis. However, such a comparison has to be done invasively for tarsal bones. This increases the overall expenses noticeably. Furthermore, if two different kinematic measurement systems are compared with each other it is difficult to determine the origin of the error since both systems are subjected to a

certain inaccuracy. In comparison, the approach used in present study to evaluate the accuracy of MR kinematic analyses has the advantage to be less complex.

3.2.5 Conclusions

This study shows that the given MR slice orientation affected the second moments of volume of all tarsal bones up to 8%. Thus, each parameter derived from them, such as a principal axes coordinate system, is considerably influenced by the MR slice orientation. However, using principal axes systems to describe even large rotations of tarsal bones is as precise as common stereophotogrammetry ($0.5\text{-}3.7^\circ$) as long as the cuboid having similar second moments of volume is omitted. Even more precise ($0.2\text{-}1.8^\circ$) for the same rotations and suitable for all tarsal bones is an iterative closest point algorithm (ICP), by which surface point clouds are used for registration. Thus, the described MR sequence in combination with an ICP is an accurate and appropriate method to investigate tarsal bone kinematics in vivo and non-invasively.

Furthermore, it has been shown that MR slice orientation affected the tarsal bone volumes and surface areas under the described conditions up to 3.5%. Thus, to improve measurement precision for comparisons of these parameters between different subjects, it is recommended to keep the MR slice orientation identical.

3.3 A MR imaging procedure to measure tarsal bone positions in different foot excursions

3.3.1 Introduction

To date, the relationship between foot morphology and foot function is still uncertain (Cornwall and McPoil, 2004; Hunt and Smith, 2004; Razeghi and Batt, 2002) but of importance in view of an effective prevention and treatment of foot injuries (Rothstein, 1985; Scharfbillig et al., 2004).

Previous studies failed to give evidence about the mentioned relationship since conclusions were drawn from two-dimensional parameters to three-dimensional (3D) movements although both motion and morphology are 3D. Thus, both should be measured in three dimensions (Stindel et al., 1999b). Furthermore, many joints within the foot remarkably contribute to its overall motion. These joint motions are hardly detectable by skin markers which are commonly used to investigate the relationship of foot morphology and foot function. Reasons are that the talus is nearly completely covered by other bones, and that skin marker effects are to be expected (Maslen and Ackland, 1994; Tranberg and Karlsson, 1998; Westblad et al., 2002).

An alternative approach to measure 3D joint motion within the foot as well as 3D bone morphology in vivo is magnetic resonance (MR) imaging. Thereby, MR imaging is superior to any other image based procedure because it is non-invasive and without harmful radiation (Siegler et al., 2005; Udupa et al., 1998).

In the late 1990s, Stindel, Udupa, and coworkers were the first to present a MR compatible foot positioning device (Stindel et al., 1998; Udupa et al., 1998). It allowed to measure positions and morphological parameters of the tarsal bones in defined pronated and supinated foot excursions intended to classify foot types (Stindel et al., 1999ab, Stindel et al., 2001). The results were precise and promising for the distinction of normal and abnormal motion, but it had also its limitations since the test jig did not allow to bear any load. The same is true for a more recently presented positioning device of another group (Mattingly et al., 2006). However, it is evident that load does alter rearfoot joint kinematics (Fraser and Ahmend, 1983; Hintermann et al., 1994b; Michelson et al., 1990).

To our knowledge, only one MR compatible foot positioning and loading device has been reported used as a diagnostic tool for ankle ligament injuries (Ringleb et al., 2005; Siegler et al., 2005). Further adequate devices are needed to profit from MR imaging to investigate fundamental foot joint mechanics.

In the present study, a MR imaging procedure to determine positions of the tarsal bones (calcaneus, cuboid, navicular, and talus) in different foot excursions under bodyweight is

presented. Having shown the reliability and accuracy of the MR data processing (see chapter 3.1 and 3.2) the current study focused on the development of a foot positioning and loading device. Thereby, the study aimed to quantify quasi-static tarsal joint motions. Additionally, the minimum difference within these motions was estimated which enables to differentiate between subjects. Overall, the presented procedure is thought to provide a new basis to investigate the relationship between foot morphology and foot function.

3.3.2 Methods

The study was conducted on one female and two male volunteers without signs of musculoskeletal diseases aging 28, 31, and 35 years, being 166, 179, and 180 cm high, and weighing 60, 71, and 80 kg. Informed written consent in accordance to the local research ethics committee was obtained from all subjects.

Foot loading and positioning device

The developed foot loading and positioning device consisted mainly of a wooden support, a dolly linked with a double pulley, different foot blocks, a load box, and two shoulder blocks (Fig. 3-6). The cushioned shoulder blocks worked as a counter bearing ensuring that the applied load did not shift the subject cranially. This shoulder support was easily displaceable enabling investigations of subjects with a height between 1.50 and 2.00 m. The size of the developed device and of the MR scanner tube (Intera 3T, Philips Medical Systems, Best, The Netherlands) restricted the maximum foot length that could be measured to 0.31 m (see detail of Fig. 3-6 showing biggest feasible foot length).

The dolly and the double pulley were fixed on the wooden support so that tarsal bone motion of the right foot was acquirable. The dolly rolled on radial ball bearings guided by

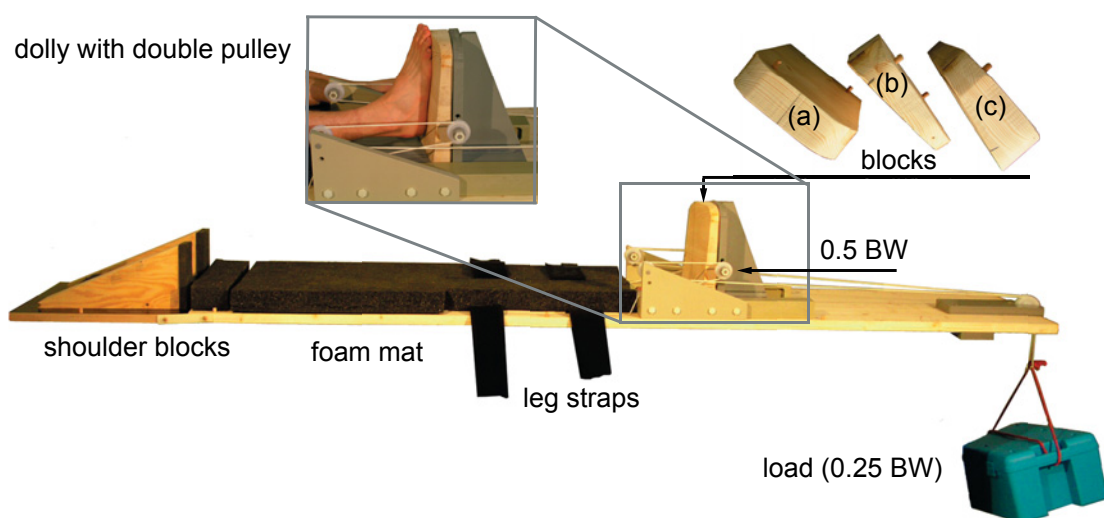


Fig. 3-6 The foot loading and positioning linkage and in detail, the dolly with a supinated foot placed on it. The foot was only fixed by the load of half bodyweight (0.5 BW) transferred by a double pulley. The used blocks are shown from above: (a) was the neutral one, (b) induced foot supination, (c) induced foot pronation.

two slots restricting the dolly to move in the forward-backward direction only. The pulleys on the dolly were symmetrically placed at malleolar height transferring load axially through the rearfoot into the straight leg. Straps above and under the knee supported the knee in full extension. A second block was fixed next to the dolly to position the contra-lateral foot to ensure a neutral pelvis position. The neutral position of the lower extremities was additionally achieved by aligning the subject's right hip with the right heel.

The blocks causing the excursion of the foot were fixed on the dolly. In this study, three blocks with different oblique fronts were used: a neutral one (Fig. 3-6 (a)), one with a front inducing supination on the rearfoot (Fig. 3-6 (b)), and one inducing pronation (Fig. 3-6 (c)). Thereby, the extent of the pronation was based on i) the commonly reported 10° of calcaneal eversion during the initial stance phase of running (Cornwall and McPoil, 2004; Hunt et al., 2000; Stacoff et al., 2000b), and ii) on an approximated subtalar axis with an orientation of 41° relative to the transverse plane and 17° relative to the sagittal plane (Isman and Inman, 1969; Root et al., 1966). Theoretically, a rotation of 15° about this assumed axis will result in the requested eversion (precisely 10.8°) as well as in 3.3° dorsiflexion and 9.8° abduction. The supination block (Fig. 3-6 (b)) was constructed to induce an exactly opposite rotation of the calcaneus: 10.8° inversion, 3.3° plantarflexion, and 9.8° adduction.

To finally chamfer the fronts of the blocks, the position of the subtalar axis had to be known, too. Based on the work of van Langelaan (1983), it was derived that 5 cm away from the posterior, 4 cm away from the lateral, and 5 cm away from the distal part of the calcaneus the subtalar axis would pass the Sinus tarsi. Furthermore, a heel fat pad of 2 cm thickness was supposed. Hence, the intersection of the axis with the front of the blocks was known, and, the front could be rotated about the assumed axis whereby the piercing point was kept in place (In the height of this point the contralateral foot was placed to keep the pelvis even). Relative to the piercing point, the positions of the most distal heel point and of the second metatarsal joint were known, too; in consequence, two points of the longitudinal axis of the foot were known. Thus, the foot could be placed in the correct manner on the different blocks. Note, the foot was only fixed on the block by the applied load which was in the order of half bodyweight reflecting normal standing. The value was chosen since it was close to the threshold that could be comfortably tolerated by the subject during MR imaging of each foot position over a total of 15 min including placement and prescans.

Each excursion was performed twice on the same day. Between the measurements, the subject was completely repositioned.

Image acquisition and data processing

Imaging was performed on a 3 Tesla whole-body MR unit (Intera 3T, Philips Medical Systems). A 3D T1 weighted gradient echo sequence with water selective excitation and second order shimming was used to obtain fat suppressed, high-contrast and high-resolution images of the tarsal bones. Sequence parameters were as follows: repetition time 16 ms, echo time 4 ms, and flip angle 11° ; 200 mm field of view; a 288×273 acquisition matrix; Fourier interpolated to 512×512 pixels; 1.4 mm

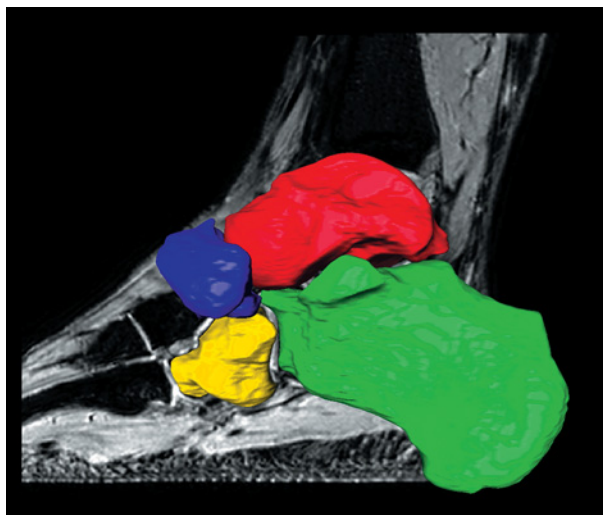


Fig. 3-7 Medial view of 3D reconstructed tarsal bones: calcaneus (green), cuboid (yellow), navicular (blue), and talus (red).

thick overcontinuous slices with 50% slice overlapping. Thus, the resolution of the reconstructed images was $0.39 \times 0.39 \times 0.7 \text{ mm}^3$, see Fig. 3-7. For each subject and test condition 130 sagittal slices were acquired during about 9 min.

The 3D reconstruction of the tarsal bones was performed by one operator with AMIRA (Mercury Computer Systems, Berlin) as described before (see chapter 3.1).

The resulting surface points were read in MatLab (MathWorks, Massachusetts) to determine the transformations of 'neutral' surface point clouds into the surface point clouds of pronation and supination, respectively, by an iterative closest point algorithm (Besl and McKay, 1992).

Feasibility

The feasibility of the presented procedure was checked by the quantification of the motion transfer from externally applied foot excursion to internal absolute calcaneal rotation. Furthermore, the relative helical axis rotations in the four tarsal joints (calcaneus relative to talus, cuboid relative to calcaneus, cuboid relative to navicular, and navicular relative to talus) were computed, converted into the cardinal body planes, and compared to the literature. Lastly, the differences between the repeated excursions were separately calculated for each tarsal joint and cardinal body plane. The mean of these differences plus one standard deviation was used to estimate the required degrees to distinguish between quasi-static tarsal bone rotations.

3.3.3 Results

The externally applied 15° of pronation resulted in 6.6° to 10.6° absolute calcaneal helical axis rotation and the externally applied 15° of supination resulted in 11.3° to 14.3° absolute calcaneal helical axis rotation (see appendix B, Tab. B-1 and B-2).

The extent of tarsal joint rotations in response to the pronation block is qualitatively exemplified in Fig. 3-8. Eversion (EV) of the calcaneus, cuboid, and navicular relative to the talus are clearly visible as well as abduction (ABD) of the cuboid and navicular relative to the talus. The use of the supination block resulted in opposite rotations as shown in Fig. 3-9: Both inversion (INV) of the calcaneus, cuboid, and navicular relative to the talus, and adduction (ADD) of the cuboid and navicular relative to the talus are noticeable.

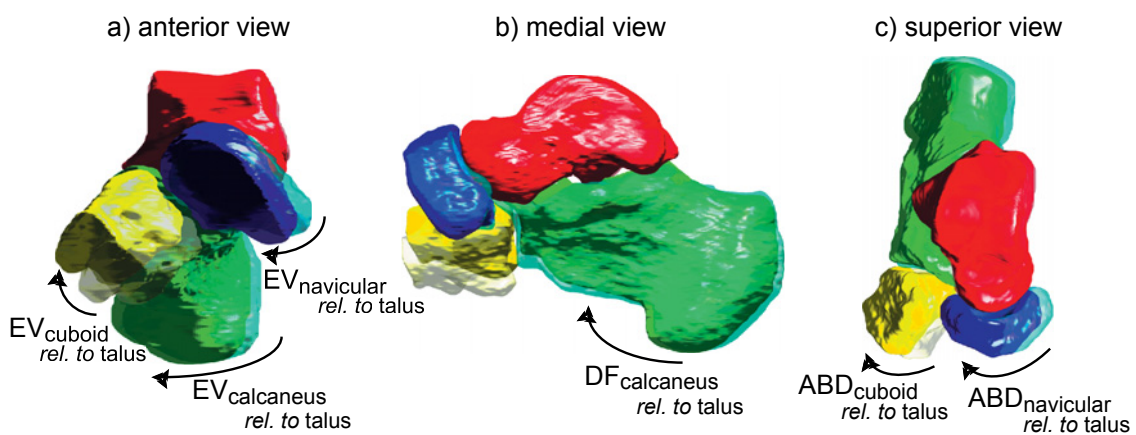


Fig. 3-8 Motion of the talar bones due to foot pronation. Neutral positions are plotted transparently. Anterior view (a): qualitatively evident eversion (EV) of calcaneus, cuboid, and navicular relative to talus. Medial view (b): visible dorsiflexion (DF) of calcaneus relative to talus. Superior view (c): noticeable abduction (ABD) of cuboid and navicular relative to talus.

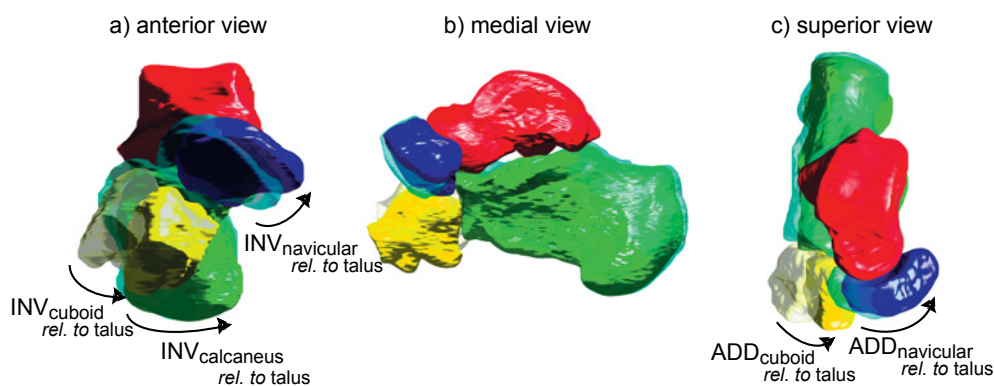


Fig 3-9 Motion of the talar bones due to foot supination. Neutral positions are plotted transparently. Anterior view (a): qualitatively remarkable inversion (INV) of calcaneus, cuboid, and navicular relative to talus. Superior view (c): obvious adduction (ADD) of cuboid and navicular relative to talus.

The quantified relative rotations in the tarsal joints are shown in Fig. 3-10 to Fig. 3-13. In all cases, the external supinated foot position led to more relative tarsal joint motion than the pronated foot position. Thereby, the talo-navicular joint exhibited the largest rotations (up to 21.5°, see Fig. 3-11) which is nearly twice as large as the corresponding rotations in the subtalar joint (see Fig. 3-10). Only small rotations were found between the cuboid and calcaneus, and between the cuboid and navicular (see Fig. 3-11 and 3-12). Translations along each finite helical axis of all tarsal joint motions were smaller than 0.5 mm.

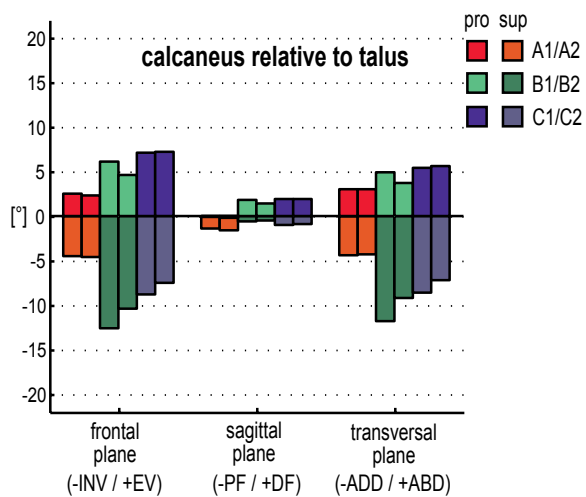


Fig. 3-10 Relative motion in the subtalar joint due to pro(nated) and sup(inated) foot positions. Each bar represents one foot excursion of the subjects A, B, C. Same coloured bars are repeated excursions.

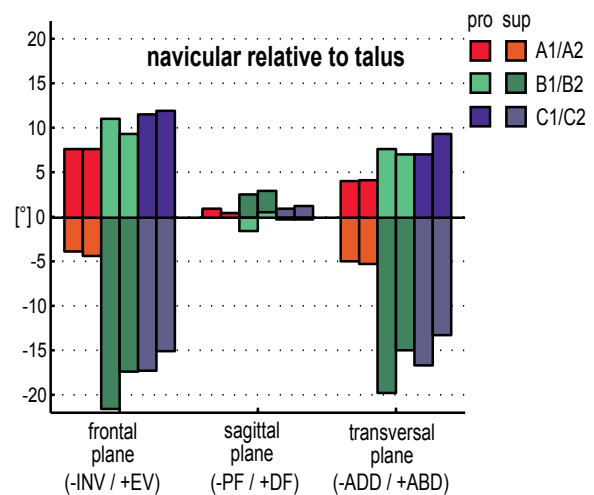


Fig. 3-11 Relative motion in the talo-navicular joint due to pronated and supinated foot positions. Each bar represents one foot excursion of the subjects A, B, C. Same coloured bars are repeated excursions.

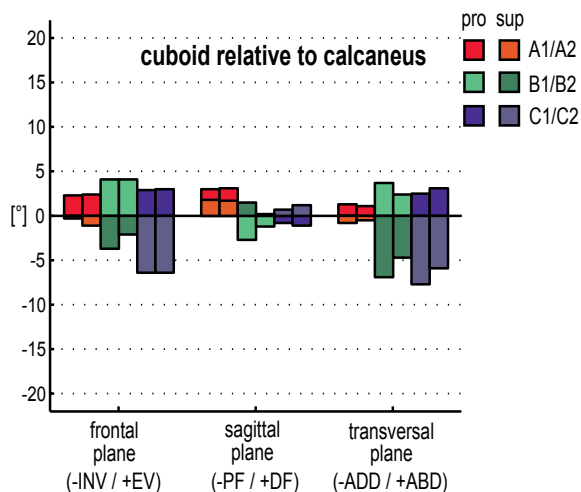


Fig. 3-12 Motion of the cuboid relative to the calcaneus due to pronated and supinated foot positions. Each bar represents one foot excursion of the subjects A, B, C. Same coloured bars are repeated excursions.

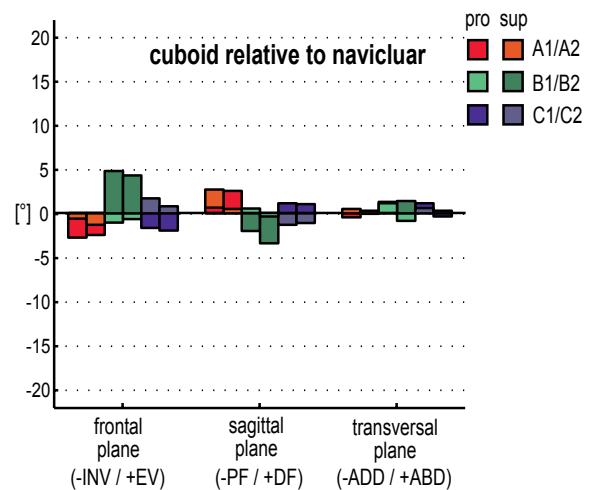


Fig. 3-13 Motion of the cuboid relative to the navicular due to pronated and supinated foot positions. Each bar represents one foot excursion of the subjects A, B, C. Same coloured bars are repeated excursions.

Based on the six available differences between repeated measurements (3 subjects, 2 repetitions of pronation and supination) the mean and standard deviation of these differences were calculated for each tarsal joint and cardinal body plane. An addition of them can be used to estimate the required rotational degrees allowing a distinction between kinematics of these joints. The largest difference plus one standard deviation was about 3.8° calculated for the talo-navicular joint. In the other joints the sum were about $0.7\text{-}1.9^\circ$ (see Tab. 3-14).

Tab. 3-14 Mean differences (\pm standard deviation) of once repeated measurements per tarsal joint and anatomical plane. In total, six differences were available each (3 subjects, pronation and supination).

| | frontal plane [°] | sagittal plane [°] | transversal plane[°] |
|------------------------------------|----------------------|-----------------------|-------------------------|
| calcaneus <i>rel. to talus</i> | 0.9 \pm 0.9 | 0.2 \pm 0.1 | 0.9 \pm 1.0 |
| cuboid <i>rel. to</i> calcaneus | 0.4 \pm 0.6 | 0.6 \pm 0.6 | 1.1 \pm 0.8 |
| cuboid <i>rel. to</i> navicular | 0.4 \pm 0.3 | 0.6 \pm 0.5 | 0.8 \pm 0.8 |
| navicular <i>rel. to talus</i> | 1.5 \pm 1.6 | 0.6 \pm 0.8 | 1.9 \pm 1.9 |

3.3.4 Discussion and conclusions

In this study, a new procedure to investigate positions of the tarsal bones in vivo in different foot excursions under bodyweight is presented. In this chapter, the applicability of the developed foot loading and positioning device is discussed in terms of the transferred motion, the resulting quasi-static tarsal joint motion, and the repeated excursions.

Transferred motion

In response to different blocks the calcaneus rotated absolutely 6.6 to 10.6° (11.3 to 14.3°) in the pronated (supinated) foot position which is equal to a transfer of $45\text{-}70\%$ ($75\text{-}95\%$) of the externally applied 15° . With regard to the roughly 2 cm thick heel fat pad and the arbitrary chosen rotation axis these differences between external foot and internal calcaneal rotations were to be expected: The heel fat pad was distorted and displaced under load and excursion. Thereby, the magnitude of motion transfer is comparable with the literature reporting a transfer in the order of 44% during foot plantarflexion (Mattingly et al., 2006).

Lundberg and coworkers (1989b) showed in vivo and under bodyweight that subtalar joint motion was twice as large in foot inversion than in foot eversion. This confirmed the rather restricted movement of the calcaneus in pronation compared to supination of the present work; hence, foot pronation was more performed by heel fat pad deformation than by calcaneal motion.

Thus, the transferred motion from the test device to the calcaneus was in agreement with the literature and transfer loss can be explained by anatomical boundary conditions.

Quasi-static tarsal joint motion

As shown above, the pronation block induced a pronation of the distal tarsal bones relative to the talus, and analogously, the distal tarsal bones supinated relative to the talus in response to the supination block (see Fig. 3-8 and 3-9).

Because the presented procedure is the first to induce rotations about an assumed subtalar axis under considerable load, the quantified motions in each tarsal joint of the three investigated subject were difficult to compare with previous literature: In former tarsal joint investigations input movements about an anterior posterior axis were used (Benink, 1985; Lundberg et al., 1989b; van Langelaan, 1983) or load was applied in another direction (Ringleb et al., 2005; Siegler et al. 2005) or disregarded (Parks et al., 1994; Udupa et al., 1998). Nevertheless, general findings were in agreement: Firstly, in the present study most motion occurred in the talo-navicular joint (up to 20° in frontal and transversal plane), followed by nearly half of that in the subtalar joint (see Fig. 3-10 and 3-11). Larger rotations in the talo-navicular joint compared to the subtalar joint had already been reported during internal/external tibia rotation (Benink, 1985; van Langelaan, 1983) as well as during eversion/inversion (Lundberg et al., 1989b) and pronation/supination of the foot (Parks et al., 1994).

Secondly, less tarsal joint motion was observed during internal tibia rotation (Benink, 1985; van Langelaan, 1983), foot eversion (Lundberg et al., 1989b), and foot pronation (Parks et al., 1994) compared to the opposite input movement. The same relation was found in the present study: Nearly half of the magnitude of subtalar and talo-navicular joint motion occurred during pronation in contrast to supination (see Fig. 3-10 and 3-11).

Finally, considerably less motion was found between the cuboid and calcaneus, and the cuboid did nearly not move relative to the navicular (see Fig. 3-12 and 3-13). Again, this is in agreement with others studies (Benink, 1985; van Langelaan, 1983) beside the generally accepted assumption that cuboid and navicular act as a unit (Shepard, 1951; Manter, 1941).

Thus, the observed quasi-static tarsal joint motions were in agreement with the literature.

Repeated excursions

In the present study, the foot excursions of three subjects were measured twice. The sum of the mean and one standard deviation of the resulting differences between these repetitions (see Tab. 3-14) were used to estimate the required amount of rotation necessary to distinguish between quasi-static kinematic behaviour: At least 2° are required to differentiate rotations between the calcaneus and talus, between the cuboid and calcaneus, and between the cuboid and navicular. In the same manner, at least deviations of 4° in talo-navicular joint motions are necessary to show intersubject differences reasonably.

The differences between repeated measurements can partly be explained by the determined reproducibility and accuracy of the data processing which was estimated to be 0.6 to 1.8° depending on tarsal bone and excursion (see chapter 3.2). And, although before each measurement the position of the lower leg was carefully controlled, it must be assumed that subtle positioning changes (e.g. of the hip) led to considerable changes in the whole tarsal bone configuration. The foot placement onto the block may be excluded as a potential source of precision errors: In a pilot study the repeatability of tarsal joint motion was not improved by using an individual thermoplastic shell fixed onto the block providing the identical calcaneal position during repeated measurements (Keller Chandra, 2005).

To the best of the authors' knowledge the feet as well as the gait of the subjects showed no abnormal morphology or pathology. But, subject A showed remarkably different quasi-static tarsal joint motion compared to the other two subjects: In particular, the navicular moved relative to the talus 10° less in the frontal and transversal plane in foot supination (pronation: -4°), see Fig. 3-11. Thus, talo-navicular joint motion of more than 4° may occur even among visually normal feet and could be considerably more in subjects with foot deformities.

In the relevant literature only one other group has focused on tarsal bone kinematics investigated by MR imaging as well (Ringleb et al., 2005; Siegler et al., 2005). Their imaging and segmentation were also time consuming (4-5h). This might limit the applicability of MR procedures if a clinical use is intended but not if basic research of tarsal bone mechanics is facilitated. Recently, stress MR imaging of subtalar and ankle joint motion was also repeatedly performed (Siegler et al., 2005). Unfortunately, the reproducibility of the rotations in these joints was not reported. But, Siegler and coworkers (2005) provided a comparison of in vitro joint motion evaluated with MR imaging and bone pins emphasising the potential of the non-invasive procedure. Therefore, it would make sense to compare in vivo quasi-static tarsal bone motion gained with the presented MR procedure and with intracortical pins in a future study.

In conclusion, a MR compatible foot positioning and loading device was presented. It facilitated arbitrary foot excursions by easy to build wooden blocks whereby a reasonable motion transfer to the calcaneus was warranted resulting in quasi-static tarsal joint motion. Thereby, it was estimated that only a few degrees (1-4°, depending on tarsal joint) are necessary to distinguish between tarsal bone kinematic behaviour. Thus, the procedure was found to be feasible to investigate tarsal bone mechanics non-invasively and in vivo. Particularly, the possibility to evaluate 3D tarsal joint motion in combination with bone morphology (e.g. joint curvature) may provide new insights into the still uncertain relationship between foot function and foot morphology.

3.4 Tarsal bone positions in different foot excursions: MR imaging vs. intracortical pins

3.4.1 Introduction

Magnet resonance (MR) imaging is increasingly important in the study of foot biomechanics. In contrast to common video motion analyses, MR imaging offers unique insights into three-dimensional (3D) foot bone morphology and quasi-static motion (Mattingly et al., 2006; Ringleb et al., 2005; Siegler et al., 2005). However, MR imaging typically relies on the subject lying supine and it is not clear whether the position of the foot in the MR relates to any foot position during the more commonly investigated standing or gait conditions. Ideally, when in the MR, a subject's foot should be loaded and positioned such that for instance, the position of the tarsal bones coincides with that during relaxed standing, or is equivalent to the tarsal bone position of a defined point in time during the stance phase of gait.

To address this problem, a MR compatible device has been developed which enables imaging to be performed whilst physiological loads are applied to the foot, and wedged blocks position the foot in either pronation or supination (see chapter 3.3): The primary role of this device is to recreate the standing posture of the foot whilst in the MR, but it is also assumed that the foot might be in a position similar to that during walking and running. To validate this approach, it was aimed to compare tarsal bone motion induced by these wedged blocks when in the MR and when standing on them. Kinematic data from lying would be derived from the MR images, and data from standing would be derived from marker arrays attached to intracortical pins. Since it is also of interest whether the tarsal bone positions in the MR relate to any position during stance, tarsal bone rotations derived by MR imaging were also compared to tarsal bone rotations during the stance phase of running (opto-electrical registration of markers on intracortical pins). These comparisons should provide further insights into the feasibility of non-invasive quasi-static procedures such as MR imaging to investigate tarsal bone mechanics.

3.4.2 Methods

The study was conducted on three male volunteers without signs of musculoskeletal diseases aged 28, 33, and 55 years, 175, 180, and 182 cm high, and weighing 71, 75, and 80 kg, respectively. Informed written consent in accordance to the local research ethics committee was obtained from all subjects.

MR procedure

Subjects lay on the MR table and their right foot was fixed into the foot loading and positioning device (detailed description of the device in chapter 3.3). A load of 0.5 body weight was applied to the board under the right foot, simulating the standing position. Three different wooden blocks were placed under the feet to control foot position: a flat block (neutral), a 15° wedged ‘pronating’ block (10.8° eversion, 3.3° dorsiflexion, 9.8° abduction), and a 15° wedged ‘supinating’ block (10.8° eversion, 3.3° dorsiflexion, 9.8° abduction), see Fig. 3-14a.

Imaging was performed on a 3 Tesla whole-body MR unit (Intera 3T, Philips Medical Systems). A 3D T1 weighted gradient echo sequence with the following parameters was used: repetition time 16 ms, echo time 4 ms, and flip angle 11°; 200 mm field of view; a 288 x 273 acquisition matrix; Fourier interpolated to 512 x 512 pixels; 1.4 mm thick overcontinuous slices with 50% slice overlapping. Thus, the resolution of the reconstructed images was 0.39 x 0.39 x 0.7 mm³, see Fig. 3-14b. For each subject and test condition 130 sagittal slices were acquired during about 9 min.

The 3D reconstruction of the tarsal bones was performed by one operator using AMIRA (Mercury Computer Systems, Berlin) as described in chapter 3.1.

The resulting surface points were read in MatLab (MathWorks, Massachusetts) to determine the transformations of ‘neutral’ surface point clouds into the surface point clouds of pronation and supination, respectively, by an iterative closest point algorithm (Besl and McKay, 1992).

Intracortical pin measurement

Intracortical pins (1.6 mm in diameter) were inserted under local anaesthetic into the calcaneus, cuboid, navicular, and talus, and a reflective marker triad attached to each, see Fig. 3-15 (pins were inserted into other bones for a different study).

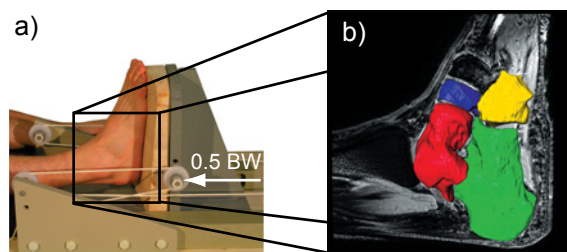


Fig. 3-14 (a) Positioning and loading device of the MR imaging procedure. A load of half bodyweight is axially applied under the heel. (b) MR image with 3D reconstructed tarsal bones: calcaneus (green), cuboid (yellow), navicular (blue), and talus (red).

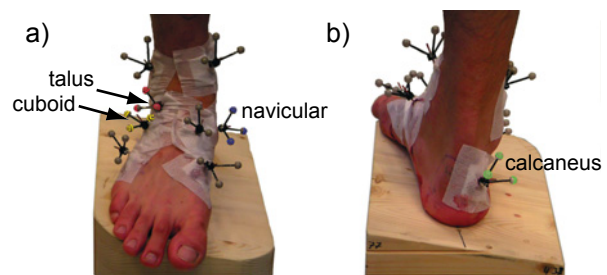


Fig. 3-15 (a) Anterior view of standing on pronation block. The marker triad of the intracortical pins of the cuboid (yellow), navicular (blue), and talus (red) are emphasised. (b) Posterior view of standing on supination block. The calcaneal marker triad is highlighted in green.

Kinematic data was collected using a ten camera opto-electrical system (Qualysis, Göteborg, Sweden) at 240 Hz.

The wooden blocks of the MR procedure were used to investigate quasi-static tarsal bone motion during standing. As in the MR, the right foot of each subject was placed on the pronation and supination block, respectively. The contra-lateral foot stood on the neutral block enabling straight leg standing and a neutral pelvis position. Each foot excursion was repeated five times. The subjects descended from the blocks between the trials.

Running data was collected from one of the subjects (9 trials, barefoot, mean velocity: 2.2 m/s). Force plate data was collected at 960 Hz and compared to running without the bone pins. The mean vertical force curve was within the 99% confidence interval of the corresponding curve of running without intracortical pins. Thus, it was concluded that the intracortical pins did not adversely affect the running pattern.

Tarsal bone positions measured with intracortical pins were calculated relative to a relaxed standing trial whereby the subject stood normally on a flat surface. Tarsal joint rotations were computed as finite helical axis rotations projected into the cardinal body planes. The analysis focused on the talo-calcaneal and talo-navicular joints since rotations between other tarsal bones were found to be small (calcaneo-cuboid: 2-6°) or were even considered to be negligible (naviculo-cuboid: <2°), see chapter 3.3.

3.4.3 Results

Rotations of the calcaneus relative to the talus in response to the quasi-static foot pronation and supination, respectively, are presented in Fig. 3.16.

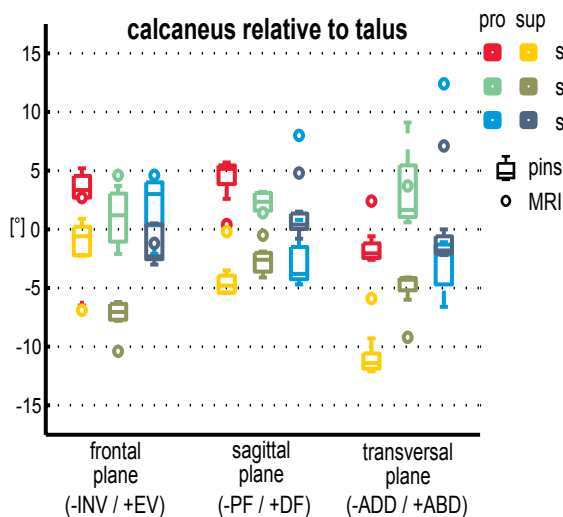


Fig. 3-16 Talo-calcaneal rotations in response to quasi-static foot pronation and supination. The results of the repeated intracortical pin measurements are shown as box plots, the results of the MR imaging as circles.

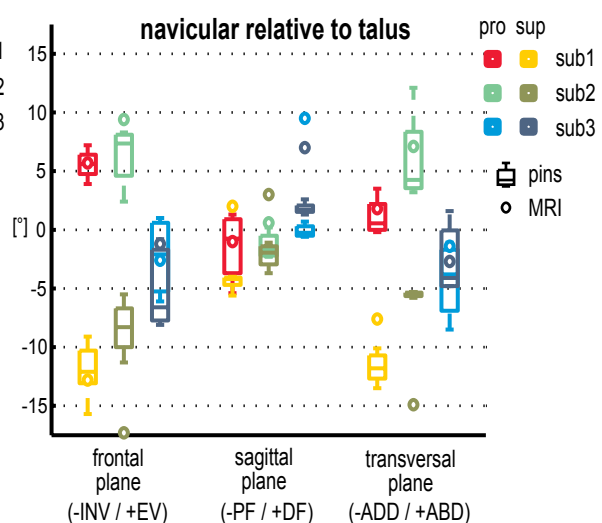


Fig. 3-17 Talo-navicular rotations. Lying supine (during the MR) and standing led to different rotations since the results of the MR procedure were not consistently within the lower and upper quartile of the pin trials.

Rotations determined with the MR procedure (circles) were only occasionally within the lower and upper quartile of the five standing trials measured with intracortical pins, and no systematic shift was present. Similar results were found for the talo-navicular joint: No subject showed consistently comparable rotations in lying supine and standing upright, see Fig. 3.17.

Talo-calcaneal and talo-navicular rotations during the stance phase of running with intracortical pins are presented in Fig. 3.18 and Fig. 3.19. At 20% stance, the magnitude of dynamic joint motion was similar, i.e. not significantly ($p=0.01$) different from the corresponding quasi-static joint motion during foot pronation measured with MR imaging.

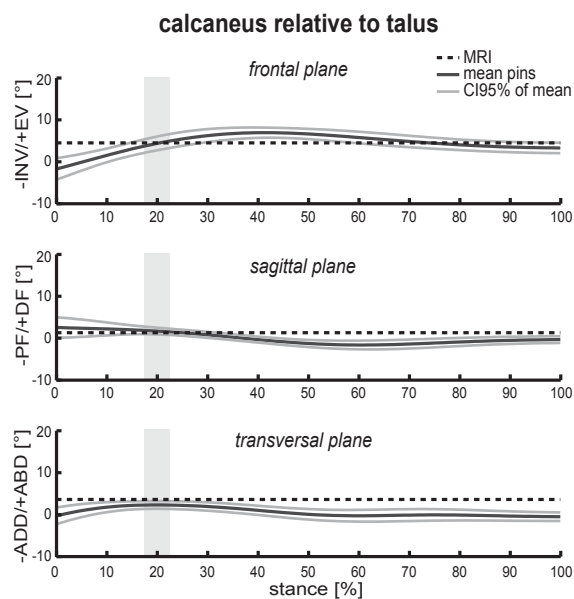


Fig. 3-18 Talo-calcaneal rotations in response to quasi-statically foot pronation in the MR (dashed line) and mean subtalar rotations during the stance phase of running (dark line with 95% confidence limits as bright line). In all cardinal body planes, the rotations of the different analyses were most similar at 20% stance phase.

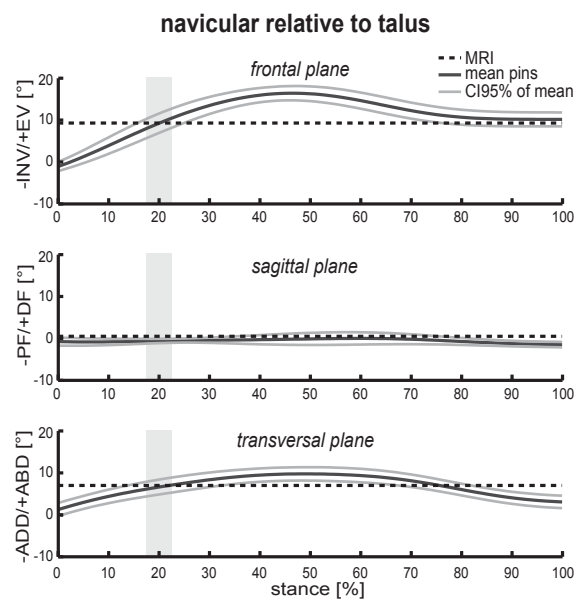


Fig. 3-19 Talo-navicular rotations during foot pronation in the MRI (dashed line) and mean talo-navicular rotations during the stance phase of running (dark line with 95% confidence limits). In all cardinal body planes, the rotations of the different analyses were most similar at 20% stance phase.

At 20% stance, the mean vertical force during running was also similar to the loading applied during the MR procedure that attempted to simulate standing, see Fig. 3.20.

3.4.4 Discussion and conclusions

In this study, it was investigated whether a MR procedure is feasible to imitate quasi-static tarsal joint rotations in upright posture as well as a point in time during the stance phase of running.

The results show that quasi-static tarsal joint rotations while lying supine in the MR do not systematically match with corresponding rotations while standing upright (see Fig. 3.16 and 3.17). Differences between the median intracortical pin and the MR imaging results were in

the magnitude of up to 10° which is up to 10 times greater than the accuracy of the two methods (see chapter 3.2). Thus, although knee flexion and externally applied load were carefully controlled during lying and standing, the motion of the tarsal joints in the MR do not imitate those in upright posture. Perhaps subtle changes in hip position in combination with slightly different points of load application (particularly during the intracortical pin measurements) may have contributed to the different tarsal joint rotations. Furthermore, in contrast to standing upright, lying supine does not require activity of the following muscles all inserting at midfoot: tibialis anterior, tibialis posterior, peroneus brevis, and peroneus longus. Activity in these muscles may result in tarsal bone rotations and thus may also account for the observed differences.

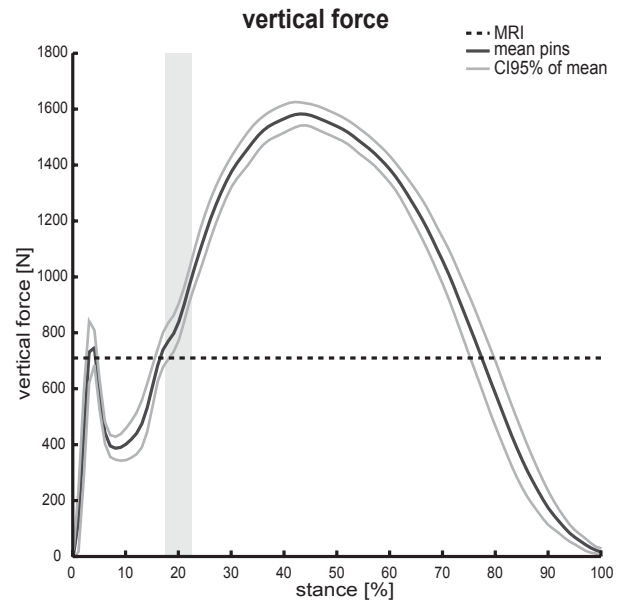


Fig. 3-20 Vertical force simulated during the MRI procedure in the magnitude of standing (dashed line) and mean vertical force with 95% confidence limits during the stance phase of running (dark and bright lines). At 20% stance phase, the simulated force of the MRI procedure was about 100 N less than the mean vertical force during running.

The MR procedure in combination with foot pronation of 15° under load simulating standing imitated a point in time at about 20% stance phase of running: rotations in the major tarsal joints were equal and the vertical forces nearly similar (see Fig. 3.18 to Fig. 3.20). Although this finding was only based on nine trials of one subject, it indicates a certain applicability of the non-invasive approach to investigate foot kinematics which would otherwise only be available by the use of invasive techniques such as intracortical pins. Perhaps, with further study and adjustment, protocols can be developed to place and load the foot in the MR in other positions used during running, walking or other activities, further increasing the value of using MR for foot biomechanics research.

In conclusion, it has been shown that despite of using a loading and positioning device, lying supine on the MR table and standing upright result in different tarsal joint rotations. The hip position, the activity of muscles inserting at midfoot, and the point of load application are likely factors affecting the foot when lying supine compared to when standing. However, the loading and positioning device did place the tarsal bones in a position corresponding to a specific phase during running stance. Thus, MR imaging of defined quasi-static foot positions is a promising approach to investigate tarsal bone mechanics non-invasively and without harmful radiation.

Chapter 4

Tarsal joint kinematics and morphology of dynamically classified runners

Based on the literature review it was concluded that an investigation of the foot morphology of subjects showing different foot kinematics during running should provide a better understanding of the still uncertain relationship of foot morphology and foot function (see chapter 2). Thus, the following chapter is dedicated to the application of the newly developed MRI procedure to evaluate tarsal mechanics of dynamically classified subjects, the second main purpose of this thesis.

The first section of this chapter is related to the quasi-static tarsal joint motion of the dynamically classified runners, and, it addresses the correlations within the tarsal joint rotations. Thereafter, tarsal joint curvatures are compared between the two classifications. Finally, the new insights into tarsal bone kinematics of dynamically classified runners are discussed in general, and a short outlook of possible next steps is given.

4.1 Quasi-static tarsal bone motion of dynamically classified runners

The kinematics of the lower extremity during running is commonly registered using skin markers. Thereby, skin markers are limited to bones which are palpable beneath the skin; related to the lower leg and rearfoot, these are the calcaneus and tibia. Although no joint surface exists between these bones, their kinematics is linked by various ligaments and the talus which is also part of the closed kinematic chain within the tarsus, the so called tarsal gear (see chapter 2.1.4). Hence, several kinematic parameters between these bones, i.e. maximal calcaneal eversion relative to the tibia, have been used in the past to classify runners as overpronators (i.e. McClay and Manal, 1997).

In contrast to video motion analysis with skin markers, the newly developed magnetic resonance (MR) imaging procedure offers a more comprehensive description of rearfoot kinematics since all tarsal joint rotations are quantifiable. These new insights into quasi-static tarsal joint motion may have the potential to interpret lower leg and rearfoot kinematics during running. Thus, the first part of the study concerning dynamically classified runners is addressed to quasi-static tarsal bone motions. These motions are further used to determine the orientation of finite helical axes. Additionally, morphological parameters of the entire bone (volume, second moments) are calculated to improve knowledge of the relation between foot morphology and foot function.

4.1.1 Dynamic foot classification

Assignment of classification parameter

To date, certain running injuries are thought to be related to kinematic parameters such as the range of calcaneal eversion and abduction relative to the lower leg (Clement et al.,

1981; Clarke et al., 1983 Stergiou, 1996). Hence, it makes sense to classify runners based on these kinematic parameters.

Ideally, to comprehensively understand joint kinematics at the tarsus, all parameters influencing its kinematics should be monitored during a motion of interest. Thereby, tarsal bone kinematics itself is already difficult to measure beside the even more demanding evaluation of tarsal ligament properties and quantification of muscle forces inserting at the tarsal bones. Thus, if the influence of tarsal bone morphology on tarsal kinematics is of interest, like in this thesis, the influence of other factors on kinematics that can not be measured should be minimised. Neuromuscular reaction can be excluded by considering only calcaneal motion during the first 50 ms of stance (assuming a stance duration of about 250 ms, the first 50 ms are also equal to 20% stance, the point in time that is probably related to MR measurements in combination with the wedged ‘pronating’ block (see chapter 3.4)). Thus, it was decided to use the range of calcaneal eversion and abduction relative to the lower leg during the first 50 ms of stance phase to classify the runners into two groups.

Assignment of subjects to two groups

Because the above mentioned classification is new, a larger pool of rearfoot kinematics during running was required. Sixteen volunteers were recruited for whom informed written consent in accordance to the local research ethics committee was obtained. Barefoot running with skin markers was captured with a twelve camera motion analysis system (Vicon MX 612, Oxford Metrics, UK) at 100 Hz. Thereby, six skin markers represented the right lower leg segment (see Fig. 4.1). They were placed on the tuberositas tibiae (RTTT), on the head of the fibula (RTHF), in the mid of the tibia and fibula each (RTMT, RTLFL), and on both malleoli (RTMM, RTLM). The right calcaneal segment based on four markers: one just below the insertion of the Achilles tendon (right superior calcaneal marker: RTSC), another vertically beneath, just above the heel fat pad (right inferior calcaneal marker: RTIC), and a marker each beneath the medial and lateral malleoli (RTMC, RTLC).

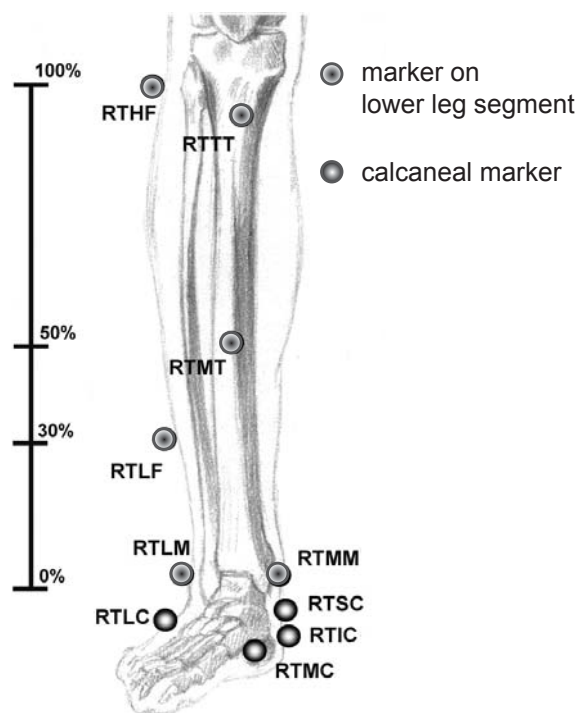


Fig. 4-1 Skin marker placement during video motion analysis of running.

The subjects performed at least five valid heel strike runs including left and right ground contact (stance phase) at a speed between 2.0 to 3.6 m/s. The positions of the different segments during stance were calculated relative to a relaxed standing trial. Relative segment motions were computed as finite helical axis rotations projected into the cardinal body planes. The resulting mean range of calcaneal eversion against calcaneal abduction is shown in Fig. 4-2. The results of ten subjects were found to be close to each other within a window of 3° calcaneal eversion and abduction, respectively (red marked area in Fig. 4-2). Thus, these subjects were defined as members of a ‘normal’ group, the other six subjects represented the ‘outlier’ group. The runners who had shoulder problems or ran very slow (2.0 m/s) were excluded for the MR investigation. Lastly, out of both groups three subjects each were investigated in the MR (emphasised circles in Fig. 4-2).

The demography of the chosen subjects is given in Tab. 4-1: Both groups consisted of one woman and two men, and in both groups the subjects were of similar age (23-35 years), height (162-184 cm), and weight (54-76 kg). Thus, the demography of the ‘normal’ and ‘outlier’ group did not contribute to the differences observed in dynamic foot motion. Furthermore, in each group subjects of similar running speed were measured (see Tab. 4-1); thus, running speed did also not contribute to the different calcaneal motion.

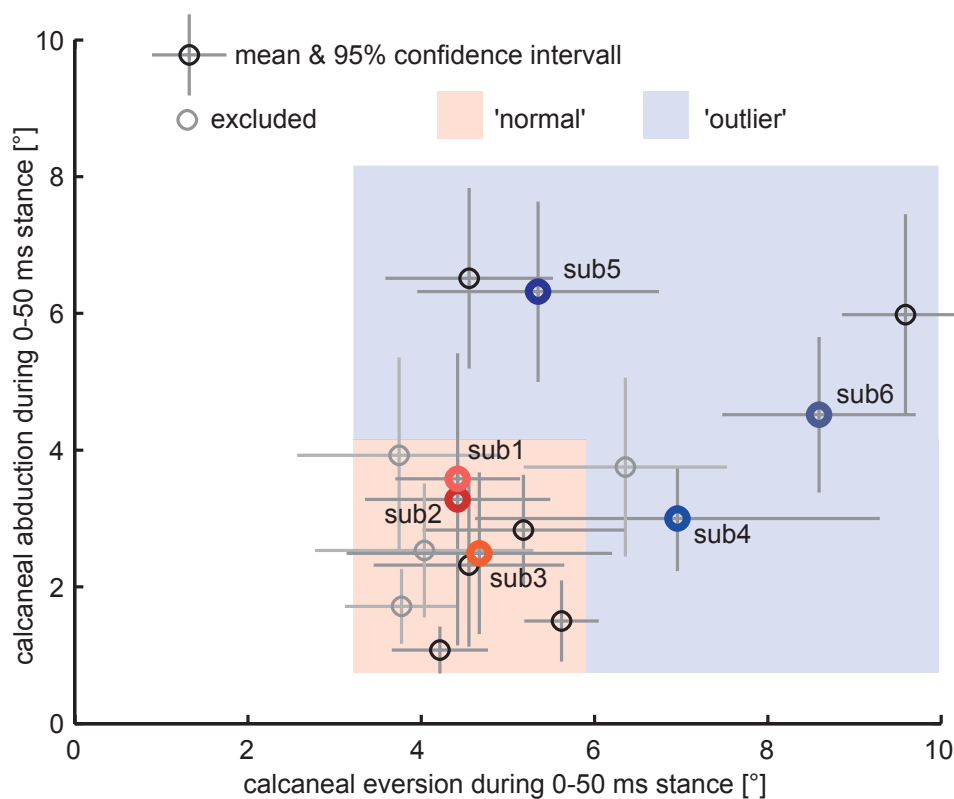


Fig. 4-2 Calcaneal eversion and abduction of the right foot during running. The subject's mean of at least 5 valid trials is given as a circle, the cross lines mark the 95% confidence limits. To the MR investigation recruited subjects are given in bold. The defined groups are highlighted in red ('normal') and blue ('outlier').

Tab. 4-1 Demography of the ‘normal’ and ‘outlier’ group. Similar subject are present in each group.

| group | id | sex | age [years] | height [cm] | weight [kg] | speed [m/s] | stance duration [ms] |
|------------------|------|-----|----------------|----------------|----------------|----------------|-------------------------|
| <i>‘normal’</i> | sub1 | w | 35 | 166 | 60 | 2.7 | 270 |
| | sub2 | m | 29 | 180 | 70 | 3.6 | 251 |
| | sub3 | m | 32 | 179 | 71 | 3.3 | 258 |
| <i>‘outlier’</i> | sub4 | w | 23 | 162 | 54 | 2.8 | 268 |
| | sub5 | m | 32 | 180 | 71 | 3.0 | 240 |
| | sub6 | m | 34 | 184 | 76 | 3.6 | 237 |

And finally, stance phase duration of all subjects was very similar such that the 50 ms (or 5 frames of the motion analysis), in which calcaneal motion was measured, were comparable to 20% stance phase.

4.1.2 MR data acquisition and processing

Tarsal bone positions of all six subjects were acquired and processed as already described in chapter 3.3.2 with two minor exceptions:

- (1) As proposed in chapter 3.2, the ‘outlier’ group was measured with transversal MR slices. The ‘normal’ group had already been measured before with sagittal MR slices. Because sagittal MR slices provide reasonably accurate tarsal bone positions as well ($<1^\circ$; navicular: $<2^\circ$, see chapter 3.2), the time consuming MR procedure was not repeated for the three ‘normal’ subjects.
- (2) Additionally to tarsal bone positions, tibia positions and motion were determined: As this bone was not entirely seen in the MR images, the tibia matching of different foot excursions was based only on a point cloud of the distal end of the tibia including the medial malleoli and the tibial joint surface of the ankle warranting that the iterative closed point (ICP) algorithm converged.

The quasi-static tarsal bone motions in response to the wedged ‘pronating’ and ‘supinating’ block (as described in chapter 3.3.2) were quantified. The motions were used to estimate the orientation of the finite helical axis of the subtalar joint, an occasionally used parameter to classify foot kinematics (i.e. Nigg et al., 1992). Additionally, based on the MR images of the ‘neutral’ foot, morphological parameters such as tarsal volumes and second moments of volume were computed (as described in chapter 3.2.2) to get new insights into the relation between foot morphology and foot function.

4.1.3 Results

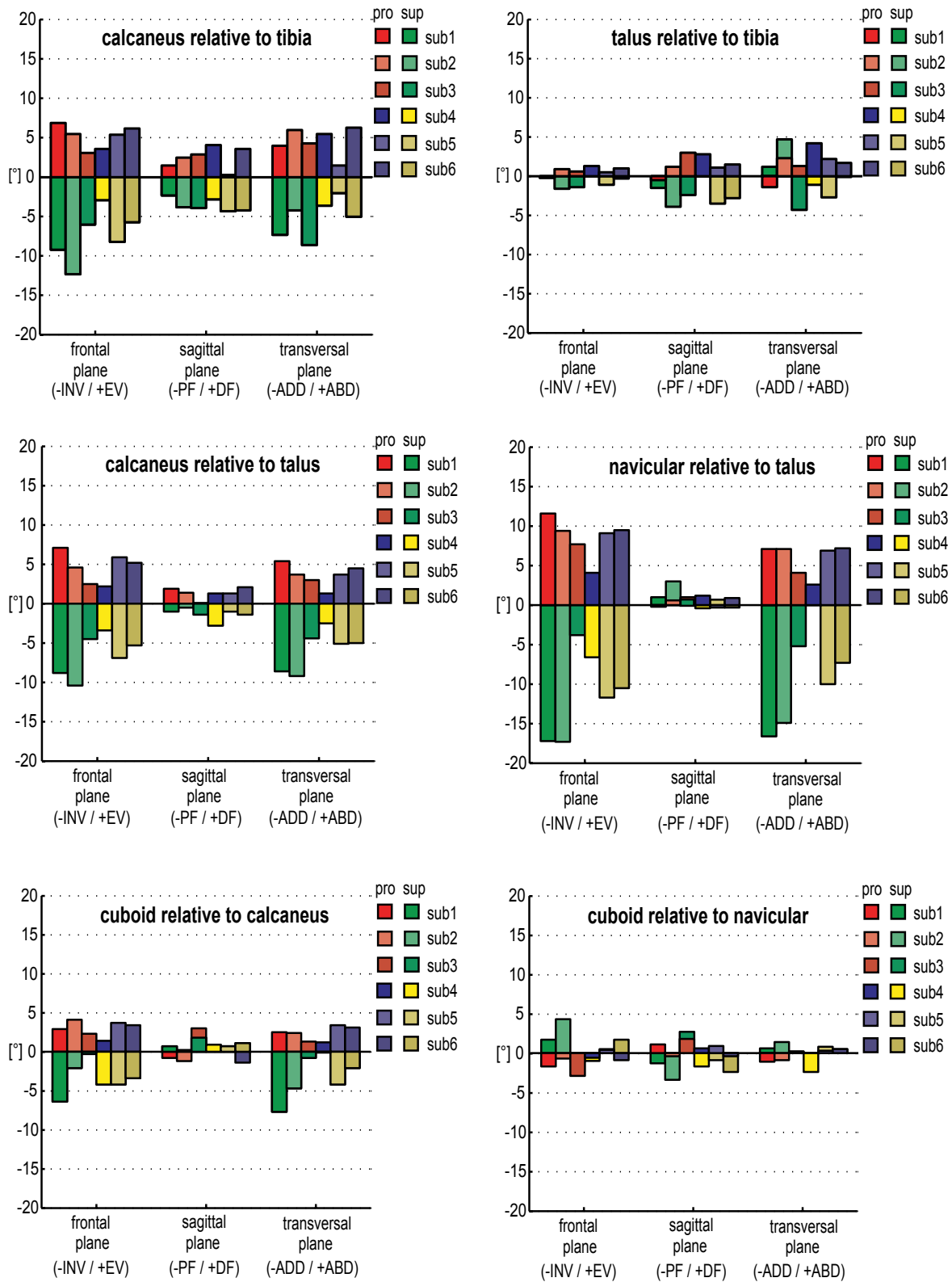


Fig. 4-3 Tarsal joint rotations in response to foot excursions in the MR under bodyweight. Neither during pronation (pro) nor during supination (sup) group differences between the 'normal' (sub1-sub3) and the 'outlier' (sub4-sub6) subjects emerged.

The quantified relative rotations between the tarsal bones are shown in Fig. 4-3. In general, the magnitude of these rotations was larger in foot supination than in foot pronation, and no group differences between the ‘normal’ and ‘outlier’ subjects emerged.

The inclination (in terms of Inman (1976): angle to transversal plane) of the finite subtalar joint axis during quasi-static foot pronation and supination is plotted in Fig. 4.4, the deviation (angle of projected axis in transversal plane to sagittal plane) in Fig. 4.5. Mostly, ‘outlier’ subjects demonstrated a lower inclination compared to the ‘normal’ subjects.

The tarsal bone volumes of all subjects are listed in Tab. 4-2. Both the ‘normal’ and the ‘outlier’ subjects covered more or less the same bone size.

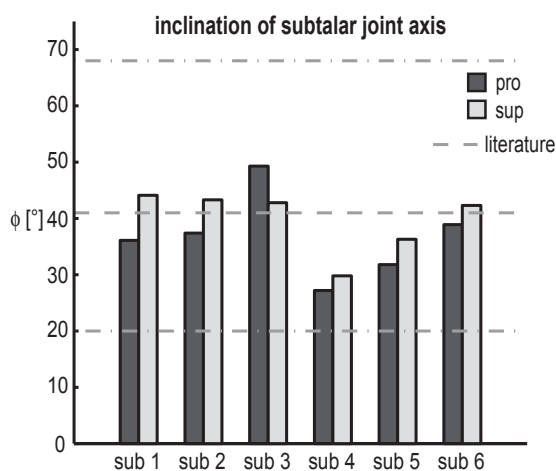


Fig. 4-4 Inclination of the finite subtalar joint axis (angle to transversal plane) during quasi-static foot pronation (pro) and supination (sup) under bodyweight. Values from the literature (mean and range, Inman, 1976) are given as lines. All ‘outlier’ subjects (sub4-sub6) demonstrated a lower inclination compared to the ‘normal’ subjects (sub1-sub3).

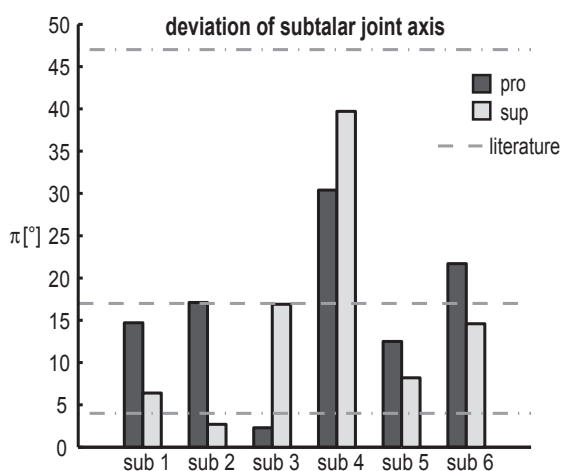


Fig. 4-5 Deviation of the finite subtalar joint axis (angle of projected axis in transversal plane to sagittal plane) during quasi-static foot pronation and supination under bodyweight. Values from the literature (mean and range, Inman, 1976) are given as lines. No obvious differences between the ‘normal’ subjects (sub1-sub3) and the ‘outlier’ subjects (sub4-sub6) emerged.

Tab. 4-2 Tarsal bone volumes [cm³] of the two groups.

| group | id | calcaneus [cm ³] | cuboid [cm ³] | navicular [cm ³] | talus [cm ³] |
|-----------|------|------------------------------|---------------------------|------------------------------|--------------------------|
| ‘normal’ | sub1 | 62.3 | 10.7 | 7.9 | 30.2 |
| | sub2 | 86.5 | 12.2 | 10.9 | 41.2 |
| | sub3 | 78.7 | 12.5 | 10.5 | 40.0 |
| ‘outlier’ | sub4 | 45.1 | 8.9 | 7.8 | 26.3 |
| | sub5 | 83.0 | 14.3 | 11.8 | 41.4 |
| | sub6 | 68.4 | 10.4 | 10.6 | 33.6 |

The second moments of volume representing the principal axes of the tarsal bones are given in the appendix C, Tab. C-1 to Tab. C-4. The relations between these second moments were similar for both groups except for the calcaneus: In contrast to the ‘normal’ subjects, the ‘outlier’ subjects had smaller second moments of volume about the (most) anterior posterior axis in relation to the other two moments (see last two columns in Tab. C-1).

4.1.4 Discussion

The following discussion of the above listed results is divided into three sections covering quasi-static tarsal bone motion, the orientation of the subtalar joint axis, and the moments of inertia of the tarsal bones.

Quasi-static tarsal bone motion

The classification of the runners was based on the magnitude of calcaneal motion relative to the lower leg during running at the beginning of stance phase (0-50 ms). To better understand the differences between the ‘normal’ and ‘outlier’ group, quasi-static tarsal bone motion of three subjects out of each group were acquired in the MR. The results show variations in individual kinematics, e.g. talo-calcaneal rotations of subject 2 and 4; but the groups can not be separated due to their quasi-static tarsal joint kinematics, neither during foot pronation nor during foot supination (see Fig. 4-3). In other words, although a detailed description of tarsal bone motions was provided by the developed MR procedure, the loading conditions in the MR did not result into different tarsal bone kinematics between the groups; particularly in contrast to running, the calcaneal motion relative to the tibia was similar in both groups (see Fig. 4-3). Thus, the dynamics of running must be considered if the group differences of calcaneal motion during running are to be interpreted.

Subtalar joint axis

The orientation of the subtalar joint axis has occasionally been used to classify foot function, in particular the relation of calcaneal motion relative to the lower leg in the frontal and transversal plane, respectively. The orientation of this axis is not assessable by skin markers but has been estimated by i.e. the arch height (Nigg et al., 1992). However, quasi-static foot excursions measured in the MR offer a precise determination of a finite subtalar joint axis. In this study, the subtalar joint axis inclination of the ‘outlier’ subjects was mostly lower than those of the ‘normal’ subjects (see Fig. 4-4). In other words, compared to the ‘normal’, the ‘outlier’ group had a remarkably greater calcaneal eversion related to calcaneal abduction. Thus, assuming similar axis orientations during running, the subtalar joint axis inclination of the investigated subjects may be used to characterise the groups. This is somehow confirmed by the ‘outlier’ subjects 4 and 6 showing more calcaneal eversion than calcaneal abduction than the other four subjects, see Fig. 4-2. Note that the orientation of the finite helical joint axis is defined by the motion of the articulating bones

without explicitly defining the type of linkage characterising the joint. The subtalar joint has been modelled manifold before, i.e. as a hinge or cardan joint, and none of these models has provided a comprehensive understanding of subtalar joint kinematics so far (see chapter 2.1). Therefore it is concluded that the orientation of a subtalar finite helical axis monitors the relation between the spatial rotations of the calcaneus relative to the talus; an information practical to classify foot function, but of minor substance to understand tarsal bone mechanics.

Tarsal bone morphology

Overall, neither tarsal bone volumes nor second moments of volume were found to be different between the subjects of the ‘normal’ and ‘outlier’ group, see Tab. 4-2 and appendix C. Only the calcaneal second moment about the anterior posterior axis was an exception of this general finding; it was smaller in relation to the other two second moments of volume for the ‘outlier’ group in comparison to the ‘normal’ group. There are two reasons why the significance of this result must be questioned: Firstly, since the acquired MR images provide no density information, the second moments were normalised with an arbitrary defined homogeneous density. This is a clear limitation of the computation of the moments. Secondly, on the one hand, tarsal bones weigh in the order of less than 10 % of the effective mass of the shank and foot during the impact (assuming an effective mass of 3.6 kg (Ker et al., 1989), an average volume of all tarsal bones of 150 cm³ (Tab. 4-2), and a bone density of 2 g/cm³). Consequently, impact forces are rather influenced by the inertia of the shank (Ker et al., 1989), the deformation of the heel pad and other structures (Ker et al., 1989), and the vertical velocity (Whittle, 1999) than by the inertia of the tarsal bones. On the other hand, the tarsal bones are almost immediately after ground contact in an anatomical configuration in which dynamic effects of tarsal moments of inertia are negligible (and tarsal bone motion is influenced by joint contact forces): Considering a moment of inertia of 1 kg cm² which based on a ‘geometrical’ moment of about 500 cm⁵ (see Tab. C-1) and a density of 2 g/cm³, and assuming a moment of 0.5 Nm shortly after ground contact, this would result in an angular acceleration of 5000 rad/s². Consequently, the bone rotates directly in a position determined by anatomical boundary conditions. Based on this deduction it is concluded that the observed differences of the geometrical shape of the calcaneus are of minor importance and do not contribute essentially to the different kinematics of the ‘normal’ and ‘outlier’ subjects during running.

In summary, it can be stated that the different calcaneal kinematics of the two groups during running is dependent on the dynamic conditions of running. Further, the morphological parameters calculated in this chapter do not allow an interpretation with respect to the registered kinematics. However, joint curvatures may significantly contribute to different kinematics. This morphological parameter will be evaluated in chapter 4.3.

4.2 Transmission within the tarsal gearbox

To enhance the significance of this chapter, two further subjects (of the pilot studies, chapter 3.4) were included beside the six subjects of the dynamic foot classification.

4.2.1 Introduction

Movements of the talus, calcaneus, cuboid, and navicular have been described as a closed kinematic chain in which motion of one tarsal bone is followed by motion of other tarsal bones (Huson, 1961). A few elaborated studies have confirmed the coupling of the tarsal bone movements in general whereby the closed kinematic chain was driven by lower leg rotation or rearfoot excursion (Benink, 1985; Lundberg et al., 1989c; van Langelaan, 1983). However, knowledge is still limited related to the magnitude of this movement transmission within the tarsal bones during spatial foot motion which is fundamental in modelling the so called tarsal gearbox (see chapter 2.1).

Limitations came about when trying to measure tarsal bone motion: Due to their invasive or ionising character, motion analysis with intracortical pins or X-ray stereophotogrammetry are not feasible as a routine tool in living subjects. And since the talus is nearly covered by other bones, and the navicular and cuboid are relatively small, motion analysis with skin markers is mainly limited to monitor calcaneal movements. Overcoming these limitations, magnetic resonance (MR) procedures have recently been developed offering insights into discrete tarsal bone positions of different spatial foot excursions (Siegler et al., 2005). Thus, a larger data pool concerning movement transfer between the different tarsal joints can now be established providing information about the function of the tarsal gearbox.

The quantified relation between tibio-calcaneal motion and a joint of the tarsal kinematic chain is of interest because a meaningful established relation would allow the use of common motion analysis with skin markers to model the tarsal gears, a major step towards of the understanding the kinematics of the tarsus.

Thus, this study aimed to determine the movement transmission within the tarsal gearbox as well as between the tibio-calcaneal rotations and single tarsal joints. It is focused on rotations in the frontal and transversal plane because in the sagittal plane, rotations within the tarsal kinematic chain are small, and tibia flexion and extension are mainly performed at the upper ankle without influencing the configuration within the tarsal kinematic chain.

4.2.2 Methods

The study was conducted on two female and six male volunteers without signs of musculoskeletal diseases being 28-35 years old, 165-180 cm high, and weighing 60-82 kg.

Informed written consent in accordance to the local research ethics committee was obtained from all subjects.

Data acquisition

The subjects lay on the MR table and their right foot was fixed into the foot loading and positioning device (see chapter 3.3). A load of 0.5 body weight was applied to the board under the right foot, simulating relaxed standing. Wooden blocks were placed under the feet to control foot position: a flat block (neutral), a 15° wedged ‘pronating’ block (10.8° eversion, 3.3° dorsiflexion, 9.8° abduction), and a 15° wedged ‘supinating’ block (10.8° inversion, 3.3° plantarflexion, 9.8° adduction), see Fig. 3-14a.

Imaging was performed on a 3 Tesla whole-body MR unit (Intera 3T, Philips Medical Systems). A 3D T1 weighted gradient echo sequence with the following parameters was used: repetition time 16 ms, echo time 4 ms, and flip angle 11°; 200 mm field of view; a 288 x 273 acquisition matrix; Fourier interpolated to 512 x 512 pixels; 1.4 mm thick overcontinuous slices with 50% slice overlapping. Thus, the resolution of the reconstructed images was 0.39 x 0.39 x 0.7 mm³, see also Fig. 3-14b. For each subject and test condition 130-160 slices were acquired during about 7-10 min.

Data processing

The 3D reconstruction of the tarsal bones was performed by one operator using AMIRA (Mercury Computer Systems, Berlin, Germany). The resulting surface points were read in MatLab (MathWorks, Massachusetts) to determine the transformations of ‘neutral’ surface point clouds into the surface point clouds of foot pronation and supination, respectively, by an iterative closest point algorithm (Besl and McKay, 1992).

Relative to the neutral foot position, tarsal joint rotations were calculated as finite helical axis rotations projected into the cardinal body planes. To determine the transmission within the tarsal kinematic chain, regression analyses were performed between the rotations of the subtalar, the talo-navicular, and calcaneo-cuboid joint, each in the frontal and transversal plane. A linear relation between these joint rotations was assumed since the joint rotations based rather on foot excursion ($\pm 15^\circ$) in the midst of the physiological range than close to the border (where a non-linear relation should better fit). The regression analysis was extended by tibio-calcaneal rotations to evaluate the potential of skin markers to describe tarsal joint behaviour.

4.2.3 Results

The observed tarsal joint rotations in response to the foot pronation and supination are plotted against each other in the Fig. 4-6 and Fig. 4-7 whereby talo-calcaneal rotations were each defined as independent. In general, the greatest rotations were observed for the talo-

navicular joint, followed by the talo-calcaneal joint; even smaller rotations were found for the calcaneo-cuboid joint.

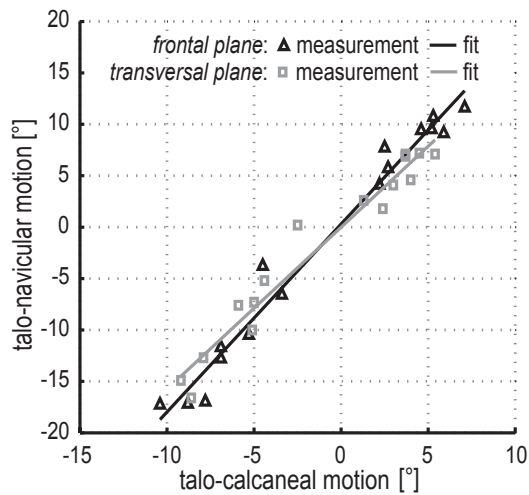


Fig. 4-6 Plot of talo-calcaneal against talo-navicular rotations. A linear curve fit represent both the results of the frontal and the transversal plane whereas the slope of the curve correspond to the transfer of talo-calcaneal into talo-navicular rotations (for more details of the curve fit, see Tab. 4-7).

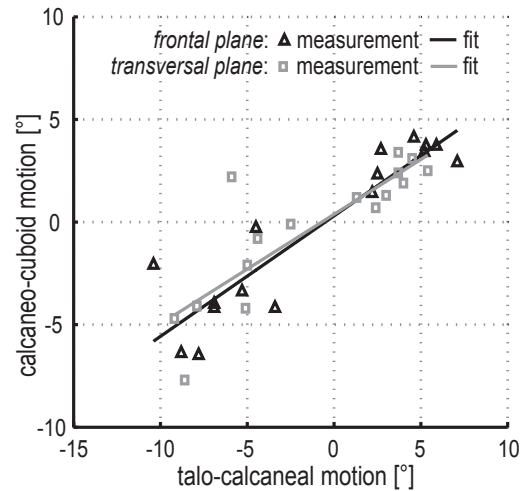


Fig. 4-7 Plot of talo-calcaneal against calcaneo-cuboid rotations. A linear curve fit represent both the results of the frontal and the transversal plane whereas the slope of the curve correspond to the transfer of talo-calcaneal into calcaneo-cuboid rotations (for more details of the curve fit, see Tab. 4-7).

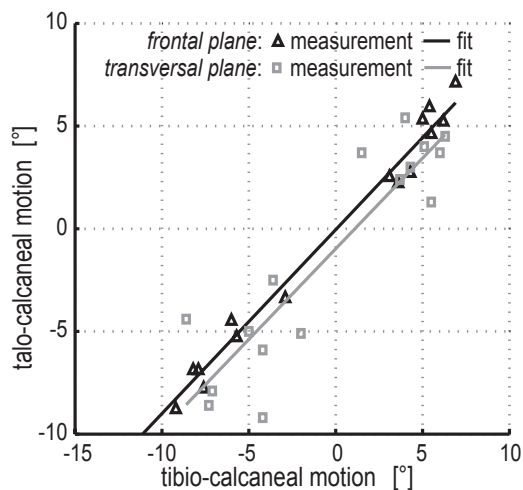


Fig. 4-8 Plot of tibio-calcaneal against talo-calcaneal rotations. A linear curve fit represent both the results of the frontal and the transversal plane whereas the slope of the curve correspond to the transfer of tibio-calcaneal into talo-calcaneal rotations (for more details of the curve fit, see Tab. 4-7).

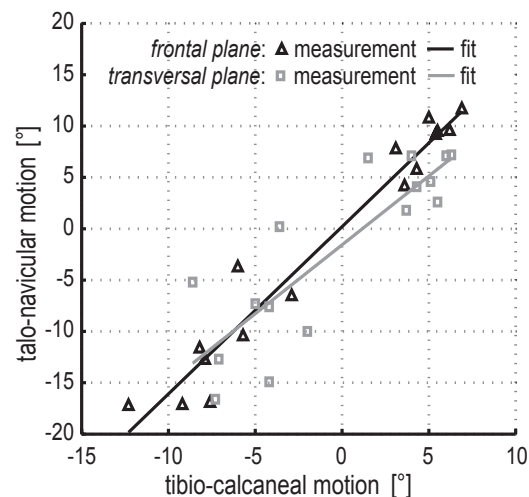


Fig. 4-9 Plot of tibio-calcaneal against talo-navicular rotations. A linear curve fit represent both the results of the frontal and the transversal plane whereas the slope of the curve correspond to the transfer of tibio-calcaneal into talo-navicular rotations (for more details of the curve fit, see Tab. 4-7).

Tab. 4-3 Result and goodness of each linear regression calculated within the tarsal kinematic chain and between tibio-calcaneal and tarsal joint rotations.

| independent vs dependent tarsal motion | plane | a (slope) [-] (CI 95%) | b [°] (CI 95%) | r ² | SD of residuals [°] |
|---|-------------|---------------------------|--------------------|----------------|---------------------|
| <i>talo-calcaneal vs talo-navicular motion</i> | frontal | 1.83 (1.66,2.00) | 0.29 (-0.72,1.31) | 0.97 | 1.8 |
| | transversal | 1.58 (1.38,1.77) | -0.02 (-1.05,1.02) | 0.95 | 1.8 |
| <i>talo-calcaneal vs calcaneo-cuboid motion</i> | frontal | 0.59 (0.44, 0.74) | 0.30 (-0.61,1.21) | 0.83 | 1.6 |
| | transversal | 0.53 (0.34,0.73) | 0.38 (-0.62,1.38) | 0.72 | 1.8 |
| <i>tibio-calcaneal vs talo-calcaneal motion</i> | frontal | 0.90 (0.83,0.96) | -0.05 (-0.48,0.38) | 0.98 | 0.8 |
| | transversal | 0.88 (0.64,1.12) | -0.98 (-2.23,0.27) | 0.82 | 2.3 |
| <i>tibio-calcaneal vs talo-navicular motion</i> | frontal | 1.63 (1.45,1.84) | 0.20 (-1.23, 1.62) | 0.95 | 2.5 |
| | transversal | 1.34 (0.87,1.8) | -1.57 (-4.05,0.90) | 0.73 | 4.4 |

The result and goodness of the linear fit between these rotations are listed in Tab. 4-3. It was found that in corresponding cardinal body planes, talo-calcaneal motion explained between 72% and 97% of the other tarsal joints motion. In particular, the talo-navicular joint is linearly linked with talo-calcaneal joint ($r^2 = 0.95-0.97$): Each degree of frontal and transversal plane rotation of the latter joint resulted in 1.8° and 1.6° talo-navicular motion, respectively.

In Fig. 4-8 and Fig. 4-9, the tibio-calcaneal motion is plotted against the motion in the subtalar and the talo-navicular joint. The result and goodness of the matching fit showed that particularly tibio-calcaneal rotation in the frontal plane is linked with subtalar ($r^2 = 0.98$) and talo-navicular ($r^2 = 0.95$) joint rotations, see Tab. 4-7.

4.2.4 Discussion and conclusions

In this study, quasi-static tarsal bone positions were monitored during foot pronation and supination in the MR. The coupling of the resulting tarsal joint rotations was quantified by a linear regression analysis to determine the function of the tarsal kinematic chain. Since the investigated foot excursions were in the middle of the physiological range linear models were assumed to describe tarsal joint rotations based on subtalar motion. The results show that this assumption was reasonable because (i) the linear curves intersect the y-axis close to zero (see Fig. 4-6 and Fig. 4-7) which ensures that both joint rotations are simultaneously in neutral position, and (ii) the standard deviations of the residuals are in the order of the

precision of the whole MR procedure (see Tab. 4-3) which means that the measurement accuracy mainly contributed to the resting deviation of the depending motion.

One degree of quasi-static talo-calcaneal rotation resulted in talo-navicular rotation of 1.8° (frontal plane) and of 1.6° (transversal plane). This generally confirms the results of earlier quasi-static investigations of lower leg and rearfoot kinematics: Using 10° of tibia external rotation as an input movement, a quotient between resulting talo-navicular and talo-calcaneal finite helical axis rotation of 1.7 was found by van Langelaan (1983). The work of Lundberg and coworkers (1989c) provided also similar quotients between talo-navicular and talo-calcaneal rotations in the frontal and transversal plane: 2.2 and 1.6, respectively. The minor discrepancies between these studies and the present work can be explained by slightly different foot positions and loading conditions. It is also expected that the remarkably different loading condition, i.e. dynamic loading instead of quasi-static, would result in another configuration of the tarsal gearbox. Thus, the observed in vivo transfers of tarsal joint rotations provide a basis for modelling tarsal gears of quasi-static conditions. In dynamic conditions like i.e. running, the required tarsal kinematics have not been quantified so far.

Currently, tarsal kinematics during walking and running may only accurately be measured by intracortical pins. However, since tibio-calcaneal motion in the frontal and transversal plane can be measured with skin markers, and since this motion is mainly performed about the subtalar joint axis, common motion analysis with skin markers may also be used to predict the behaviour of the tarsal kinematic chain. This approach was also evaluated in this study by comparing tibio-calcaneal motion with talo-calcaneal and talo-navicular motion. The results show, that the frontal plane rotations of the talo-calcaneal ($r^2 = 0.98$) and talo-navicular ($r^2 = 0.98$) joint are predictable by tibio-calcaneal rotations. A linear model based only on transversal plane rotations of the tibio-calcaneal joint seems not appropriate enough to explain corresponding tarsal joint rotations since the y-axis intersection of the fitted curve was found not to be close to zero (see Tab. 4-3). It is suggested that transversal plane rotations in the ankle also contribute to the tarsal kinematic chain behaviour. This was subsequently proofed and confirmed: a multiple linear regression analysis with transversal plane motion of the tibio-calcaneal and tibio-talar joint as predictors improves the determination of transversal plane motion of the talo-calcaneal ($r^2 = 0.89$) and talo-navicular ($r^2 = 0.80$) joint remarkably.

In conclusion, this study provided detailed information about the transfer within the tarsal kinematic chain: During quasi-static foot pronation and supination, talo-calcaneal rotation in the frontal plane (transversal plane) are transferred by factor 1.8 (1.6) and 0.6 (0.5) into talo-navicular and calcaneo-cuboid rotations, respectively. Therewith, a basis to model the tarsal gearbox under quasi-static conditions is given; an equivalent basis for dynamic

conditions would be an outstanding project for future investigations. Based on the newly developed MR procedure it was also shown that particularly in the frontal plane, rearfoot concepts can be investigated by tibio-calcaneal rotations because these are correlated with tarsal joint rotations.

4.3 Tarsal joint curvature

The expectation that tarsal joint curvatures offer new insights into the fundamental understanding of tarsal joint rotations is based on the following considerations:

Articulation between i.e. the navicular and the talus is kept by the joint capsule, by ligament and muscle forces acting on the joint. Due to the tarsal joint congruency and the deformable joint cartilage, the articulating area is characterised by a relatively constant surface. If the navicular rotates relative to the talus, the curvature of the talar joint surface will define the movement of the navicular surface being in contact with the talus. In other words, the movement of the whole navicular is prescribed by talo-navicular joint curvature. Of course, knowing the curvature does not provide information concerning the magnitude of joint rotation. However, the navicular is likely to rotate not a lot in a plane in which very small talo-navicular curvatures occur since rotations would require a remarkable movement. Thereby, spatial movements of the navicular as well as of the other tarsal bones are noticeably restricted by anatomical conditions, i.e. the joint capsule. Thus, based on the curvature one can deduce which joint is likely to show large or small rotations. Related to this study this means, subjects with a greater i.e. talo-calcaneal joint curvature may show a larger calcaneal rotation.

4.3.1 Method to analyse tarsal joint curvature

The curvature analysis was based on the MR images acquired during the ‘neutral’ foot excursion as described in chapter 4.1.2. This defined foot orientation ensured the use of the MR coordinate system to analyse the joint curvature. The analysis was performed on the bony surface beneath the articulating joint cartilage. The cartilage layer was not considered since the cartilage-cartilage border could not be segmented in the acquired MR images (Fig. 4-10).

Disregarding the cartilage would not have resulted in different joint curvatures than an investigation of the bony surface beneath the joint since (i) the cartilage layer is evenly thick (Adam et al., 1998; Al-Ali et al., 2002), (ii) the layer are very small compared to the radii of tarsal joint



Fig. 4-10 Sagittal MR image of the right foot. The talus is emphasised. The cartilage layers of the talar joints are thin and the cartilage-cartilage border is hardly detectable.

curvature (Beillas and Lavaste, 1999), and (iii) the cartilage surface is of equal size compared to the cartilage-bone interface (Al-Ali et al., 2002), see Fig. 4-15. Hence, each tarsal joint surface was reasonably marked on the tarsal bone surface.

Description of joint surface by points evenly distributed in one plane

A plane grid was computed for each spatial tarsal joint surface based on the coordinates along the two largest dimensions of the joint surface points (like the entire analysis, this was done in MatLab (MathWorks, Massachusetts)). Thereby, hundred lines were chosen per dimension to mesh the surface points, and intersections of these lines constituted the evenly distributed points of the grid. This grid determined the lines/points of the curvature analysis. This means that depending on the tarsal joint size every 0.02 - 0.04 cm the curvature was evaluated which was almost in the order to the resolution of the acquired surface point cloud: The mean distance between neighbouring points was 0.02 cm. Note, that the fineness of the mesh did not contribute to the curvature analysis if at least thirty lines per dimension were used: From this point on, resulting difference were randomly distributed and in the order of less than 0.1 cm.

Since the talo-navicular joint is spherically shaped and the articulating surface of the calcaneo-cuboid joint is almost parallel to the frontal plane, an orientation of the grid parallel to that plane was chosen (see Fig. 4-11a: red and green lines of the mesh are going from inferior to superior and medial to lateral, respectively). This warranted a straight comparison of joint curvatures along the grid lines with the corresponding joint rotations in the cardinal body planes (dorsi/plantarflexion and ab/adduction). The grid of the posterior talo-calcaneal joint was orientated such that one dimension of the grid was along the largest dimension of the joint surface (see Fig. 4-12a). Thus, the curvatures offered information about the cylindrical shape of the subtalar joint providing an interpretation of the calcaneal motion of the dynamically classified runners.

The plane grid, given by points with (x,y) cartesian coordinates, was then fitted to the remaining dimension of the joint surface such that $z = f(x,y)$. Thereby, a triangle-based cubic interpolation was used to calculate the surface 'height' at the points of the grid.

Curvature analysis

Based on the resulting mesh, the curvature was computed at the intersecting points in x and y direction. Therewith, the complete joint surface was defined by the radii of curvature as shown in Fig. 4-11b for the navicular surface articulating with the talus and in Fig. 4-12b for the posterior talar surface articulating with the calcaneus.

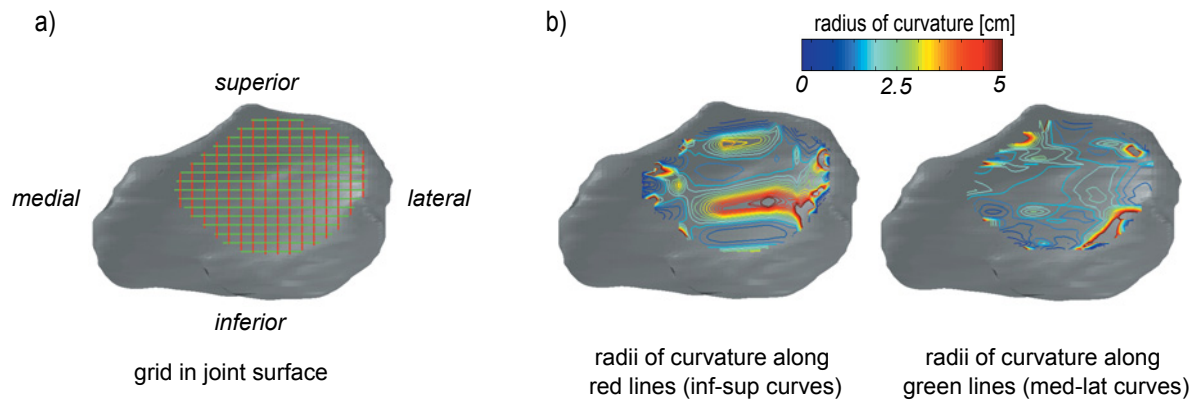


Fig 4-11 Illustration of navicular joint curvature analysis. At first, a regularly grid in the frontal plane was fitted into the joint surface (a). Along the dimensions of the grid, the radii of curvature were determined (b).

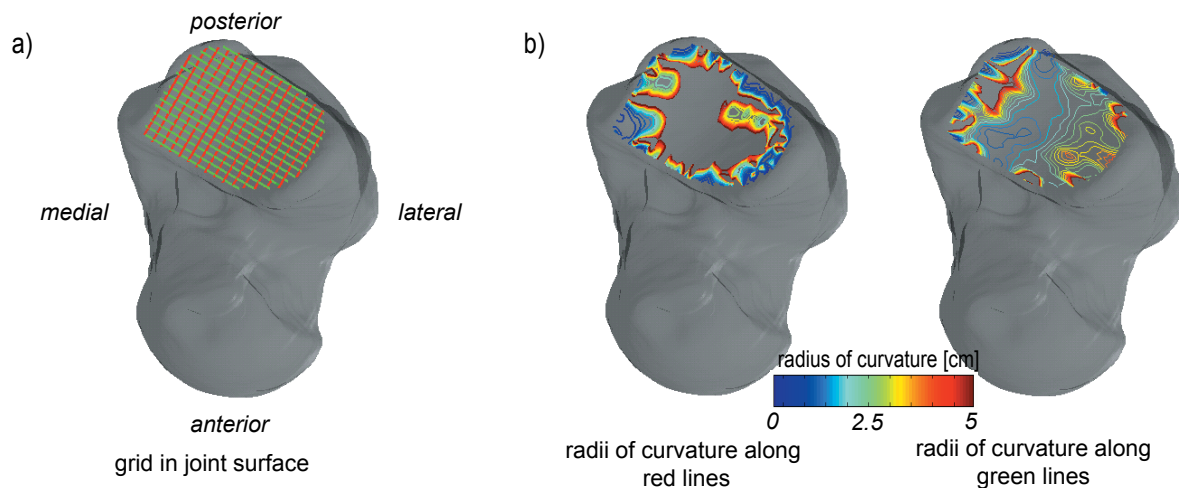


Fig. 4-12 Illustration of the joint curvature analysis at the posterior talar surface articulating with the calcaneus. A grid was orientated along the two greatest dimensions of the joint surface and then fitted to it (a). Again, along to the dimensions of the grid, the radii of curvature were computed (b).

With respect to the talo-navicular and calcaneo-cuboid joint, the comparison of joint motion and joint curvature focused on the transversal plane. Motion in the frontal plane could not be compared since the curvature computation based on a grid in this plane; consequently, only curvatures of the joint surface in the other planes were available. Because tarsal joint rotations were remarkably small in the sagittal plane (see Fig. 4-3), comparisons in this plane were also disregarded.

With respect to the talo-calcaneal joint, the analysis focused on the curvature along the greatest dimension of the joint surface (green lines in Fig. 4-12a). In the other evaluated dimension, corresponding rotations were expected to be negligible since the related curvatures were found to be very small (see Fig. D-1 and Fig. D-3 in the appendix D of this thesis showing mainly radii of curvatures greater than 5 cm of the talar and calcaneal surface of the subtalar joint).

To characterise the radii of joint curvatures of the six subjects, and to provide a comparison of radii of joint curvature and joint motion, two approaches were chosen to summarise the relevant curvatures:

- (1) Including the beginning and ending of the mid line, ten equally spaced points on the mid line of the surface grid were selected. Disregarding the two outmost points at each border, the radii of curvature at these points were computed and compared between the subjects (see Fig. 4-13). This approach was chosen on the very reasonable assumptions that the mid of the joint surfaces is mainly in contact during physiological joint motion.
- (2) The second approach based on the distribution of the radii of curvatures. Assigning the radii into ‘bins’ with a range of 0.1 cm, a gaussian distribution was computed to describe the relation of the radius (x) and its relative frequency (y), see also Fig. 4-14:

$$y = a e^{-0.5((x-\mu)/\sigma)^2} \quad \text{with } a = 1/((2\pi)^{0.5} \sigma) \quad (\text{eq. 4-1})$$

The mean μ and the standard deviation σ of the fitted distribution function are then used to characterise the joint surface radii of curvature of the six subjects each.

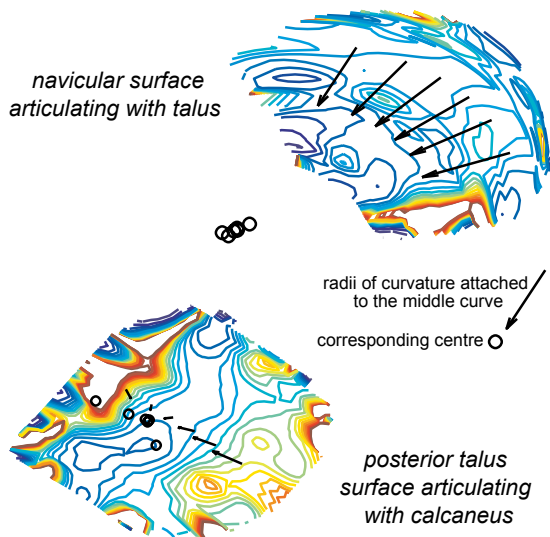


Fig. 4-13 Contour plots of the navicular surface articulating with the talus and of the posterior talar surface articulating with the calcaneus. The six points of each mid curve were highlighted which were each used for the curvature comparison between the subjects.

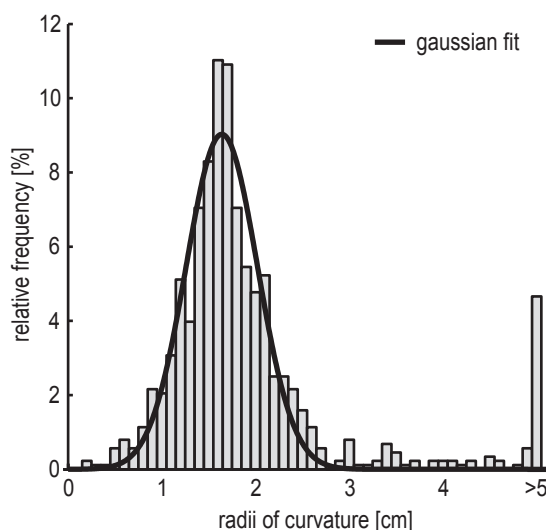


Fig. 4-14 Example of a distribution of the radii of curvature at the navicular surface articulating with the talus. A gaussian fit was computed to describe the relation of the radii and the relative frequencies. Mean and standard deviation of the fitted distribution were used for the curvature comparison between the subjects.

4.3.2 Results of the tarsal joint curvature analysis

The projected tarsal joint surfaces of all subjects with contour plots of radii of curvature are shown in the appendix D of this thesis, Fig. D-1 to Fig. D-12. Box plots of the radii of curvature calculated each on the mid line of the articulating surfaces are presented for the subtalar (Fig. 4-15) and the talo-navicular joints (Fig. 4-16), respectively. Both joints showed similar results: In agreement with tarsal joint congruency, the subjects' median radii were each almost equal for both articulating surfaces. But although individual differences occurred, the overlapping notches of 'normal' and 'outlier' subjects revealed no significant distinction between the groups. This curvature comparison was not performed on the calcaneo-cuboid joint since a great radius variability in the mid line occurred (see Fig. D-10 and Fig. D-12, radii parallel to x-axis in the mid of z-values).

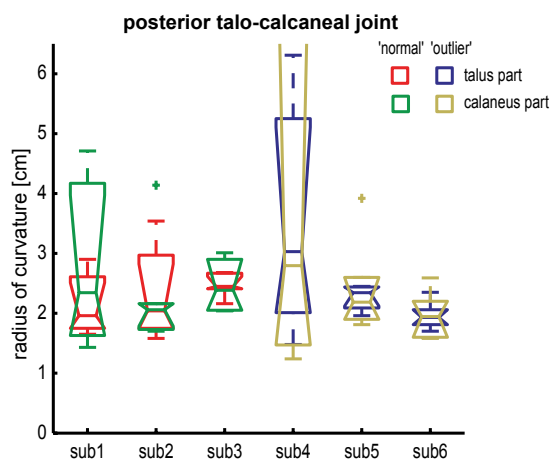


Fig. 4-15 Box plots of the radii of curvature on the mid line of the posterior articulating surfaces at the subtalar joint. Both the calcaneal and the talar side showed similar radii for each subject. And, the radii of 'normal' and 'outlier' subjects were not significant different.

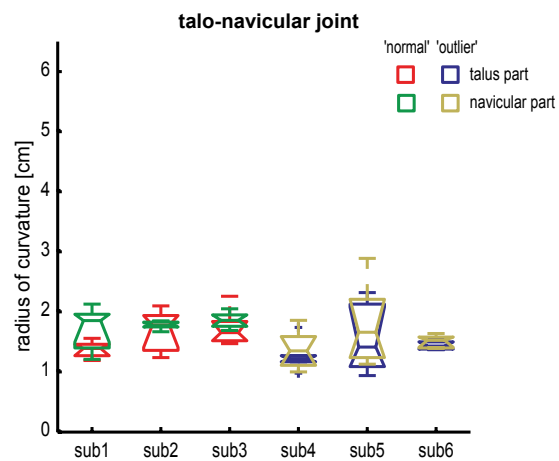


Fig. 4-16 Box plots of the radii of curvature on the mid line of the articulating surfaces at the talo-navicular joint. Both the talar and the navicular side showed similar radii for each subject. And, the radii of 'normal' and 'outlier' subjects were not significant different.

The gaussian distribution of the radii of curvature computed for all subjects and tarsal joints are presented in Fig. 4-17. The results and goodness of each fit are listed in Tab. 4-4. In general, the subjects of the 'normal' and 'outlier' group showed similar distributions in each tarsal joint surface. Thereby, a gaussian function describes the curvature distribution quite well, particularly of the subtalar ($0.60 < r^2 < 0.95$) and talo-navicular joint ($0.91 < r^2 < 0.99$). Lower correlation coefficients were found in the calcaneal-cuboid joint ($0.37 < r^2 < 0.82$) because no distinct frequency of radii of curvature occurred between 0 and 5 cm; see also the relatively flat curvature distribution of this joint in Fig. 4-17.

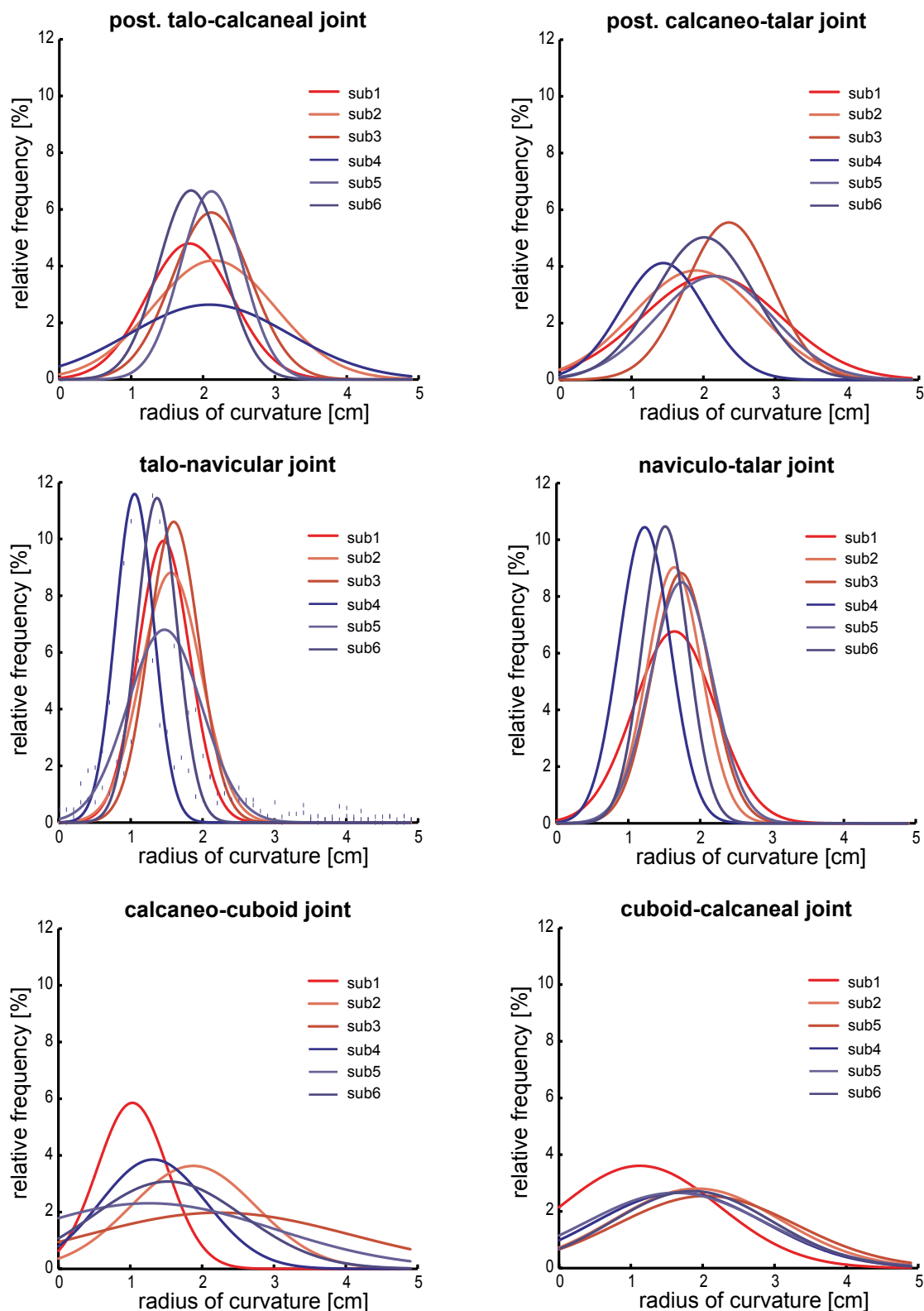


Fig. 4-17 Gaussian distribution of the radii of curvature computed for all subjects and tarsal joints. The evaluated surface of the joint is named first in each figure title. At each articulating surface, the distribution of the radii of all subjects were close to each other. For more details of the gaussian fit, see Tab. 4-4.

Tab. 4-4 Results and goodness of each gaussian fit computed for the tarsal joint radii of curvature. The gaussian parameters were the mean μ and the standard deviation σ .

| joint | bone | gaussian parameter | 'normal' group | | | 'outlier' group | | |
|------------------|-----------|--------------------|----------------|-------------|-------------|-----------------|-------------|-------------|
| | | | <i>sub1</i> | <i>sub2</i> | <i>sub3</i> | <i>sub4</i> | <i>sub5</i> | <i>sub6</i> |
| subtalar | talus | μ | 1.81 | 2.15 | 2.11 | 2.09 | 2.12 | 1.83 |
| | | σ | 0.85 | 1.21 | 0.77 | 1.58 | 0.61 | 0.64 |
| | | r^2 | 0.76 | 0.81 | 0.94 | 0.72 | 0.90 | 0.87 |
| | calcaneus | μ | 2.11 | 1.90 | 2.36 | 1.44 | 2.16 | 2.01 |
| | | σ | 1.37 | 1.24 | 0.85 | 0.83 | 1.14 | 0.98 |
| | | r^2 | 0.78 | 0.76 | 0.84 | 0.61 | 0.78 | 0.88 |
| talo-navicular | talus | μ | 1.46 | 1.56 | 1.60 | 1.06 | 1.47 | 1.37 |
| | | σ | 0.51 | 0.59 | 0.49 | 0.38 | 0.73 | 0.40 |
| | | r^2 | 0.95 | 0.98 | 0.96 | 0.93 | 0.94 | 0.91 |
| | navicular | μ | 1.64 | 1.64 | 1.73 | 1.23 | 1.74 | 1.51 |
| | | σ | 0.80 | 0.53 | 0.57 | 0.51 | 0.61 | 0.45 |
| | | r^2 | 0.95 | 0.93 | 0.97 | 0.97 | 0.97 | 0.93 |
| calcaneal-cuboid | calcaneus | μ | 1.03 | 1.88 | 2.24 | 1.32 | 1.26 | 1.53 |
| | | σ | 0.69 | 1.23 | 2.60 | 1.05 | 2.48 | 1.48 |
| | | r^2 | 0.74 | 0.82 | 0.37 | 0.70 | 0.50 | 0.71 |
| | cuboid | μ | 1.13 | 1.92 | 2.05 | 1.68 | 1.62 | 1.86 |
| | | σ | 1.56 | 1.65 | 1.76 | 1.68 | 1.78 | 1.58 |
| | | r^2 | 0.68 | 0.74 | 0.75 | 0.56 | 0.73 | 0.67 |

4.3.3 Discussion of the tarsal joint curvatures

It is a common opinion that foot function and foot morphology depend on each other (Inman, 1976; Sammarco et al., 1973). However, this relationship has rarely been quantified, in particular it is not known how joint curvatures influence joint rotations. To get more insights, runners were initially classified based on their tibio-calcaneal motion during the beginning of the stance phase during running. Then, tarsal joint curvatures of the 'normal' and 'outlier' classified runners were investigated since tibio-calcaneal motion is linked with talo-calcaneal motion, and rotations in the talar joints are coupled in the so called tarsal gearbox (see chapter 4.2).

Both the curvature analysis of the mid part of the joint surface and the analysis of the curvature distribution of the complete joint surface showed similar results for the 'normal' and 'outlier' group in all investigated tarsal joint surface curvatures. Individual differences of the radii of curvature were in the order of 0.5 cm (see Fig. 4-15 to Fig. 4-17 and

Tab. 4-8). Assuming a large rotation of 20° , this radius difference of 0.5 cm would result in an arc length difference of less than 0.2 cm. It can be argued that this spatial movement is too small to be really restricted by anatomical conditions. Considering again a large rotation of 20° , the spatial movement would be different in the order of 0.5 cm if the radii of curvature differed by 1.4 cm. However, it is not known whether such a large variability in a curvature is present in healthy tarsal joints. There is something to be said against such a variability: The radii of curvature of the tarsal joints of female and male subjects with a shoe size of EU 36 to EU 46 varied only up to 0.5 cm. Thus, and further based on the multiplicity of other parameters influencing tarsal joint kinematics, i.e. those of muscles and ligaments, it is concluded that the contribution of tarsal joint curvatures on the magnitude of tarsal joint rotations is negligible. Of course, joint curvature may contribute to the relation of joint rotations in different cardinal body planes, but in this thesis, the classification of the runners was based on either small or large joint rotations (see Fig. 4-2) and not on quotients of these rotations.

In summary, tarsal joint curvatures provide no interpretation of the tibio-calcaneal kinematics of the 'normal' and 'outlier' subjects. Hence, a distinct dependence of the magnitude of foot motion on foot morphology is not supported by this work. In other words, morphological parameters of the tarsal bones, even three-dimensionally and precisely measured, seem to be the wrong approach to classify feet in view of a prediction of tarsal bone or rearfoot motion during quasi-static or dynamic movements. Consequently, other parameters than the morphology seem to define the magnitude of tarsal kinematics. One of them, the stiffness of the ligaments, will be discussed in the following chapter.

4.4 Ligament properties: a discussion and an outlook

As shown in the previous chapters, the different calcaneal motion of the ‘normal’ and ‘outlier’ subjects can not be explained based on:

- (1) the demography of subjects, since both groups included both one woman and two men, and subjects were of similar age, height, and weight (see Tab. 4-1),
- (2) the running speed, since in each group subjects with similar running speed were measured (see Tab. 4-1),
- (3) the neuromuscular control, since only calcaneal motion during the first 50 ms of stance phase was considered,
- (4) the tarsal joint curvatures, since the differences between the subjects were too small to remarkably contribute to the magnitude of tarsal joint rotations (conclusion of chapter 4.3).

Hence, the cause of the observed different calcaneal motion remains unclear. In the present study, no further factor influencing tarsal joint rotations was quantified, i.e. external forces, muscle forces or ligament properties. Thus, only hypothetical considerations can be made upon their contribution. In this manner, the influence of ligament properties on calcaneal motion is discussed in the first part of this chapter. Due to the apparent lack of appropriate methods measuring ligament properties, the second part of this chapter presents an outlook how ligament length during the stance phase of walking or running may be assessable.

4.4.1 Influence of initial ligament properties on calcaneal motion

The sixteen subjects whose kinematics of the lower extremities were used to classify feet (see chapter 4.1) were all injury free during at least 6 months before the investigation. However, the anamneses of the subjects showed an unexpected correlation between the classification as a ‘normal’ or ‘outlier’ subject and previously torn ankle ligaments (supination trauma) or ankle sprains: None of the ‘normal’ subjects had ever had an ankle injury, but the lateral ligaments of the right ankle of all but one of the ‘outlier’ subjects were torn or heavily strained, see Fig. 4-18 (A clinician diagnosed the remaining ‘outlier’ subject with ‘slacking foot joints’. Biomechanically, this was confirmed by the fact that this subject showed the greatest range of calcaneal motion out of all subjects. This indicates why this subject was classified as an ‘outlier’).

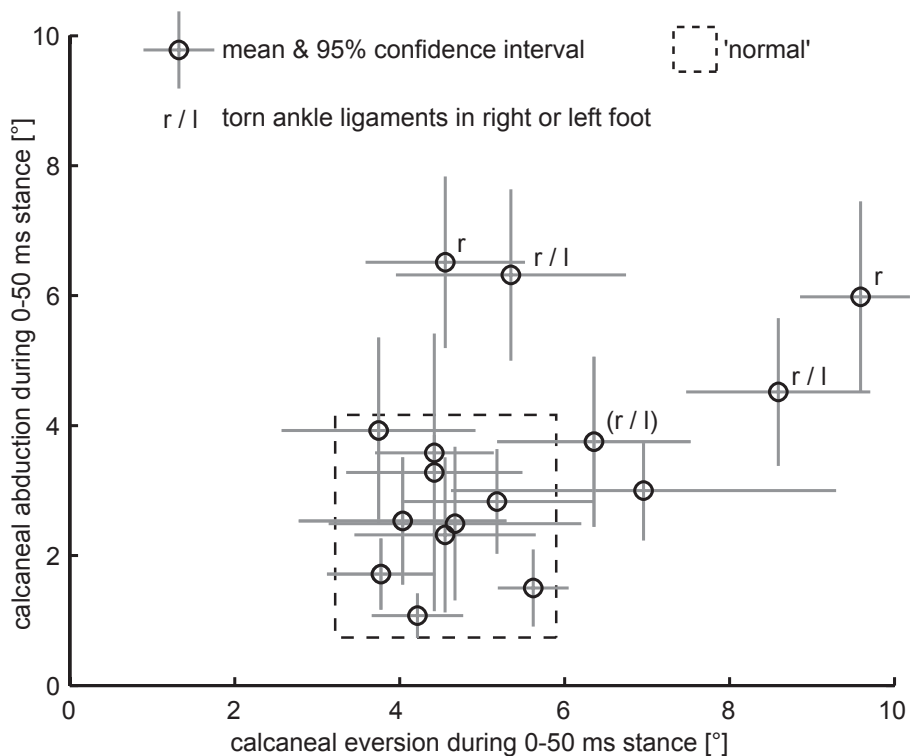


Fig. 4-18 Calcaneal eversion and abduction of the right foot during running. The as 'normal' defined motion is framed. Additionally, the occurrence and side of torn ankle ligaments or of heavily sprained ankles are given.

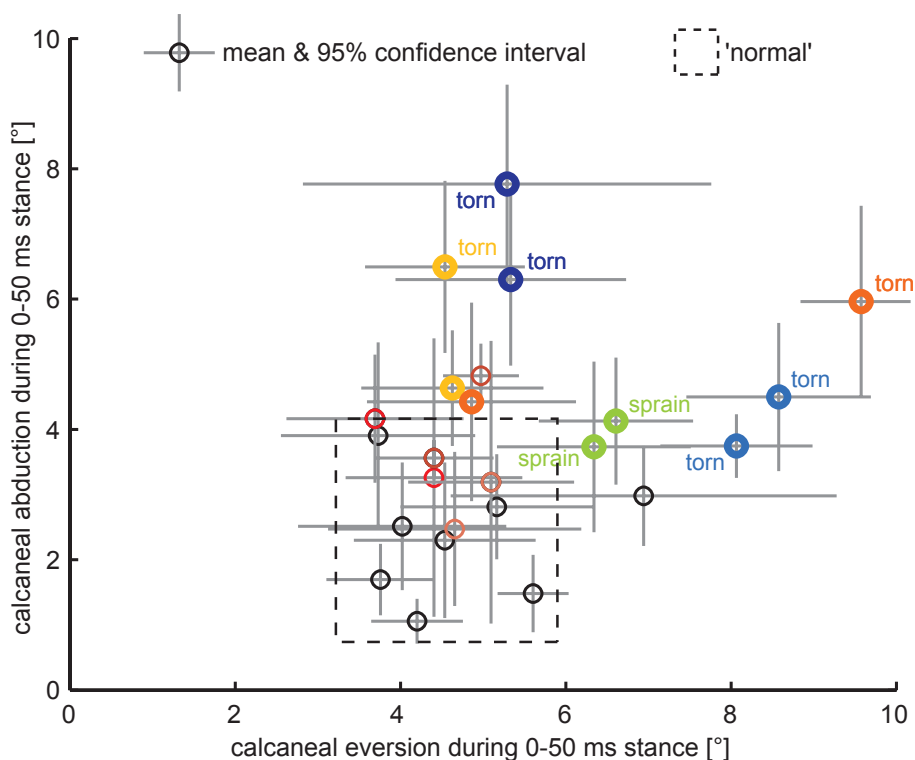


Fig. 4-19 Calcaneal eversion and abduction during running. Right and left calcaneal motion are given in the same colours for the subjects with torn ligaments (or heavily sprained ankles) as well as for the 'normal' subjects of the MR investigation.

Considering that ankle ligaments restrict calcaneal motion, in particular, the calcaneofibular ligament calcaneal abduction (Colville et al., 1990; Nigg et al., 1990; Renstrom et al., 1988) and the anterior talofibular ligament calcaneal reduces abduction (Cawley and France, 1991; Colville et al., 1990; Nigg et al., 1990) and eversion (Cawley and France, 1991), it may be concluded that the initial properties of these ligaments were not restored during the healing process. Consequently, subjects with previously torn ankle ligaments showed more calcaneal abduction and/or eversion, and hence, were assigned to the ‘outlier’ group.

The tenability of this hypothetical consideration was checked by additionally evaluating calcaneal kinematics of the contra-lateral foot: Compared to ‘previously injured’ feet, contra-lateral ‘healthy’ feet should show ‘normal’ calcaneal motion during the first 50 ms of stance phase ($<4^\circ$ abduction and $<6^\circ$ eversion). The comparison shows that calcaneal motion of both feet was only greater than ‘normal’ if both ankles were injured once (see (light) blue and green marked subjects in Fig. 4-19). Further, if the contra-lateral ankle was not injured, its calcaneal motion was almost ‘normal’ (see yellow and orange marked subjects in Fig. 4-19). And, subjects with no ankle injuries such as the chosen ‘normal’ subjects of the morphology investigation (marked in red colours in Fig. 4-19) showed ‘normal’ calcaneal kinematics for both feet. Thus, the hypothetical consideration that the initial ligament properties contribute to the magnitude of calcaneal motion during the begin of stance phase was confirmed. However, the precise quantification of the influence of ligament properties on three-dimensional tarsal joint kinematics should be aimed in future investigations.

4.4.2 An approach to measure ligament lengths during the stance phase of gait

The following approach to measure ligament lengths during the stance phase of gait is based on a combination of i) the newly developed MR imaging procedure of this thesis and ii) foot bone kinematics investigated in a study of the Karolinska Institutet, Stockholm, in collaboration with the Centre for Rehabilitation and Human Performance Research, University of Salford, and the Institute for Biomechanics, ETH Zurich.

Although it was not intended to determine ligament insertions, the MR sequence provided at least a few of them, i.e. those of the posterior tibiotalar ligament, see Fig. 4-20a. On the other hand, accurate kinematic data during running with intracortical pins (Fig. 4-20c) was opto-electrically registered.

To match both data, a coordinate system had to be defined for both registrations in which the ‘neutral’ positions of the foot bones were equally positioned (have the same coordinates). Therefore, a marker of similar size was placed just to the most posterior part of the rearfoot both during neutral foot excursion in the MR (registration A) and the relaxed

standing with intracortical pins (registration B). These markers defined the origin of the required coordinate system. Considering also that during both registrations the foot length axis (most posterior part of the rearfoot to second toe) was placed parallel to an axis of the global coordinate system, bony positions in both registrations were equal, except for a permutation of the coordinates. Thus, the ‘neutral’ location of the bones assessable in the MR were transferable to the relaxed standing trial of the opto-electrical measurement. Since the markers opto-electrically registered during running were rigidly attached to the bones, their transformation (Fig. 4-20d) was equal to that of the linked bone². This means that ligament insertions were computable during the entire stance phase of running. And consequently, the ligament strain relative to relaxed standing and absolute ligament length, respectively, were quantifiable during motion.

This approach was exemplified on the length behaviour of the posterior tibiotalar ligament

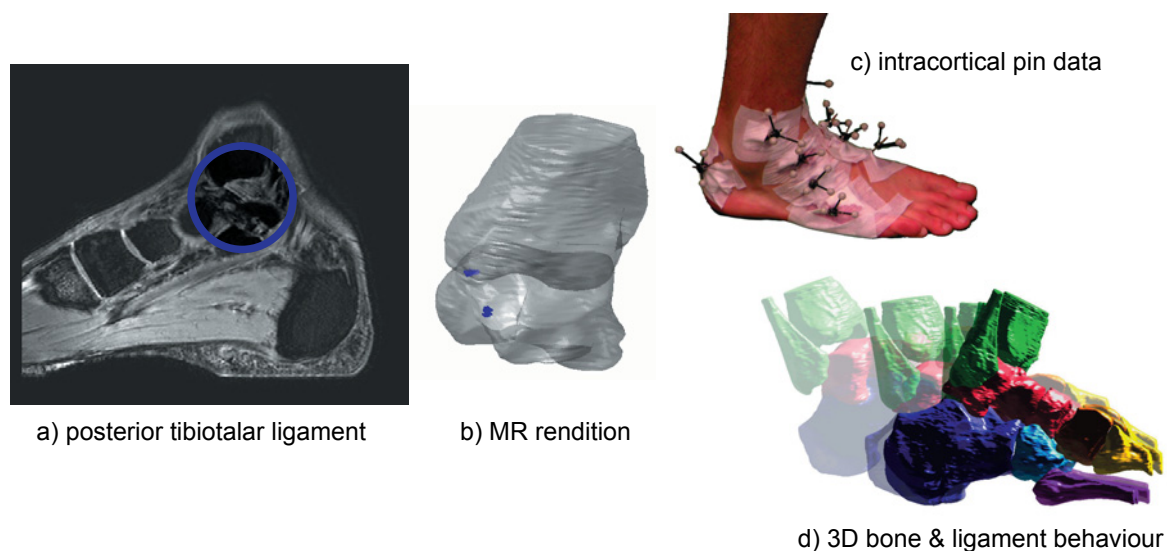


Fig. 4-20 Procedure to investigate ligament behaviour during motion. At first, ligament insertions were gained in the MR, i.e. for the posterior tibiotalar ligament (1a). Therewith, the spatial position of the ligaments on the reconstructed bones was given (1b). On the other hand, foot bones with intracortical pins were opto-electrically registered during motion (2). Matching the references of the MR and pin measurement allowed to track bone motion (3) and thus, provided data of ligament length behaviour.

of one subject during running. The insertion area was determined in the MR images acquired during the ‘neutral’ foot position (for MR sequence and foot positioning/loading details see chapter 3.3). The distance between the centres of each insertion area was used to determine ligament length: In the ‘neutral’ foot position its length was 1.35 cm which was in the order of values provided by the literature (Luo et al., 1997; Siegler et al., 1988b).

² This requires only that the transformation between two positions is computed on a rotation before a translation.

On the other hand, kinematic data of the tibia and talus during nine running trials (mean velocity 2.2 m/s) was available providing the ligament length behaviour during motion. The mean ligament strain of these trials is plotted over the entire stance phase in Fig. 4.21 beside the tibio-talar motion in the cardinal body planes. That the posterior tibiotalar ligament was strained during ankle dorsiflexion and relaxed during plantarflexion is in agreement with in vitro studies introducing foot motion manually (Bruns and Rehder, 1993; Luo et al., 1997). Hence, it is demonstrated that MR imaging of ligament insertions in combination with a method monitoring foot bone motion during the stance phase of gait could provide new insights into foot ligament behaviour and its contribution to lower leg and rearfoot kinematics. Perhaps, even the cause of different tarsal kinematics may be clarified using this approach.

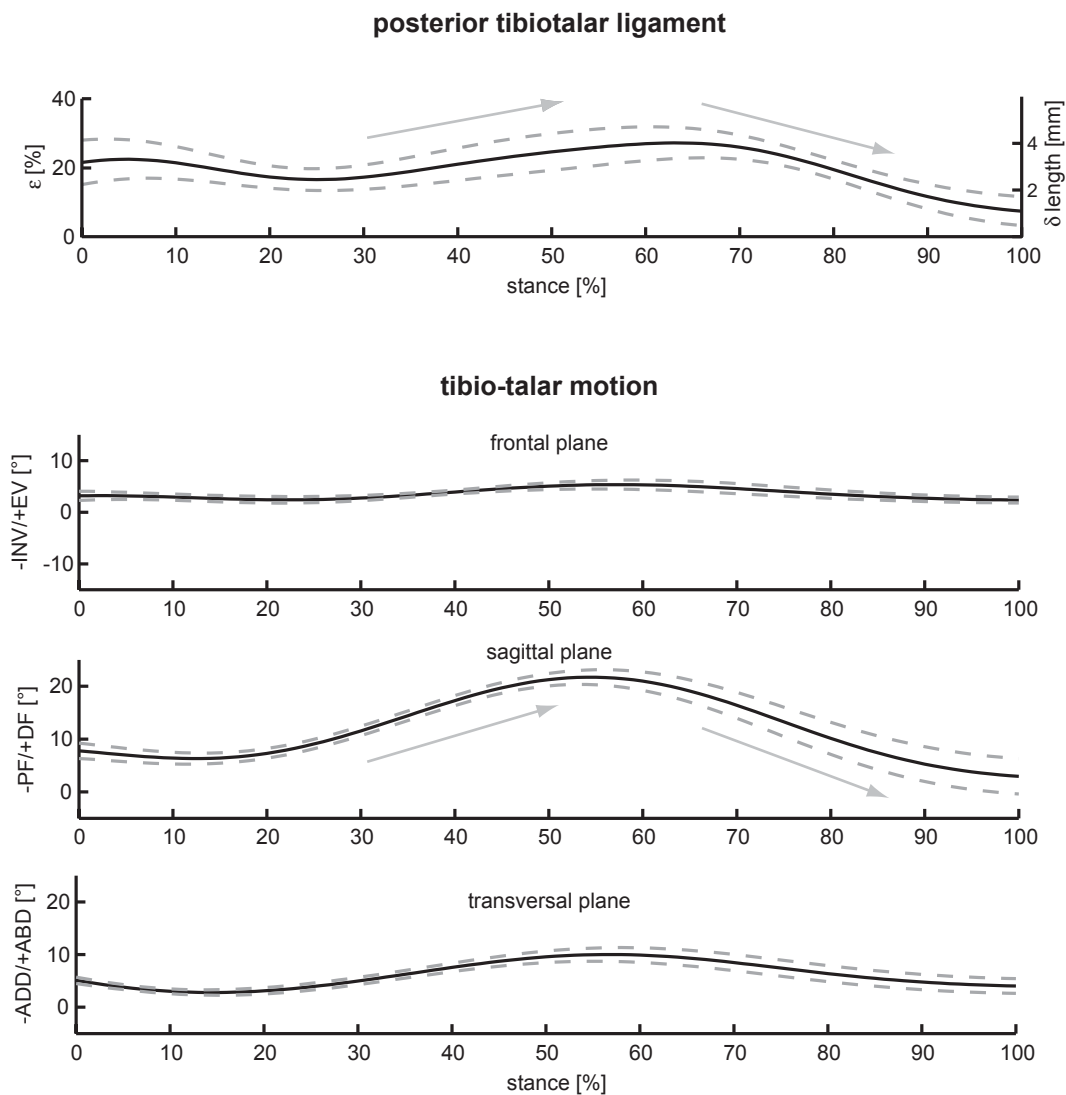


Fig. 4-21 Mean and 95% confidence limits of the posterior tibiotalar ligament strain during the stance phase of running. Additionally, relative tibio-talar motion (ankle joint) is presented in the cardinal body planes. During ankle dorsiflexion, the posterior tibiotalar ligament was strained; during plantarflexion it was relaxed.

Chapter 5

Conclusions

The general motivation behind the research in this thesis is given by the common practise to use morphological foot parameters to predict foot motion although knowledge about this deduction is very limited: There is a lack of methods to determine three dimensional foot bone morphology and kinematics. Adequate procedures would not only offer new insights into the still uncertain relationship of foot morphology and foot function but also would have an impact on the demanding validation of current concepts representing tarsal kinematics.

Thus, this thesis aims at i) the development of procedure to quantify tarsal joint motion and tarsal bone morphology based on magnetic resonance imaging (chapter 3), and ii) the application of this procedure to determine the dependence of foot motion on foot morphology (chapter 4). The most important contributions of the presented work are summarised in the following paragraphs.

5.1 Most important contributions

Chapter 3.1 addresses the reproducibility of the used semi-automatic image segmentation, as this is a mandatory prerequisite for image processing. It was shown that operators performing the segmentation are interchangeable without influencing the magnitude of reconstructed tarsal bone volume, principal axes and their related moments of inertia, and the tarsal joint surfaces. Thus, the curvature analysis based on semi-automatically segmented bones can be regarded as reliable. Further, it became evident that in contrast to an kinematic analyses method based on principal axes, a method using an iterative surface point cloud fit is negligibly affected by repeated segmentations.

Chapter 3.2 reports the influence of magnetic resonance (MR) slice orientation on the accuracy of kinematic analyses methods. The feasibility of a method evaluating kinematics acquired in the MR by a surface point cloud fit is warranted since its accuracy was estimated to be in the order of common video motion analyses. Its accuracy was also twice as good as a method based on principal axes whereas that MR kinematic analyses approach has limitations regarding symmetrical bones. It was concluded that the registration of surface point clouds acquired in the MR is an accurate and appropriate method to analyse tarsal bone kinematics in vivo and non-invasively.

Chapter 3.3 establishes a MR compatible device facilitating arbitrary spatial foot positions and axial foot loading. Compared to a ‘neutral’ foot position, an explainable motion transfer from the device to the calcaneus was found resulting in quasi-static tarsal joint motion. Repeated measurements showed that equivalent to common video motion analyses, only a few degrees are necessary to distinguish between tarsal joint kinematics. Thus, a new

MR imaging procedure was established providing investigations of spatial tarsal joint motion in combination with three-dimensional rearfoot morphology.

Chapter 3.4 presents a comparison between tarsal bone motion measured with magnetic resonance imaging and measured by opto-electrical registration of intracortical pin mounted markers. Although knee flexion and externally applied load were carefully controlled, joint rotations during lying in the MR and when standing with pins did not correlate. However, the quasi-static tarsal joint rotations acquired by magnetic resonance imaging of a pronated foot correlated significantly to tarsal joint rotations at 20% of stance phase of running. Thus, the newly developed procedure is a promising approach to investigate foot kinematics which would otherwise only be available by the use of invasive techniques.

Chapter 4.1 introduces a classification of runners based on their calcaneal kinematics during the beginning of stance phase of running. It was shown that the same runners can not be adequately classified during quasi-static foot excursions. Hence, the different calcaneal kinematics depended on the dynamic conditions of running.

Chapter 4.2 provides a basis to model the tarsal gearbox in the frontal and transversal plane under quasi-static conditions. During physiological tarsal joint rotations, linear models allow a determination of the transmission within the tarsal gearbox. Particularly in the frontal plane, rearfoot concepts like the tarsal gearbox can also be investigated by tibio-calcaneal rotations because these have been shown to be correlated with tarsal joint rotations. This means, opto-electrical registrations of tibio-calcaneal rotations can also be used to validate current concepts of the tarsal bone kinematics.

Chapter 4.3 investigates the tarsal joint curvature of subjects classified based on their calcaneal kinematics during running. A distinct dependence of the magnitude of rearfoot motion on tarsal joint curvatures is not supported. Morphological parameters of the tarsal bones are not feasible to predict the magnitude of tarsal bone or rearfoot motion. Morphological parameters, even three-dimensionally and precisely measured, seem to be the wrong approach to classify feet in view of a prediction of rearfoot motion. Thus, the results of this thesis do not support the dependence of foot motion on foot morphology.

Chapter 4.4 discusses the contribution of ligament properties on calcaneal kinematics. The results indicate that initial ligament properties changed due to an injury resulting in more calcaneal motion during the beginning of stance phase of running than normal. As exemplified on one ligament, MR imaging of ligament insertions in combination with a method to monitor foot bone motion enables investigations of foot ligament behaviour.

5.2 Outlook

The present work does not support the dependence of foot function on 'internal' tarsal bone morphology such as joint curvature which is in agreement with other studies reporting no relation between foot kinematics and predefined 'external' foot morphologies. Thus, research on foot biomechanics should change the focus away from morphology towards other factors contributing to joint mechanics. In particular, ligament properties of subjects showing different (rear-)foot kinematics should be evaluated because ligament properties may vary systematically between them as indicated in this thesis: Subjects with ankle sprains or torn ankle ligaments showed reduced ligament stiffness at touchdown resulting in enhanced rearfoot motion. Thereby, the newly developed magnetic resonance imaging procedure enables non-invasive investigations correlating of the strain behaviour of ligaments with different quasi-static tarsal joint motion.

The monitoring of ligament strain during the stance phase of gait is more challenging than during quasi-static motion. A feasible approach is to combine magnetic resonance imaging (to reconstruct bones as well as ligament insertions) with opto-electrical registrations of intracortical pins attached to lower leg and foot bones (to get kinematic data). In this thesis, this approach was exemplified on one ligament of one subject during running. The work will be extended to other ligaments and to the few further subjects of which kinematic data during walking and running is available. By doing that foot kinematics can be modelled for the first time three-dimensionally for the stance phase of gait based on in vivo ligament strain and joint motion. Ligaments behaving isometric (during a period of stance phase) may be identified and then considered as guiding elements in a kinematic chain (representing that period of stance phase).

Since intracortical pin studies are not the preferable method to investigate subjects groups on a larger scale, other methods must be developed to register bone positions and ligament insertions. One possibility is video-fluoroscopy, a method that has already been established at the Institute for Biomechanics, ETH Zurich, to register knee joint kinematics during walking. Applying this approach to the foot should provide a basis to investigate foot bone kinematics and ligament behaviour during motion. In combination with this, magnetic resonance imaging can provide the required three-dimensional reconstructions of the bones and ligament insertions. In future studies even muscle activity and ground reaction forces should be measured simultaneously. When doing that a comprehensive interpretation of different foot joint kinematics should be achieved. This may also lead into more acceptable foot classifications ensuring a more successful prevention and treatment of foot injuries than today.

References

- Adam C, Eckstein F, Milz S, Putz R (1998). The distribution of cartilage thickness within the joints of the lower limb of elderly individuals. *J Anat* 193: 203-214.
- Agartz I, Okuguwa G, Nordstrom M, Greitz D, Magnotta V, Sedvall G (2001). Reliability and reproducibility of brain tissue volumetry from segmented MR scans. *Eur Arch Psychiatry Clin Neurosci* 251: 255-261.
- Al-Ali D, Graichen H, Faber S, Englmeier KH, Reiser M, Eckstein F (2002). Quantitative cartilage imaging of the human hind foot: Precision and inter-subject variability. *J Orthop Res* 20: 249-256.
- Allinger TL and Engsborg JR (1993). A method to determine the range of motion of the ankle joint complex, in vivo. *J Biomech* 26: 69-76.
- Ambagtsheer JB (1978). The function of the muscles of the lower leg in relation to movements of the tarsus. *Acta Orthop Scand* 49 (Suppl 172): 1-196.
- Apkarian J, Naumann S, Cairns B (1989). A three-dimensional kinematic and dynamic model of the lower limb. *J Biomech* 22: 143-155.
- Arndt A, Westblad P, Winson I, Hashimoto T, Lundberg A (2004). Ankle and subtalar kinematics measured with intracortical pins during the stance phase of walking. *Foot Ankle Int* 25: 357-364.
- Astion DJ, Deland JT, Otis JC, Kenneally S (1997). Motion of the hindfoot after simulated arthrodesis. *J Bone Joint Surg Am* 79: 241-246.
- Attarian DE, McCrackin HJ, DeVito DP, McElhaney JH, Garrett WE, Jr. (1985). Biomechanical characteristics of human ankle ligaments. *Foot Ankle Int* 6: 54-58.
- Bahr R, Pena F, Shine J, Lew WD, Engebretsen L (1998). Ligament force and joint motion in the intact ankle: a cadaveric study. *Knee Surg Sports Traumatol Arthrosc* 6: 115-121.
- Ball KA and Afheldt MJ (2002a). Evolution of foot orthotics—part 1: coherent theory or coherent practice? *J Manipulative Physiol Ther* 25: 116-124.
- Ball KA and Afheldt MJ (2002b). Evolution of foot orthotics—part 2: research reshapes long-standing theory. *J Manipulative Physiol Ther* 25: 125-134.
- Bandak FA, Tannous RE, Toridis T (2001). On the development of an osseo-ligamentous finite element model of the human ankle joint. *Int J Solids Struct* 38: 1681-1697.
- Barnett CH and Napier JR (1952). The axis of rotation at the ankle joint in man - Its influence upon the form of the talus and the mobility of the fibula. *J Anat* 86: 1-9.
- Barra V and Boire JY (2002). Segmentation of fat and muscle from MR images of the thigh by a possibilistic clustering algorithm. *Comput Methods Programs Biomed* 68: 185-193.
- Bartlett TQ, Vannier MW, McKeel DW, Jr., Gado M, Hildebolt CF, Walkup R (1994). Interactive segmentation of cerebral gray matter, white matter, and CSF: photographic and MR images. *Comput Med Imaging Graph* 18: 449-460.
- Beillas P, Lavaste F (1999). Foot and ankle finite element modeling using CT-scan data. *Proceedings of the 43rd Stapp Car Crash Conference*: 171-184.
- Benink RJ (1985). The constraint mechanism of the human tarsus. *Acta Orthop Scand* 56 (Suppl 215): 49-68.
- Besl PJ and McKay ND (1992). A method for registration of 3-D shapes. *IEEE Trans Patt Anal Machine Intell* 14: 239-256.
- Bogdan RJ, Jenkins D, Hyland T (1978). The runner's knee syndrome. *Sports Medicine* 78: 159-177.

References

- Boutry N, Cortet B, Chappard D, Dubois P, Demondion X, Marchandise X, Cotten A (2004). Bone structure of the calcaneus: Analysis with magnetic resonance imaging and correlation with histomorphometric study. *Osteoporos Int* 15: 827-833.
- Bottlang M, Marsh JL, Brown TD (1999). Articulated external fixation of the ankle: minimizing motion resistance by accurate axis alignment. *J Biomech* 32: 63-70.
- Braus H (1921). *Anatomie des Menschen. Vol 1: Bewegungsapparat*. Berlin: Springer Verlag.
- Bruns J and Rehder U (1993). Ligament kinematics of the ankle joint. *Z Orthop Grenz* 131: 363-369.
- Burdett RG (1982). Forces predicted at the ankle during running. *Med Sci Sports Exerc* 14: 308-316.
- Camacho DL, Ledoux WR, Rohr ES, Sangeorzan BJ, Ching RP (2002). A three-dimensional, anatomically detailed foot model: a foundation for a finite element simulation and means of quantifying foot-bone position. *J Rehabil Res Dev* 39: 401-410.
- Cawley PW and France EP (1991). Biomechanics of the lateral ligaments of the ankle: an evaluation of the effects of axial load and single plane motions on ligament strain patterns. *Foot Ankle Int* 12: 92-9.
- Chan CW and Rudins A (1994). Foot biomechanics during walking and running. *Mayo Clin Proc* 69: 448-461.
- Cheung JT, Zhang M, Leung AK, Fan YB (2005). Three-dimensional finite element analysis of the foot during standing—a material sensitivity study. *J Biomech* 38: 1045-1054.
- Chiara L, Croce UD, Leardini A, Cappazzo A (2005). Human movement analysis using stereophotogrammetry. Part 2: Instrumental errors. *Gait Post* 21: 197-211.
- Chu WC, Lee SH, Chu W, Wang TJ, Lee MC (1995). The use of arch index to characterize arch height: a digital image processing approach. *IEEE Trans Biomed Eng* 42: 1088-1093.
- Clarke TW, Frederick EC, Hamill CL (1983). The effects of shoe design parameters on rearfoot control in running. *Med Sci Sports Exercise* 15: 376-381.
- Clement DB, Taunton JE, Smart GW, McNicol KL (1981). A survey of overuse running injuries. *Phys Sports Med* 9: 47-58.
- Cohen ZA, McCarthy DM, Kwak SD, Legrand P, Fogarasi F, Ciaccio EJ, Ateshian GA (1999). Knee cartilage topography, thickness, and contact areas from MRI: In-vitro calibration and in-vivo measurements. *Osteoarthritis Cartilage* 7: 95-109.
- Colville MR, Marder RA, Boyle JJ, Zarins B (1990). Strain measurement in lateral ankle ligaments. *Am J Sports Med* 18: 196-200.
- Cornwall MW and McPoil TG (1995). Footwear and foot orthotic effectiveness research: a new approach. *J Orthop Sports Phys Ther* 21: 337-344.
- Cornwall MW and McPoil TG (1999). Relative movement of the navicular bone during normal walking. *Foot Ankle Int* 20: 507-512.
- Cornwall MW and McPoil TG (2004). Influence of rearfoot postural alignment on rearfoot motion during walking. *Foot* 14: 133-138.
- Cowan DN, Robinson JR, Jones BH, Polly DW, Jr., Berrey BH (1994). Consistency of visual assessments of arch height among clinicians. *Foot Ankle Int* 15: 213-217.
- Cunningham DJ (1998). *Textbook of anatomy*. London: Oxford University Press.
- Dahle LK, Mueller MJ, Delitto A, Diamond JE (1991). Visual assessment of foot type and relationship of foot type to lower extremity injury. *J Orthop Sports Phys Ther* 14: 70-74.
- Debrunner HU (1998). *Biomechanik des Fusses*. Stuttgart: Ferdinand Enke Verlag.

- Debrunner HU and Hepp WR(1994). *Orthopädisches Diagnostikum*. Stuttgart: Georg Thieme Verlag.
- Dul J and Johnson GE (1985). A kinematic model of the human ankle. *J Biomed Eng* 7: 137-143.
- Eckstein F, Heudorfer L, Faber SC, Burgkart R, Englmeier KH, Reiser M (2002). Long-term and resegmentation precision of quantitative cartilage MR imaging (qMRI). *Osteoarthritis Cartilage* 10: 922-928.
- Elftman H (1960). The transverse tarsal joint and its control. *Clin Orthop* 16: 41-45.
- Eliasziw M, Young SL, Woodbury MG, Fryday-Field K (1994). Statistical methodology for the concurrent assessment of interrater and intrarater reliability: using goniometric measurements as an example. *Phys Ther* 74: 777-788.
- Elveru RA, Rothstein JM, Lamb RL (1988). Goniometric reliability in a clinical setting. Subtalar and ankle joint measurements. *Phys Ther* 68: 672-677.
- Engsberg JR (1987). A biomechanical analysis of the talocalcaneal joint - in vitro. *J Biomech* 20: 429-442.
- Fick R (1911). *Handbuch der Anatomie und Mechanik der Gelenke*. Jena: Fischer Verlag.
- Franco AH (1987). Pes cavus and pes planus. Analyses and treatment. *Phys Ther* 67: 688-694.
- Fraser GA and Ahmed AM (1983). Passive rotational stability of the weight-bearing talocrural joint: an in vitro biomechanical study. *Trans Orthop Res Soc* 7: 248.
- Gauffin H, Areblad M, Tropp H (1993). 3-dimensional analysis of the talocrural and subtalar joints in single-limb stance. *Clin Biomech* 8: 307-314.
- Gentili A, Masih S, Yao L, Seeger LL (1996). Pictorial review: foot axes and angles. *Br J Radiol* 69: 968-974.
- Gluer CC, Blake G, Lu Y, Blunt BA, Jergas M, Genant HK (1995). Accurate assessment of precision errors: how to measure the reproducibility of bone densitometry techniques. *Osteoporos Int* 5: 262-270.
- Hamill J, Bates BT, Knutzen KM, Kirkpatrick GM (1989). Relationship between selected static and dynamic lower extremity measures. *Clin Biomech* 4: 217-225.
- Harris GF (1991). Analysis of ankle and subtalar motion during human locomotion. In Stiehl JB (ed.): *Inman's joints of the ankle*. Baltimore: Williams & Wilkins Company.
- Hawes MR, Nachbauer W, Sovak D, Nigg BM (1992). Footprint parameters as a measure of arch height. *Foot Ankle Int* 13: 22-26.
- Heil B (1992). Lower limb biomechanics related to running injuries. *Physiotherapy* 76: 400-406.
- Hicks JH (1953). The mechanics of the foot .1. The Joints. *J Anat* 87: 345-357.
- Hintermann B and Nigg BM (1993). Pronation aus der Sicht der Bewegungsübertragung zwischen Kalkaneus und Tibia. *Schw Zt Sportmed* 41: 151-156.
- Hintermann B, Nigg BM, Sommer C, Cole GK (1994a). Transfer of movement between calcaneus and tibia in-vitro. *Clin Biomech* 9: 349-355.
- Hintermann B, Nigg BM, Cole GK (1994b). Influence of selective arthrodesis on the movement transfer between calcaneus and tibia in-vitro. *Clin Biomech* 9: 356-361.
- Hintermann B and Nigg BM (1995). In vitro kinematics of the axially loaded ankle complex in response to dorsiflexion and plantarflexion. *Foot Ankle Int* 16: 514-518.
- Hintermann B, Sommer C, Nigg BM (1995). Influence of ligament transection on tibial and calcaneal rotation with loading and dorsi-plantarflexion. *Foot Ankle Int* 16: 567-571.
- Hlavac HF (1967). Differences in x-ray findings with varied positioning of the foot. *J Am Podiatry Assoc* 57: 465-471.

References

- Hollis JM, Blasier RD, Flahiff CM (1995). Simulated lateral ankle ligamentous injury. Change in ankle stability. *Am J Sports Med* 23: 672-677.
- Hogan MT and Staheli LT (2002). Arch height and lower limb pain: an adult civilian study. *Foot Ankle Int* 23: 43-47.
- Hunt AE, Fahey AJ, Smith RM (2000). Static measures of calcaneal deviation and arch angle as predictors of rearfoot motion during walking. *Austr J Phys* 46: 9-16.
- Hunt AE and Smith RM (2004). Mechanics and control of the flat versus normal foot during the stance phase of walking. *Clin Biomech* 19: 391-397.
- Huson A (1961). *Een ontleedkundig-functioneel onderzoek van de voetwortel* [PhD Thesis]. Leiden: Rijksuniversiteit te Leiden.
- Huson A, Benink RJ, van Langelaan EJ, Spoor CW (1977). Die Bewegungsart der tarsalen Gelenke. *Acta Anat* 99: 279.
- Huson A, van Langelaan EJ, Spoor CW (1986). Tibiotalar delay and tarsal gearing. *J Anat* 149: 244-245.
- Inman VT (1969). The influence of the foot-ankle complex on the proximal skeletal structures. *Artif Limbs* 13: 59-65.
- Inman VT (1976). *The joints of the ankle*. Baltimore: Williams & Wilkins Company.
- Isman RE and Inman VT (1969). Anthropometric studies of the human foot and ankle. *Bull Prosthet Res* 11: 97-129.
- James SL, Bates BT, Osternig LR (1978). Injuries to runners. *Am J Sports Med* 6: 40-50.
- Jones R (1945). The functional significance of the declination of the axis of the subtalar joint. *Anat Rec* 93: 151-159.
- Kaufmann L, Kramer DM, Crooks LE, Orthendahl DA (1989). Measuring signal-to-noise ratios in MR imaging. *Radiology* 173: 265-267.
- Keller Chandra S (2005). *Konstruktion einer Auslenkungsapparatur zur Untersuchung des Rueckfusses mittels Magnet Resonanz Tomographie* [Diploma Thesis]. Zurich: ETH Zurich.
- Ker RF, Bennet MB, Alexander RM, Kester RC (1989). Foot strike and the properties of the human heel pad. *Proc Inst Mech Eng* 203: 191-196.
- Kernozek TW and Ricard MD (1990). Foot placement angle and arch type: effect on rearfoot motion. *Arch Phys Med Rehabil* 71: 988-991.
- Kim S-J, Nigg BM, Hume PA (1995). *The effect of ankle joint complex ROM and arch height on the transfer of foot to leg in hee-toe running*. Calgary: Human Performance Laboratory.
- Knutzen KM and Price A (1994). Lower extremity static and dynamic relationships with rearfoot motion in gait. *J Am Podiatr Med Assoc* 84: 171-180.
- Lapidus PW (1963). Kinesiology and mechanical anatomy of the tarsal joints. *Clin Orthop* 30: 20-36.
- Leardini A, Benedetti MG, Catani F, Simoncini L, Giannini S (1999a). An anatomically based protocol for the description of foot segment kinematics during gait. *Clin Biomech* 14: 528-536.
- Leardini A, O'Connor JJ, Catani F, Giannini S (1999b). Kinematics of the human ankle complex in passive flexion: a single degree of freedom system. *J Biomech* 32: 111-118.
- Leardini A, O'Connor JJ, Catani F, Giannini S (1999c). A geometric model of the human ankle joint. *J Biomech* 32: 585-591.

- Leardini A (2001). Geometry and mechanics of the human ankle complex and ankle prosthesis design. *Clin Biomech* 16: 706-709.
- Leardini A, Stagni R, O'Connor JJ (2001). Mobility of the subtalar joint in the intact ankle complex. *J Biomech* 34: 805-809.
- Leardini A and O'Connor JJ (2002). A model for lever-arm length calculation of the flexor and extensor muscles at the ankle. *Gait Post* 15: 220-229.
- Leardini A and Moschella D (2002). Dynamic simulation of the natural and replaced human ankle joint. *Med Biol Eng Comput* 40: 193-199.
- Liu W, Maitland ME, Nigg BM (2000). The effect of axial load on the in vivo anterior drawer test of the ankle joint complex. *Foot Ankle Int* 21: 420-426.
- Longatti HJ (2003). *Fusstypen beim Gehen* [Medical Thesis]. Zurich: University Hospital Zurich.
- Lovett RW and Cotton FJ (1898). Some practical points in the anatomy of the foot. *Boston Med Surg J* 139: 101-107.
- Lundberg A (1988). *Patterns of motion of the ankle/foot complex*. Stockholm: Gotab.
- Lundberg A, Goldie I, Kalin B, Selvik G (1989a). Kinematics of the ankle foot complex - Plantarflexion and dorsiflexion. *Foot Ankle Int* 9: 194-200.
- Lundberg A, Svensson OK, Bylund C, Goldie I, Selvik G (1989b). Kinematics of the ankle foot complex. 2. Pronation and supination. *Foot Ankle Int* 9: 248-253.
- Lundberg A, Svensson OK, Bylund C, Selvik G (1989c). Kinematics of the ankle foot complex. 3. Influence of leg rotation. *Foot Ankle Int* 9: 304-309.
- Luo ZP, Kitaoka HB, Hsu HC, Kura H, An KN (1997). Physiological elongation of ligamentous complex surrounding the hindfoot joints: In vitro biomechanical study. *Foot Ankle Int* 18: 277-283.
- Manter JT (1941). Movements of the subtalar and transverse tarsal joints. *Anat Rec* 80: 397-410.
- Maslen BA and Ackland TR (1994). Radiographic study of skin displacement errors in the foot and ankle during standing. *Clin Biomech* 9: 291-296.
- Mathieson I, Upton D, Birchenough A (1999). Comparison of footprint parameters calculated from static and dynamic footprints. *Foot* 9: 145-149.
- Mattingly B, Talwalkar V, Tylkowski C, Stevens DB, Hardy PA, Pienkowski D (2006). Three-dimensional in vivo motion of adult hind foot bones. *J Biomech* 39: 726-733.
- Mazur JM, Schwartz E, Simon SR (1979). Ankle arthrodesis. Long-term follow-up with gait analysis. *J Bone Joint Surg Am* 61: 964-975.
- McClay I and Manal K (1997). Coupling parameters in runners with normal and excessive pronation. *J Appl Biomech* 13: 109-124.
- McClay I (2000). The evolution of the study of the mechanics of running. Relationship to injury. *J Am Podiatr Med Assoc* 90: 133-148.
- McCullough CJ and Burge PD (1980). Rotatory stability of the load-bearing ankle. *J Bone Joint Surg Br* 62: 460-464.
- McDonald SW and Tavener G (1999). Pronation and supination of the foot: confused terminology. *Foot* 9: 6-11.
- McPoil TG and Cornwall MW (1996a). The relationship between static lower extremity measurements and rearfoot motion during walking. *J Orthop Sports Phys Ther* 24: 309-314.

References

- McPoil TG and Cornwall MW (1996b). Relationship between three static angles of the rearfoot and the pattern of rearfoot motion during walking. *J Orthop Sports Phys Ther* 23: 370-375.
- McPoil TG and Cornwall MW (2000). Use of the medial longitudinal arch height to predict plantar surface contact area during walking. *J Orthop Sports Phys Ther* 30: A28-A30.
- Menz HB (1995). Clinical hindfoot measurement: a critical review of the literature. *Foot* 5: 57-64.
- Michelson JD, Clarke HJ, Jinnah RH (1990). The effect of loading on tibiotalar alignment in cadaver ankles. *Foot Ankle Int* 10: 280-284.
- Michelson JD, Ahn UM, Helgemo SL (1996). Motion of the ankle in a simulated supination-external rotation fracture model. *J Bone Joint Surg Am* 78: 1024-1031.
- Michelson JD, Schmidt GR, Mizel MS (2000). Kinematics of a total arthroplasty of the ankle: comparison to normal ankle motion. *Foot Ankle Int* 21: 278-284.
- Michelson JD, Hamel AJ, Buczek FL, Sharkey NA (2002). Kinematic behavior of the ankle following malleolar fracture repair in a high-fidelity cadaver model. *J Bone Joint Surg Am* 84: 2029-2038.
- Milgrom C, Giladi M, Simkin A, Stein M, Kashtan H, Margulies J, Steinberg R, Aharonson Z (1985). The normal range of subtalar inversion and eversion in young males as measured by three different techniques. *Foot Ankle Int* 6: 143-145.
- Morris JM (1977). Biomechanics of the foot and ankle. *Clin Orthop*: 10-17.
- Nawoczenski DA, Cook TM, Saltzman CL (1995). The effect of foot orthotics on 3-dimensional kinematics of the leg and rearfoot during running. *J Orthop Sports Phys Ther* 21: 317-327.
- Nawoczenski DA, Saltzman CL, Cook TM (1998). The effect of foot structure on the three-dimensional kinematic coupling behavior of the leg and rear foot. *Phys Ther* 78: 404-416.
- Nester CJ (1997). Rearfoot complex: a review of its interdependent components, axis orientation and functional model. *Foot* 7: 86-96.
- Nester CJ, Hutchins S, Bowker P (2000). Shank rotation: A measure of rearfoot motion during normal walking. *Foot Ankle Int* 21: 578-583.
- Nester CJ, Findlow A, Bowker P (2001). Scientific approach to the axis of rotation at the midtarsal joint. *J Am Podiatr Med Assoc* 91: 68-73.
- Nester C, Bowker P, Bowden P (2002). Kinematics of the midtarsal joint during standing leg rotation. *J Am Podiatr Med Assoc* 92: 77-81.
- Nigg BM, Skarvan G, Frank CB, Yeadon MR (1990). Elongation and forces of ankle ligaments in a physiological range of motion. *Foot Ankle Int* 11: 30-40.
- Nigg BM, Nachbauer W, Cole GK (1992). Effects of arch height of the foot on angular motion of the lower extremities in running. *Proceedings of the Second North American Congress on Biomechanics*: 233-234.
- Nigg BM, Cole GK, Nachbauer W (1993). Effects of arch height of the foot on angular motion of the lower extremities in running. *J Biomech* 26: 909-916.
- Nigg BM, Cole GK, Brüggemann GP (1995). Impact forces during heel-toe running. *J Appl Biomech* 11: 407-432.
- Okugawa G, Takase K, Nobuhara K, Yoshida T, Minami T, Tamagaki C, Magnotta VA, Anreasen NC, Kinoshita (2003). Inter- and intraoperator reliability of brain tissue measures using magnetic resonance imaging. *Eur Arch Psychiatry Clin Neurosci* 253: 301-306.

- Olerud C (1985). The pronation capacity of the foot - its consequences for axial deformity after tibial shaft fractures. *Arch Orthop Trauma Surg* 104: 303-306.
- Olerud C and Rosendahl Y (1986). Functional-anatomy of the hindfoot with special reference to its torsion transmitting properties. *Acta Orthop Scand* 57: 257-258.
- Olerud C and Rosendahl Y (1987). Torsion-transmitting properties of the hind foot. *Clin Orthop Rel Res* 214: 285-294.
- Parenteau CS, Viano DC, Petit PY (1998). Biomechanical properties of human cadaveric ankle-subtalar joints in quasi-static loading. *J Biomech Eng* 120: 105-111.
- Parks N, Hirsch HJ, Hillstrom HJ, Udupa JK (1994). Stereometry and 3-D MRI reconstructions for kinematics of the rearfoot: A cadaver study. *Proceedings of the 16th International Conference IEEE Engineering in Medicine and Biology Society*: 562-563.
- Perry J (1992). *Gait analysis*. Thorofare: Slack Incorporated.
- Pierrynowski MR, Smith SB, Mlynarczyk JH (1996). Proficiency of foot care specialists to place the rearfoot at subtalar neutral. *J Am Podiatr Med Assoc* 86: 217-223.
- Procter P and Paul JP (1982). Ankle joint biomechanics. *J Biomech* 15: 627-634.
- Rasmussen O (1985). Stability of the ankle joint. Analysis of the function and traumatology of the ankle ligaments. *Acta Orthop Scand* 56 (Suppl 211): 1-75.
- Razeghi M and Batt ME (2002). Foot type classification: a critical review of current methods. *Gait Post* 15: 282-291.
- Reinschmidt C, van den Bogert AJ, Murphy N, Lundberg A, Nigg BM (1997a). Tibiocalcaneal motion during running, measured with external and bone markers. *Clin Biomech* 12: 8-16.
- Reinschmidt C, van den Bogert AJ, Nigg BM, Lundberg A, Murphy N (1997b). Effect of skin movement on the analysis of skeletal knee joint motion during running. *J Biomech* 30: 729-732.
- Reinschmidt C, van den Bogert AJ, Lundberg A, Nigg BM, Murphy N, Stacoff A, Stano A (1997c). Tibiofemoral and tibiocalcaneal motion during walking: external vs. skeletal markers. *Gait Post* 6: 98-109.
- Reischl SF, Powers CM, Rao S, Perry J (1999). Relationship between foot pronation and rotation of the tibia and femur during walking. *Foot Ankle Int* 20: 513-520.
- Renstrom P, Wertz M, Incavo S, Pope M, Ostgaard HC, Arms S, Haugh L (1988). Strain in the lateral ligaments of the ankle. *Foot Ankle Int* 9: 59-63.
- Ringleb SI, Udupa JK, Siegler S, Imhauser CW, Hirsch BE, Liu J, Odhner D, Okereke E, Roach N (2005). The effect of ankle ligament damage and surgical reconstructions on the mechanics of the ankle and subtalar joints revealed by three-dimensional stress MRI. *J Orthop Res* 23: 743-749.
- Root ML, Weed JH, Sgarlato, TE, Bluth DR (1966). Axis of motion of the subtalar joint. *J Am Podiatr Med Assoc* 56: 149-155.
- Root ML, Orien WP, Weed JH (1977). *Clinical biomechanics: normal and abnormal function of the foot*. Los Angeles: Clinical Biomechanics Corporation.
- Rosenbaum D, Hautmann S, Gold M, Claes L (1994). Effects of walking speed on plantar pressure patterns and hindfoot angular motion. *Gait Post* 2: 191-197.
- Rothstein JM (1985). *Measurement in physical therapy*. New York: Churchill Livingstone.
- Rubin G (1971). Tibial rotation. *Bull Prosthet Res* 10: 95-101.
- Salathe EP Jr., Arangio GA, Salathe EP (1986). A biomechanical model of the foot. *J Biomech* 19: 989-1001.

References

- Salathe EP Jr., Arangio GA, Salathe EP (1990). The foot as a shock absorber. *J Biomech* 23: 655-659.
- Saltzman CL and Nawoczenski DA (1995). Complexities of foot architecture as a base of support. *J Orthop Sports Phys Ther* 21: 354-360.
- Sammerco GJ, Burstein AH, Frankel VH (1973). Biomechanics of the ankle: A kinematic study. *Orthop Clin North Am* 4: 75.
- Scharfbillig R, Evans AM, Copper AW, Williams M, Scutter S, Iasiello H, Redmond A (2004). Criterion validation of four criteria of the foot posture index. *J Am Podiatr Med Assoc* 94: 31-38.
- Scott SH and Winter DA (1991). Talocrural and talocalcaneal joint kinematics and kinetics during the stance phase of walking. *J Biomech* 24: 743-752.
- Sharkey NA and Hamel AJ (1998). A dynamic cadaver model of the stance phase of gait: performance characteristics and kinetic validation. *Clin Biomech* 13: 420-433.
- Shephard E (1951). Tarsal Movements. *J Bone Joint Surg Br* 33: 258-263.
- Shiang TY, Lee SH, Lee SJ, Chu WC (1998). Evaluating different footprint parameters as a predictor of arch height. *IEEE Eng Med Biol Mag* 17: 62-66.
- Shrout PE and Fleiss JL (1979). Intraclass correlations: Uses in assessing rater reliability. *Psychol Bull* 86: 420-428.
- Siegler S, Chen J, Schneck CD (1988a). The 3-dimensional kinematics and flexibility characteristics of the human ankle and subtalar joints. 1. Kinematics. *J Biomech Eng-Trans ASME* 110: 364-373.
- Siegler S, Block J, Schneck CD (1988b). The mechanical characteristics of the collateral ligaments of the human ankle joint. *Foot Ankle Int* 8: 234-242.
- Siegler S, Udupa JK, Ringleb SI, Imhauser CW, Hirsch BE, Odhner D, Saha PK, Okereke E, Roach N (2005). Mechanics of the ankle and subtalar joints revealed through a 3D quasi-static stress MRI technique. *J Biomech* 38: 567-578.
- Singh AK, Starkweather KD, Hollister AM, Jatana S, Lupichuk AG (1992). Kinematics of the ankle: a hinge axis model. *Foot Ankle Int* 13: 439-446.
- Sommer C, Hintermann B, Nigg BM, van den Bogert AJ (1996). Influence of ankle ligaments on tibial rotation: An in vitro study. *Foot Ankle Int* 17: 79-84.
- Stacoff A (1998). *Skeletal lower extremity motions during running* [PhD Thesis]. Calgary: University of Calgary.
- Stacoff A, Nigg BM, Reinschmidt C, van den Bogert AJ, Lundberg A (2000a). Tibiocalcaneal kinematics of barefoot versus shod running. *J Biomech* 33: 1387-1395.
- Stacoff A, Nigg BM, Reinschmidt C, van den Bogert AJ, Lundberg A, Stussi E, Denoth J (2000b). Movement coupling at the ankle during the stance phase of running. *Foot Ankle Int* 21: 232-239.
- Stacoff A, Reinschmidt C, Nigg BM, van den Bogert AJ, Lundberg A, Denoth J, Stussi E (2000c). Effects of foot orthoses on skeletal motion during running. *Clin Biomech* 15: 54-64.
- Stagni R, Leardini A, Catani F, Cappello A (2004). A new semi-automated measurement technique based on X-ray pictures for ankle morphometry. *J Biomech* 37: 1113-1118.
- Staheli LT, Chew DE, Corbett M (1987). The longitudinal arch. A survey of eight hundred and eighty-two feet in normal children and adults. *J Bone Joint Surg Am* 69: 426-428.
- Stammberger T, Eckstein F, Englmeier KH, Reiser M (1999). Determination of 3D cartilage thickness data from MR imaging: computational method and reproducibility in the living. *Magn Reson Med* 41: 529-536.

- Stauffer RN, Chao EY, Brewster RC (1977). Force and motion analysis of the normal, diseased, and prosthetic ankle joint. *Clin Orthop* 127: 189-196.
- Stephens MM and Sammarco GJ (1992). The stabilizing role of the lateral ligament complex around the ankle and subtalar joints. *Foot Ankle Int* 13: 130-136.
- Stergiou P (1996). *Biomechanical factors associated with patellofemoral pain syndrome in runners* [Master Thesis]. Calgary: University of Canada.
- Stindel E, Udupa JK, Hirsch BE, Odhner D, Couture C (1998). 3D morphology of the rearfoot from MRI data: technical validation and clinical description. *Proceedings of the Society of Photo-optical Instrumentation Engineers* 3335: 479-487.
- Stindel E, Udupa JK, Hirsch BE, Odhner D, Couture C (1999a). 3D MR image analysis of the morphology of the rear foot: application to classification of bones. *Comput Med Imaging Graph* 23: 75-83.
- Stindel E, Udupa JK, Hirsch BE, Odhner D (1999b). A characterization of the geometric architecture of the peritalar joint complex via MRI: an aid to the classification of foot type. *IEEE Trans Med Imaging* 18: 753-763.
- Stindel E, Udupa JK, Hirsch BE, Odhner D (2001). An in vivo analysis of the motion of the peri-talar joint complex based on MR imaging. *IEEE Trans Biomed Eng* 48: 236-247.
- Stormont DM, Morrey BF, An KN, Cass JR (1985). Stability of the loaded ankle. Relation between articular restraint and primary and secondary static restraints. *Am J Sports Med* 13: 295-300.
- Strasser H (1917). *Lehrbuch der Muskel- und Gelenkmechanik, III. Band: Die untere Extremität*. Berlin: Springer Verlag.
- Subotnick SI (1985). The biomechanics of running. Implications for the prevention of foot injuries. *Sports Med* 2: 144-153.
- Thoma W, Scale D, Kurth A (1993). Computerized analysis of the kinematic of the upper ankle joint. *Z Orthop Grenz* 131: 14-17.
- Tranberg R and Karlsson D (1998). The relative skin movement of the foot: a 2-D roentgen photogrammetry study. *Clin Biomech* 13: 71-76.
- Udupa JK, Odhner D, Samarasekera S, Goncalves RJ, Iyer K, Venugopal K, Furuie S (1994). 3DVIEWNIX: an open multiparametric imaging software system. *Proceedings of the Society of Photo-optical Instrumentation Engineers* 2164: 58-73.
- Udupa JK, Hirsch BE, Hillstrom HJ, Bauer GR, Kneeland JB (1998). Analysis of in vivo 3-D internal kinematics of the joints of the foot. *IEEE Trans Biomed Eng* 45: 1387-1396.
- van den Bogert AJ, Smith GD, Nigg BM (1994). In-vivo determination of the anatomical axes of the ankle joint complex - an optimization approach. *J Biomech* 27: 1477-1488.
- van Langelaan EJ, Spoor CW, Huson A (1974). A kinematical analysis of the tarsal joints. *J Anat* 117: 650.
- van Langelaan EJ (1983). A kinematical analysis of the tarsal joints. *Acta Orthop Scand* 54 (Suppl 204): 135-265.
- van Mechelen W (1992). Running injuries. A review of the epidemiological literature. *Sports Med* 14: 320-335.
- Wearing SC, Urry S, Perlman P, Smeathers J, Dubois P (1998). Sagittal plane motion of the human arch during gait: a videofluoroscopic analysis. *Foot Ankle Int* 19: 738-742.
- Westblad P, Hashimoto T, Winson I, Lundberg A, Arndt A (2002). Differences in ankle-joint complex motion during the stance phase of walking as measured by superficial and bone-anchored markers. *Foot Ankle Int* 23: 856-863.

References

- Whittle MW (1999). Generation and attenuation of transient impulsive forces beneath the foot: a review. *Gait Post 10*: 264-275.
- Wolf P, Stacoff A, Stuessi E (2004). Modelling of the passive mobility in human tarsal gears implications from the literature. *Foot 14*: 23-34.
- Wolf P, Stacoff A, Luechinger R, Arndt A, Nester C, Lundberg A, Stuessi E (2005). Tarsal bone positions in different foot excursions under bodyweight measured in vivo and non-invasively. *Proceedings of the 3th International Conference on Biomechanics of the Lower Limb in Health, Disease and Rehabilitation*: 208-209.
- Woodburn J, Udupa JK, Hirsch BE, Wakefield RJ, Helliwell PS, Reay N, O'Connor P, Budgen A, Emery P (2002). The geometric architecture of the subtalar and midtarsal joints in rheumatoid arthritis based on magnetic resonance imaging. *Arthritis Rheum 46*: 3168-3177.
- Wright DG, Desai ME, Henderson BS (1964). Action of the subtalar and ankle joint complex during the stance phase of walking. *J Bone Joint Surg Am 46*: 361-382.
- Wu G, Siegler S, Allard P, Kirtley C, Leardini A, Rosenbaum D, Whittle M, D'Lima DD, Cristofolini L, Witte H, Schmid O, Stokes I (2002). ISB recommendation on definitions of joint coordinate system of various joints for the reporting of human joint motion-part I: ankle, hip, and spine. *J Biomech 35*: 543-548.

Appendix A

The equations of the used intraclass correlation coefficients are given below. A detailed description can be found in the literature (Eliaszew et al., 1994; Shrout and Fleiss, 1979).

The intraoperator reproducibility was estimated by a covariance-variance ratio for the i^{th} tarsal bone (calcaneus, cuboid, navicular, talus) and for the j^{th} operator (A, B; C, D):

$$\text{ICC}_{3,1} = (\text{var}_{\text{bone } i} + (t-1) \cdot \text{var}_{\text{inter}/t}) / (\text{var}_{\text{bone } i} + (t-1) \cdot \text{var}_{\text{inter}/t} + \text{var}_{\text{error } j}). \quad (\text{eq. A-1})$$

Thereby, t is the number of operators who segmented the same bone. Thus, the second summand of equation 3-2 is given by the variance of the interaction within the i^{th} bone of five subjects $\text{var}_{\text{inter}}$ divided by 2. The residual error $\text{var}_{\text{error}}$ is partitioned into t components to represent the within-operator variability for each operator.

The interoperator reproducibility was estimated for each bone by the variance of this bone divided by the total variance:

$$\text{ICC}_{2,1} = \text{var}_{\text{bone } i} / (\text{var}_{\text{bone } i} + \text{var}_{\text{operator}} + \text{var}_{\text{inter}} + \text{var}_{\text{error}}). \quad (\text{eq. A-2})$$

Appendix B

Tab. B-1 Externally predefined calcaneus rotation due to pronation block and resulting absolute calcaneal rotations of each subject. The relative amount of the rotation in each plane is given as percentage, too, indicating the orientation of the helical axis.

| | helical axis rotation [°] | frontal plane (-INV / +EV) [°] | sagittal plane (-PF / +DF) [°] | transversal plane (-ADD / +ABD) [°] |
|------------|---------------------------|--------------------------------|--------------------------------|-------------------------------------|
| external | 15.0 | 10.8 (45%) | 3.3 (14%) | 9.8 (41%) |
| subject A1 | 6.6 | 4.4 (40%) | 2.4 (21%) | 4.6 (39%) |
| subject A2 | 6.6 | 4.3 (40%) | 2.3 (21%) | 4.3 (39%) |
| subject B1 | 10.6 | 9.8 (65%) | 3.5 (23%) | 1.8 (12%) |
| subject B2 | 9.2 | 7.1 (47%) | 3.4 (22%) | 4.8 (31%) |
| subject C1 | 7.6 | 7.2 (69%) | 2.3 (22%) | 0.9 (9%) |
| subject C2 | 7.9 | 7.6 (78%) | 2.2 (22%) | 0.0 (0%) |
| deviation | 6.9 ±1.6 | 4.1 ±2.1 (15% ±13) | 0.7 ±0.4 (8% ±1) | 7.1 ±2.1 (19% ±17) |

Tab. B-1 Externally predefined calcaneus rotations due to supination block and resulting absolute calcaneal rotations of each subject. The relative amount of the rotation in each plane is given as percentage, too, indicating the orientation of the helical axis.

| | helical axis rotation [°] | frontal plane (-INV / +EV) [°] | sagittal plane (-PF / +DF) [°] | transversal plane (-ADD / +ABD) [°] |
|------------|---------------------------|--------------------------------|--------------------------------|-------------------------------------|
| external | 15.0 | 10.8 (45%) | 3.3 (14%) | 9.8 (41%) |
| subject A1 | 6.6 | 4.4 (40%) | 2.4 (21%) | 4.6 (39%) |
| subject A2 | 6.6 | 4.3 (40%) | 2.3 (21%) | 4.3 (39%) |
| subject B1 | 10.6 | 9.8 (65%) | 3.5 (23%) | 1.8 (12%) |
| subject B2 | 9.2 | 7.1 (47%) | 3.4 (22%) | 4.8 (31%) |
| subject C1 | 7.6 | 7.2 (69%) | 2.3 (22%) | 0.9 (9%) |
| subject C2 | 7.9 | 7.6 (78%) | 2.2 (22%) | 0.0 (0%) |
| deviation | 6.9 ±1.6 | 4.1 ±2.1 (15% ±13) | 0.7 ±0.4 (8% ±1) | 7.1 ±2.1 (19% ±17) |

Appendix C

Tab. C-1 Calcaneal second moments of volume representing principal axes [cm⁵]. In contrast to the 'normal', the 'outlier' group has a smaller moment about the most anterior posterior axis in relation to the other two moments (see last two columns).

| group | id | 2 nd moments of volume | | | relations | |
|-----------|------|---|---|--|-----------|---------|
| | | most medial-lateral axis [cm ⁵] | most anterior-posterior axis [cm ⁵] | most superior-inferior axis [cm ⁵] | ml / ap | si / ap |
| 'normal' | sub1 | 294 | 113 | 267 | 2.6 | 2.4 |
| | sub2 | 501 | 194 | 455 | 2.6 | 2.3 |
| | sub3 | 419 | 165 | 381 | 2.5 | 2.3 |
| 'outlier' | sub4 | 177 | 63 | 162 | 2.8 | 2.6 |
| | sub5 | 497 | 170 | 455 | 2.9 | 2.7 |
| | sub6 | 400 | 118 | 362 | 3.4 | 3.1 |

Tab. C-2 Second moments of volume of the cuboid representing principal axes [cm⁵]. The 'normal' and 'outlier' subjects show similar relations.

| group | id | 2 nd moments of volume | | | relations | |
|-----------|------|---|---|--|-----------|---------|
| | | most medial-lateral axis [cm ⁵] | most anterior-posterior axis [cm ⁵] | most superior-inferior axis [cm ⁵] | ml / si | ap / si |
| 'normal' | sub1 | 10.6 | 9.7 | 6.7 | 1.6 | 1.4 |
| | sub2 | 12.6 | 12.0 | 8.4 | 1.5 | 1.4 |
| | sub3 | 14.4 | 13.5 | 8.9 | 1.6 | 1.5 |
| 'outlier' | sub4 | 8.1 | 7.2 | 5.6 | 1.4 | 1.3 |
| | sub5 | 16.6 | 15.3 | 12.2 | 1.4 | 1.3 |
| | sub6 | 10.6 | 9.8 | 6.5 | 1.4 | 1.5 |

Tab. C-3 Second moments of volume of the navicular representing principal axes [cm⁵]. The 'normal' and 'outlier' subjects show similar relations.

| group | id | 2 nd moments of volume | | | relations | |
|-----------|------|---|---|--|-----------|---------|
| | | most medial-lateral axis [cm ⁵] | most anterior-posterior axis [cm ⁵] | most superior-inferior axis [cm ⁵] | ml / ap | si / ap |
| 'normal' | sub1 | 4.0 | 9.4 | 7.4 | 2.4 | 1.9 |
| | sub2 | 7.1 | 16.2 | 13.2 | 2.3 | 1.9 |
| | sub3 | 5.9 | 14.3 | 12.9 | 2.4 | 2.2 |
| 'outlier' | sub4 | 4.3 | 9.1 | 7.1 | 2.1 | 1.7 |
| | sub5 | 7.8 | 18.1 | 15.7 | 2.3 | 2.0 |
| | sub6 | 6.0 | 14.7 | 13.0 | 2.5 | 2.2 |

Tab. C-4 Talar second moments of volume representing principal axis [cm⁵]. The 'normal' and 'outlier' subjects show similar relations.

| group | id | 2 nd moments of volume | | | relations | |
|-----------|------|---|---|---|-----------|---------|
| | | most medial-lateral axis [cm ⁵] | most anterior-posterior axis [cm ⁵] | superior-inferior axis [cm ⁵] | ml / si | ap / si |
| 'normal' | sub1 | 70 | 38 | 80 | 1.9 | 2.1 |
| | sub2 | 117 | 65 | 131 | 1.8 | 2.0 |
| | sub3 | 109 | 60 | 132 | 1.8 | 2.1 |
| 'outlier' | sub4 | 54 | 30 | 61 | 1.8 | 2.0 |
| | sub5 | 119 | 63 | 135 | 1.9 | 2.1 |
| | sub6 | 86 | 43 | 95 | 2.0 | 2.2 |

Appendix D

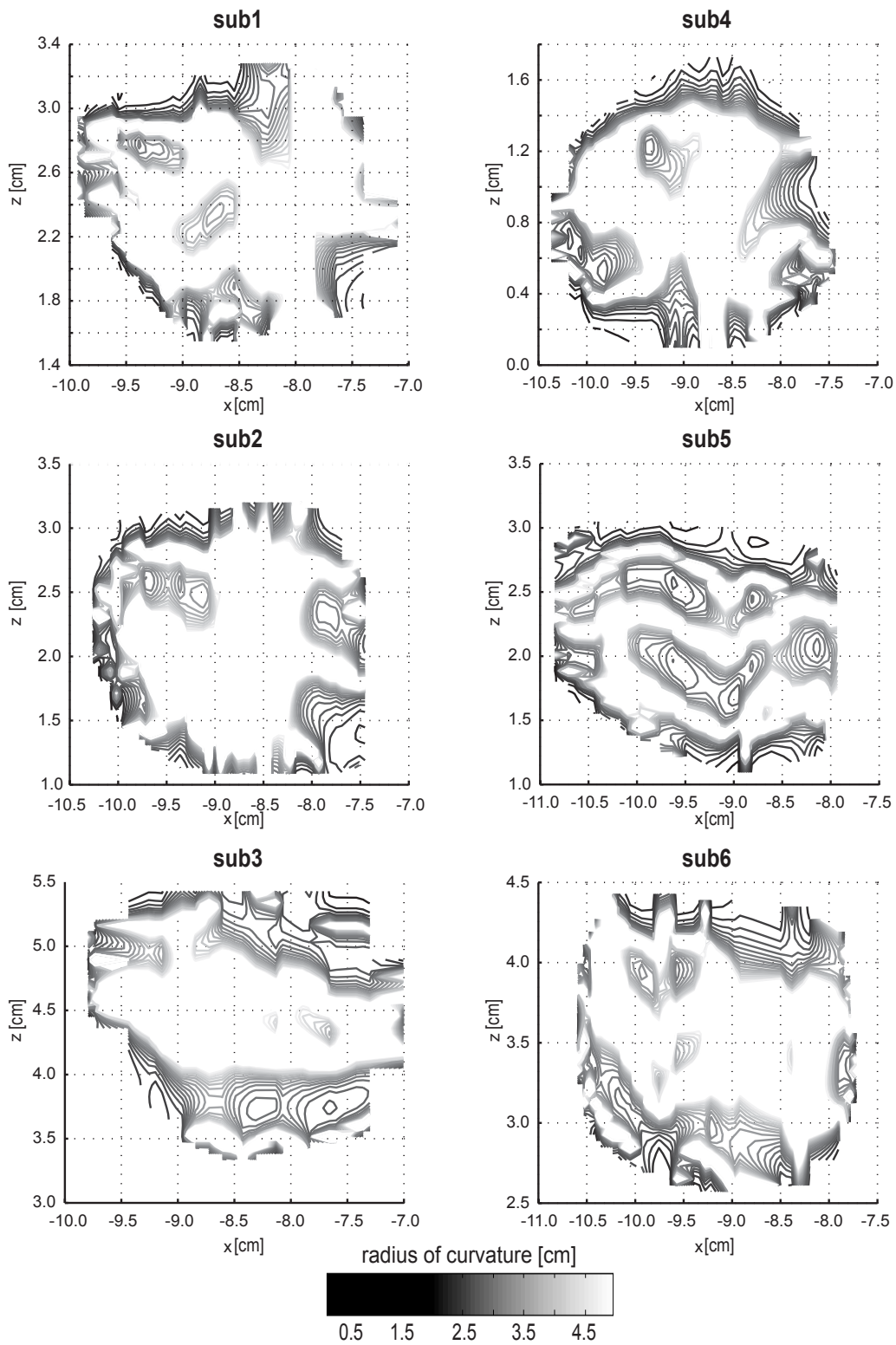


Fig. D-1 Projected radii of curvature of the posterior talar surface articulating with the calcaneus. The curvature is determined perpendicular to the greatest dimension of the joint. All subjects showed great areas of radii greater than 5 cm.

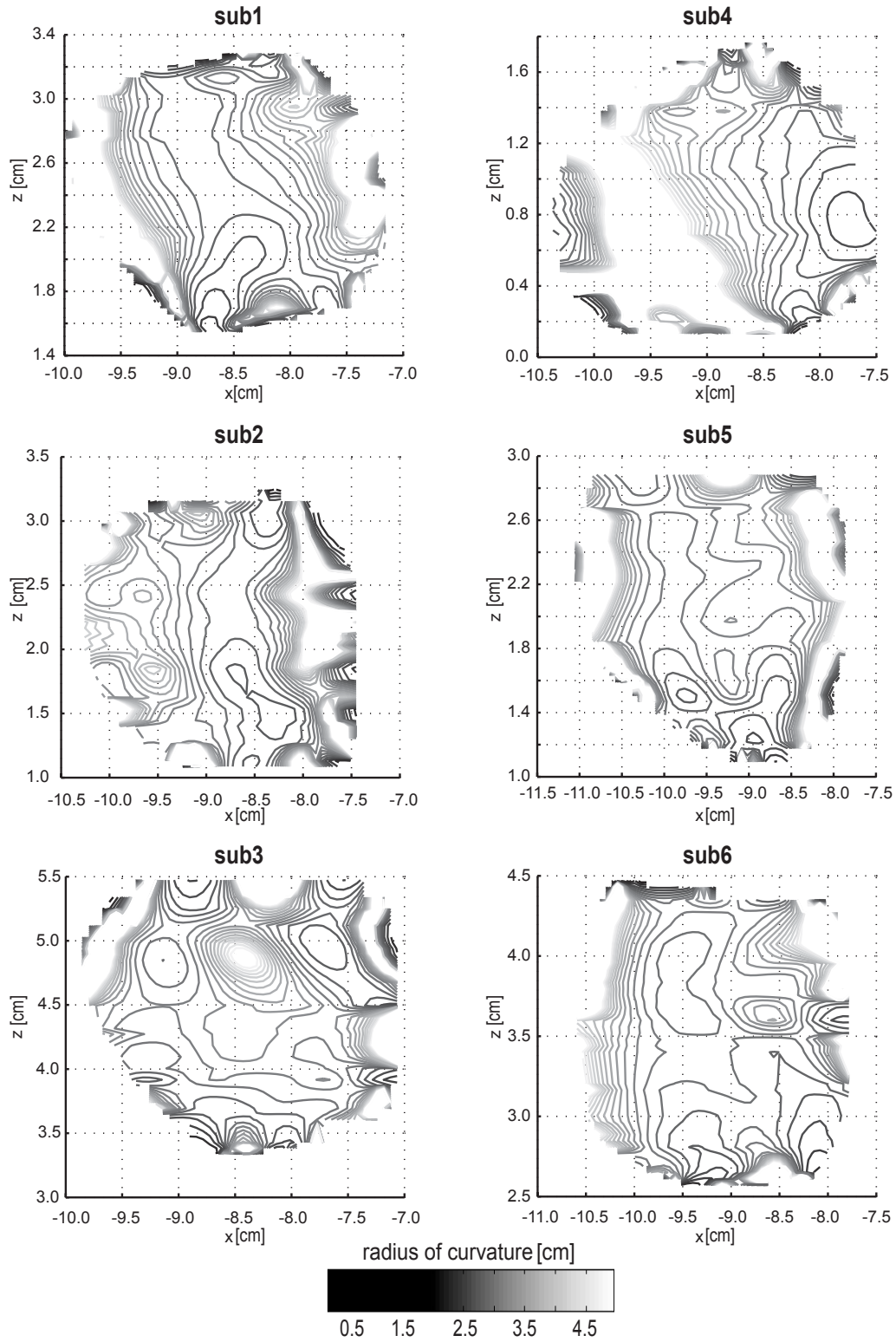


Fig. D-2 Projected radii of curvature of the posterior talar surface articulating with the calcaneus. The curvature is determined along the greatest dimension of the joint. Except for subject 4, smallest radii were found in the middle of the surface.

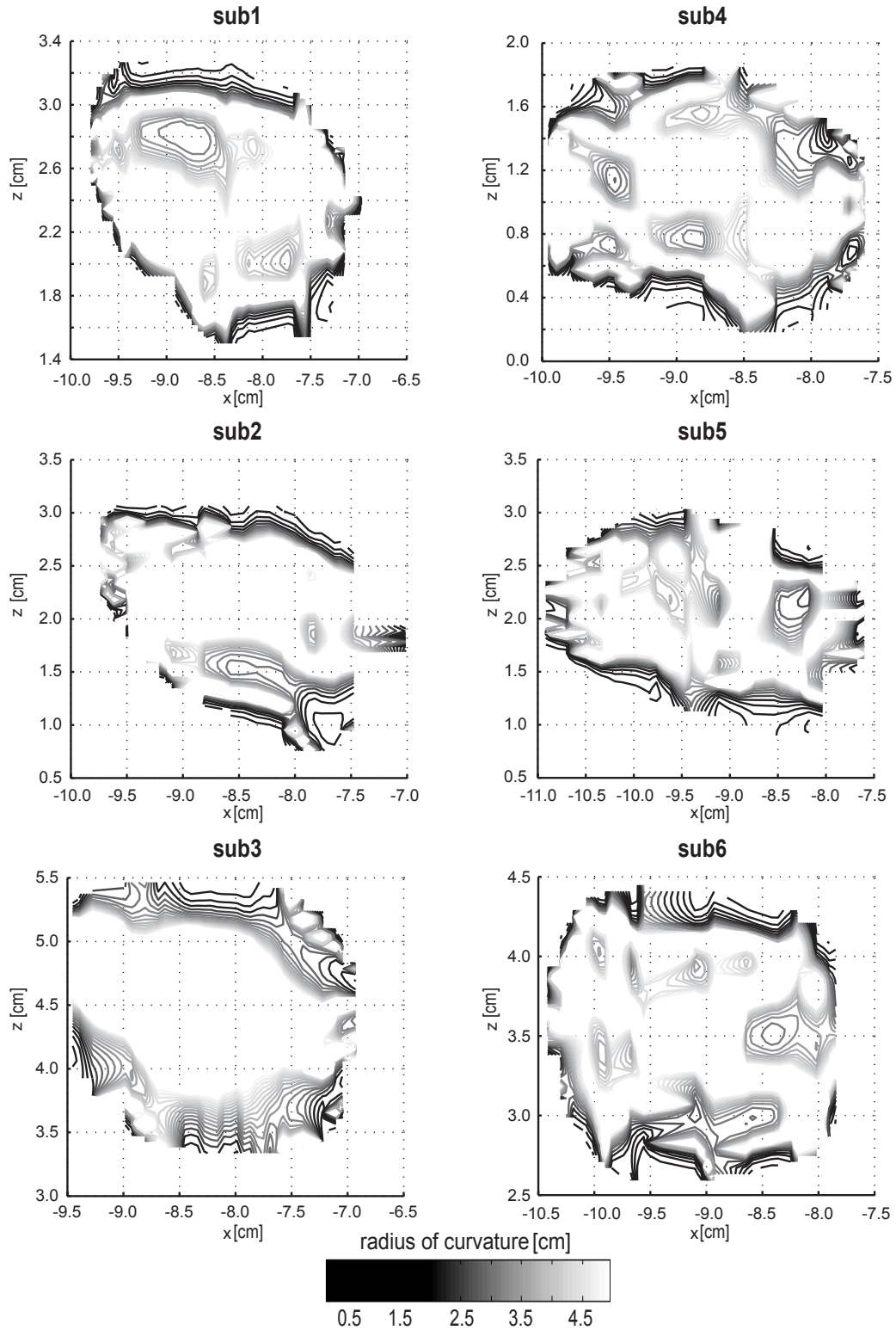


Fig. D-3 Projected radii of curvature of the posterior calcaneal surface articulating with the talus. The curvature is determined perpendicular to the greatest dimension of the joint. All subjects showed great areas of radii greater than 5 cm.

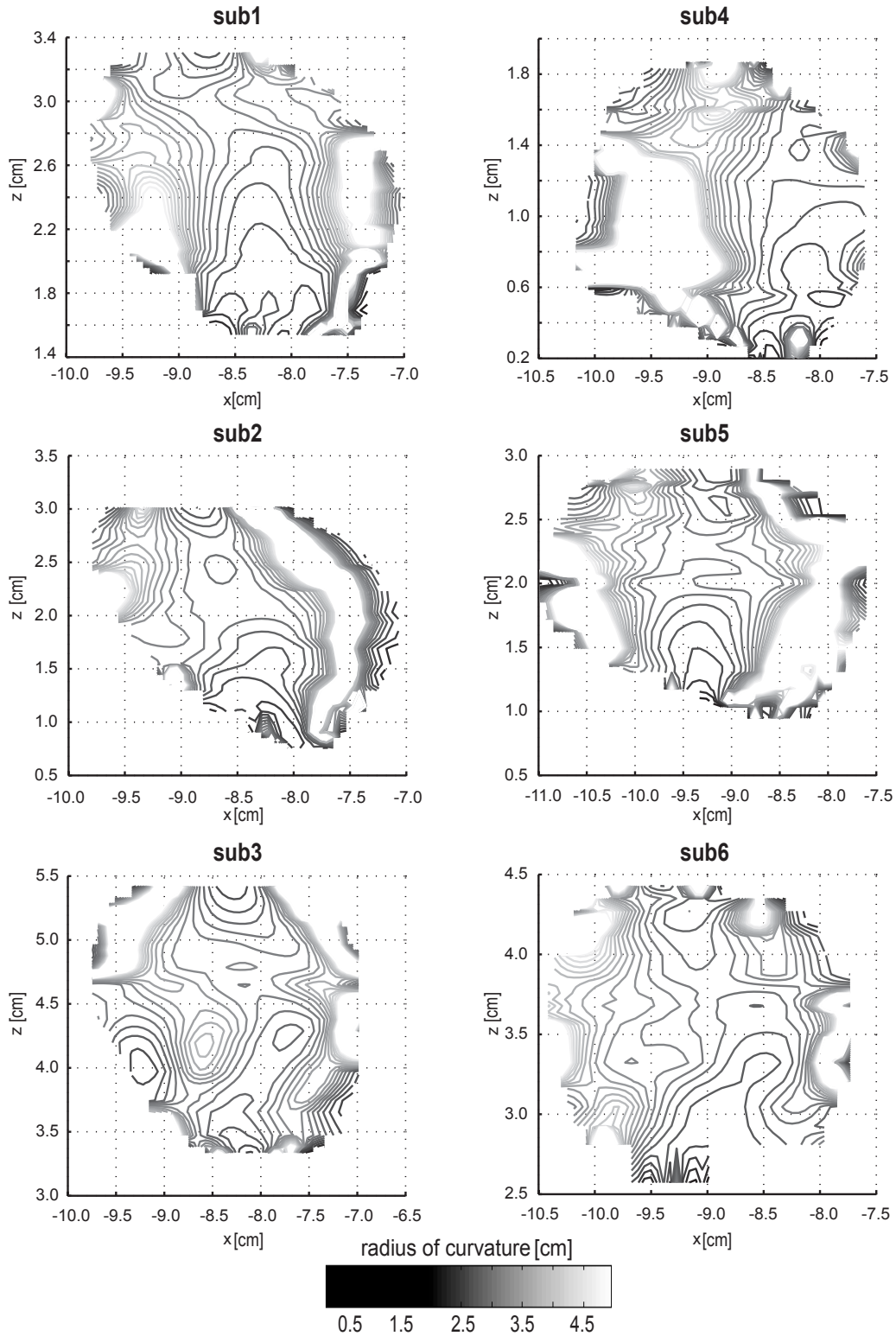


Fig. D-4 Projected radii of curvature of the posterior calcaneal surface articulating with the talus. The curvature is determined along the greatest dimension of the joint. The radii of all subjects were similar to corresponding parts on the talar articulating surface (Fig. D-2) outlining the congruency of the subtalar joint.

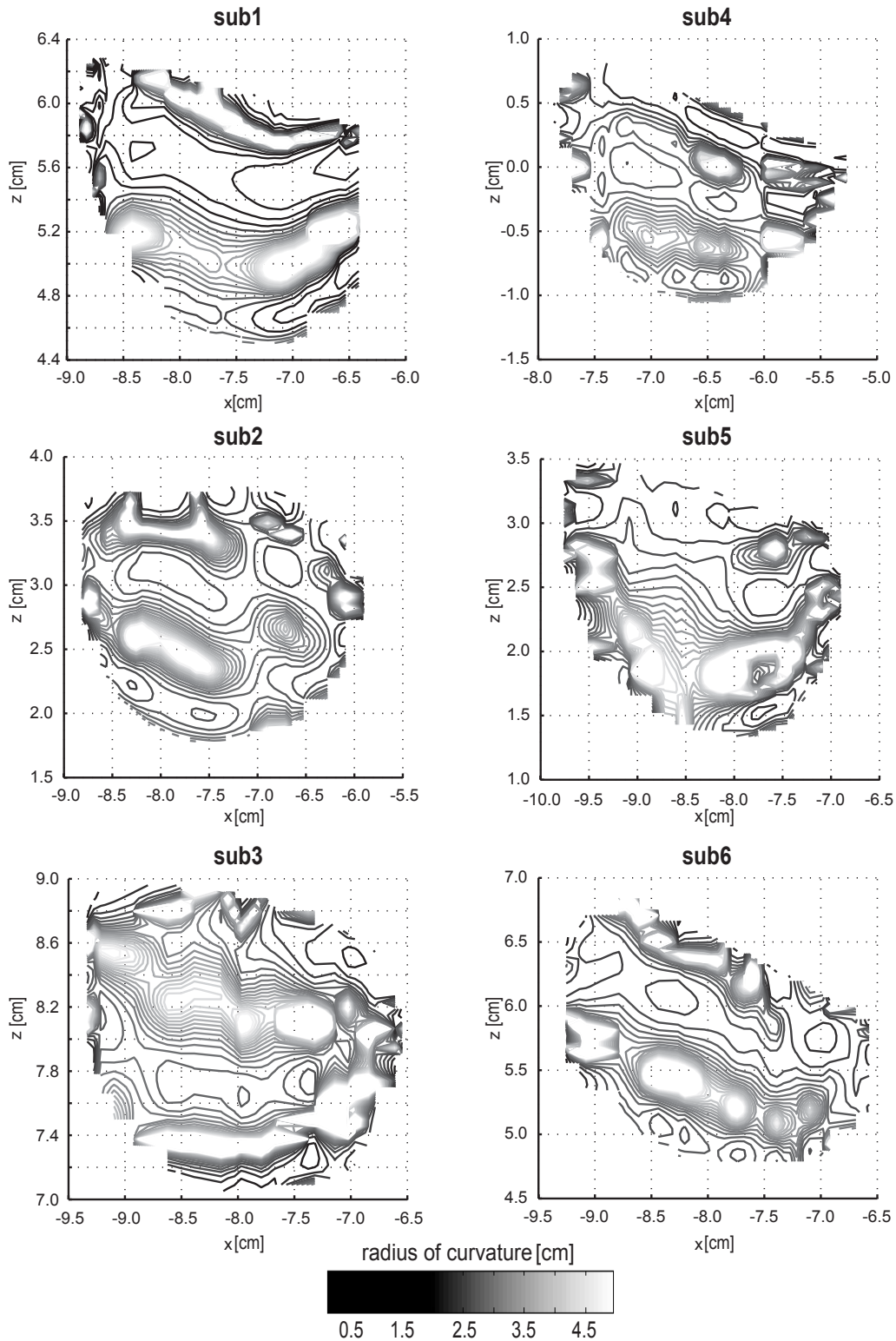


Fig. D-5 Projected radii of curvature of the talar surface articulating with the navicular. The curvature is determined in the frontal plane (hence linked with plantar- and dorsiflexion). No obvious differences between the 'normal' subjects (sub1-sub3) and the 'outlier' subjects (sub4-sub6) emerged.

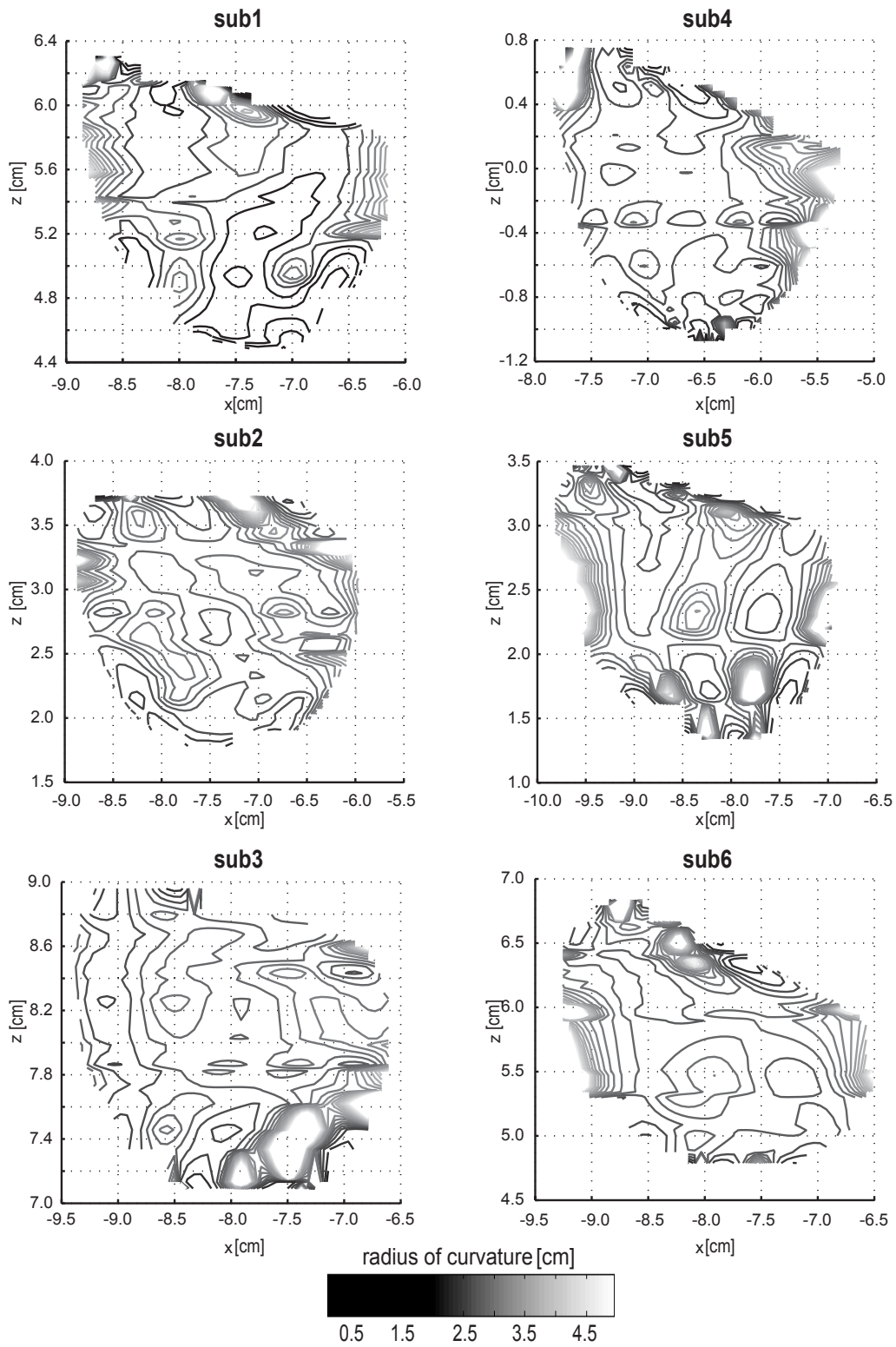


Fig. D-6 Projected radii of curvature of the talar surface articulating with the navicular. The curvature is determined in the transversal plane (hence linked with ab- and adduction). No obvious differences between the 'normal' subjects (sub1-sub3) and the 'outlier' subjects (sub4-sub6) emerged.

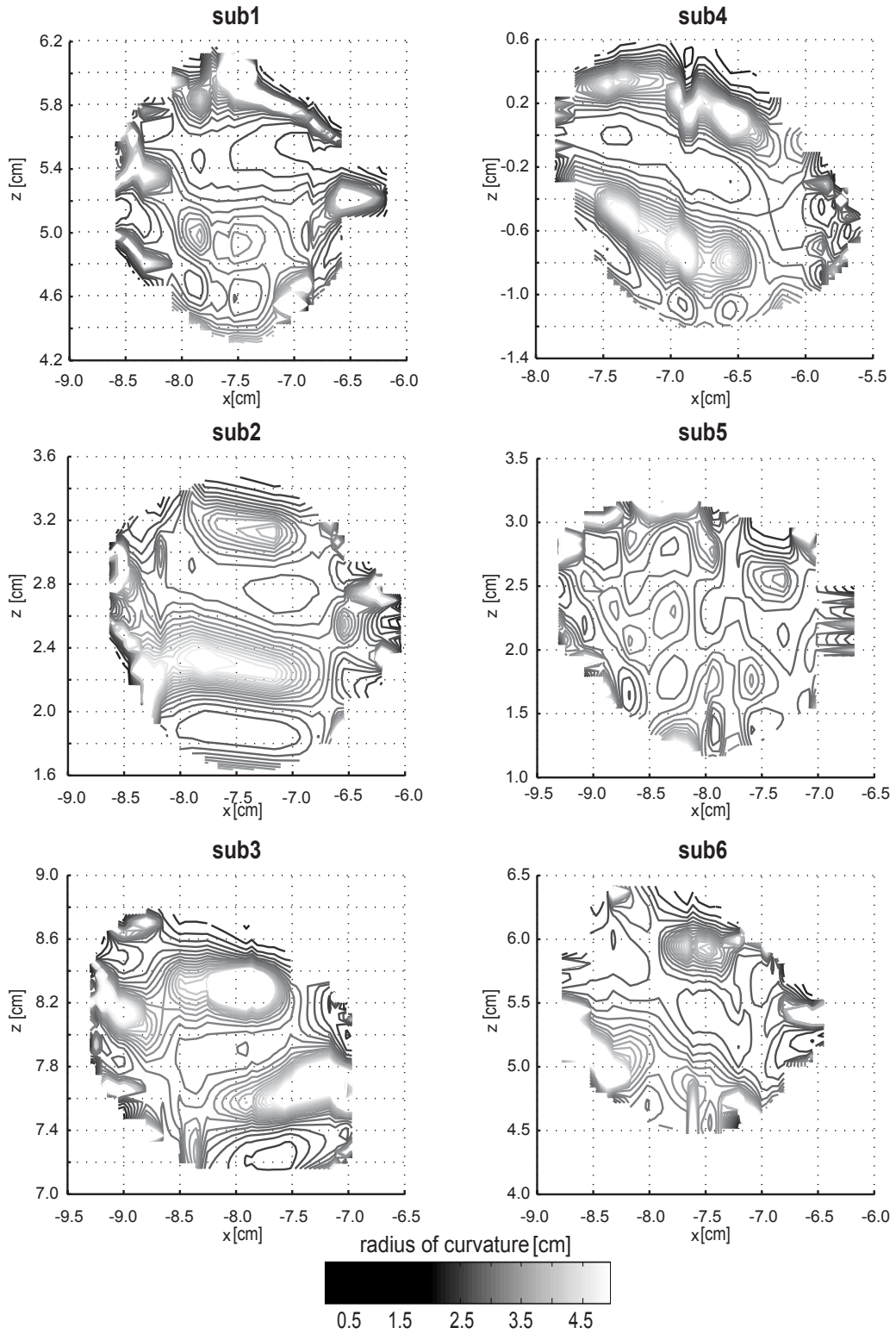


Fig. D-7 Projected radii of curvature of the navicular surface articulating with the talus. The curvature is determined in the frontal plane.

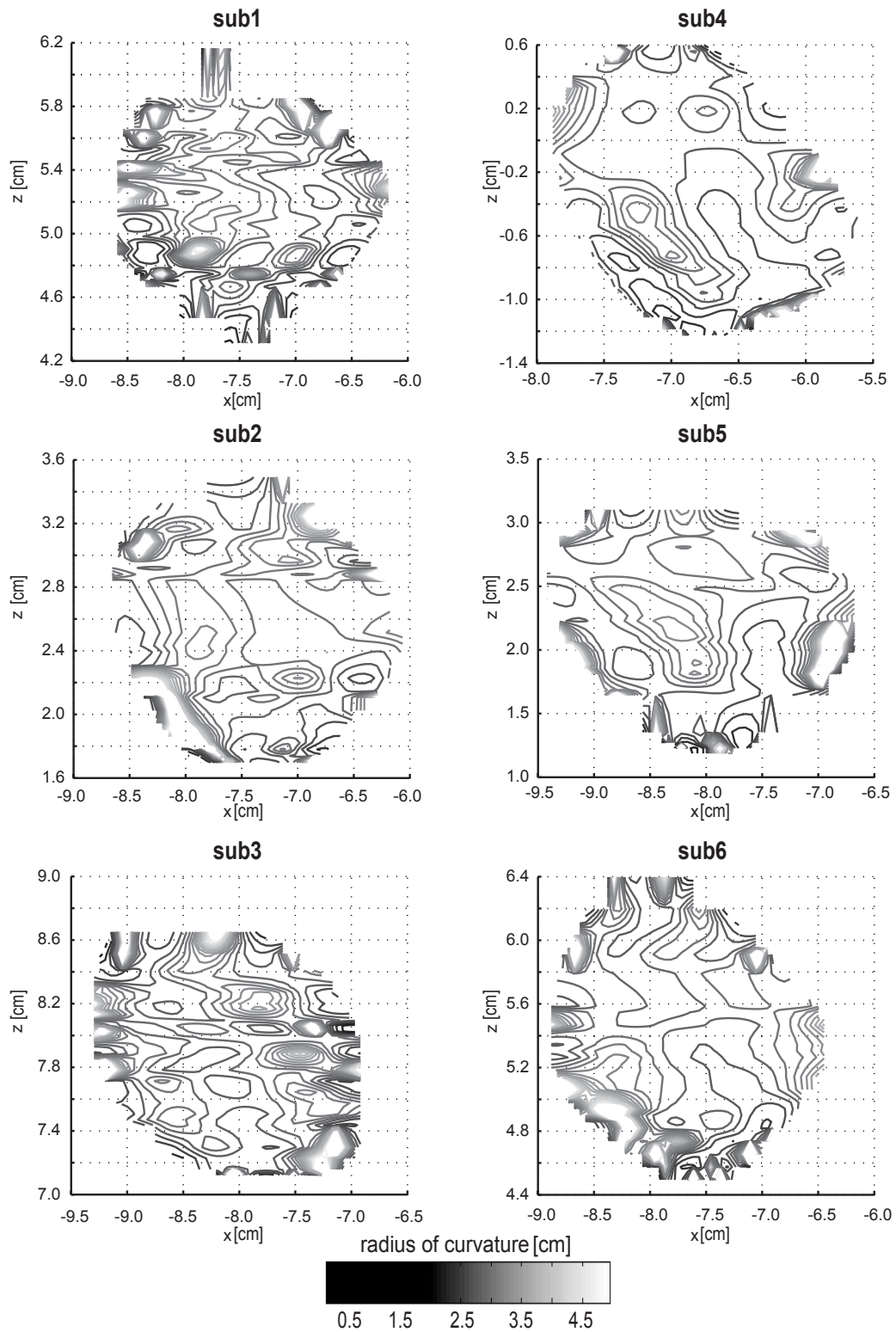


Fig. D-8 Projected radii of curvature of the navicular surface articulating with the talus. The curvature is determined in the transversal plane. No obvious differences between the 'normal' subjects (sub1-sub3) and the 'outlier' subjects (sub4-sub6) emerged.

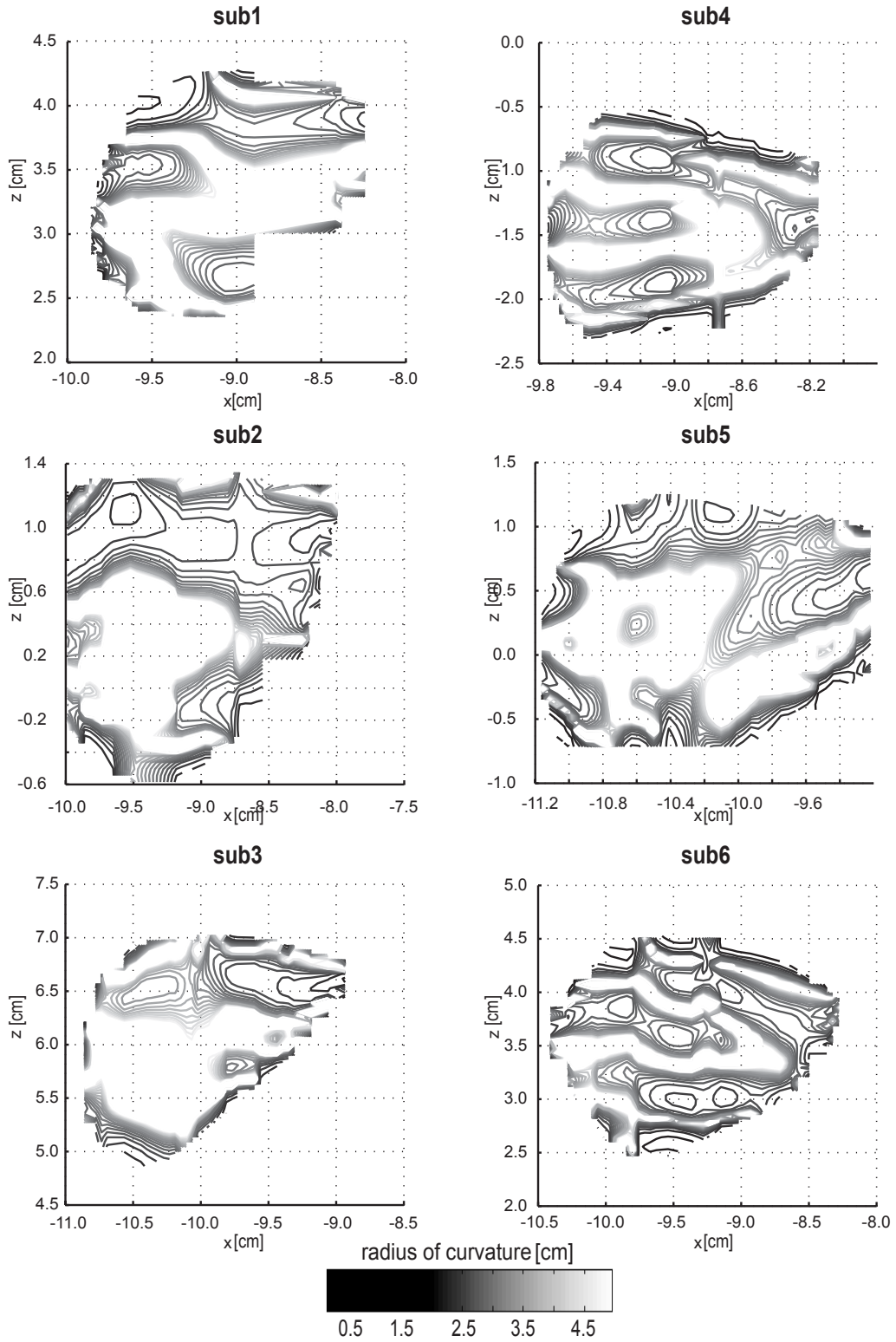


Fig. D-9 Projected radii of curvature of the calcaneal surface articulating with the cuboid. The curvature is determined in the frontal plane. All subjects showed great areas of radii greater than 5 cm.

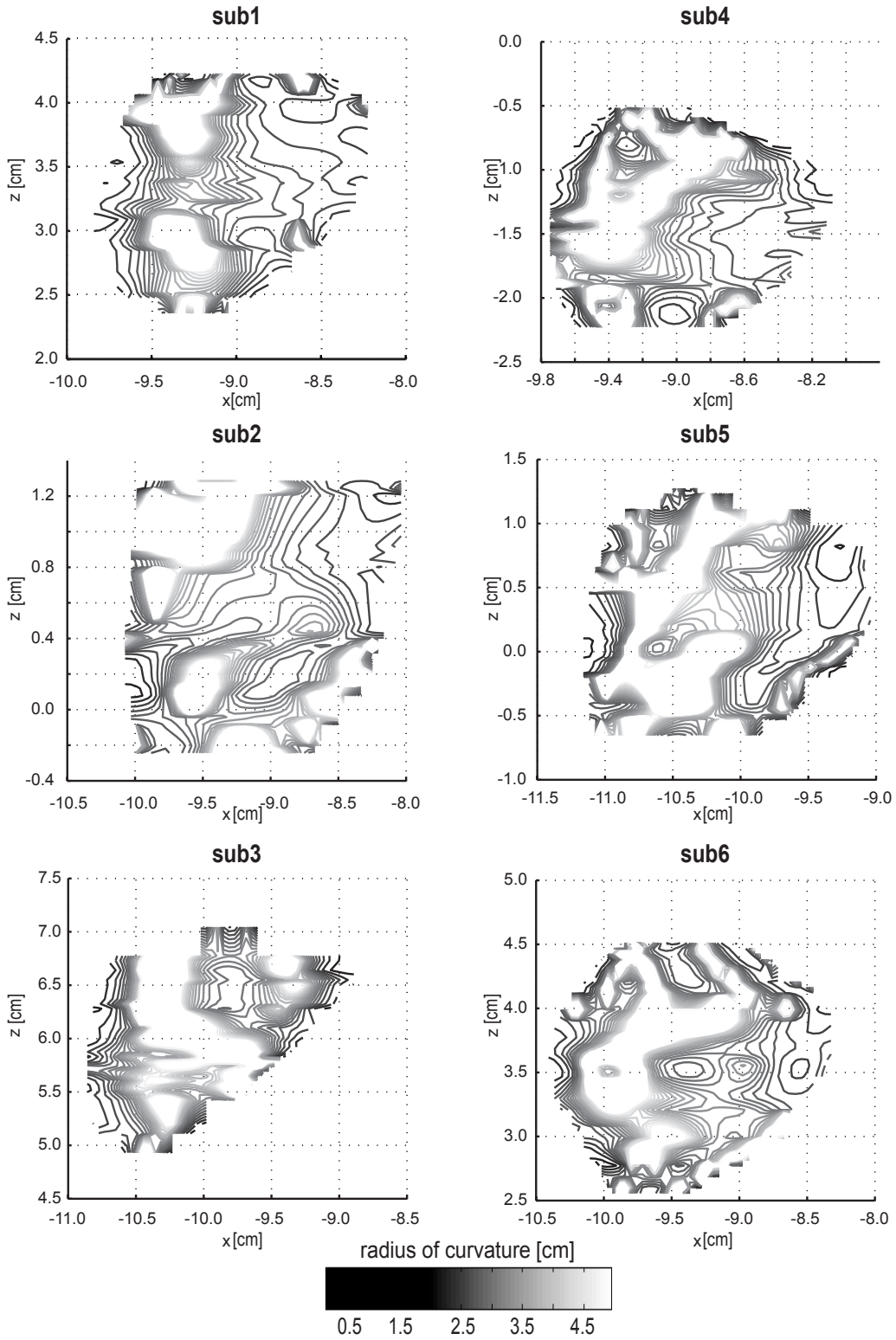


Fig. D-10 Projected radii of curvature of the calcaneal surface articulating with the cuboid. The curvature is determined in the transversal plane. Like in the frontal plane, all subjects showed great areas of radii greater than 5 cm outlining the flat character of the joint.

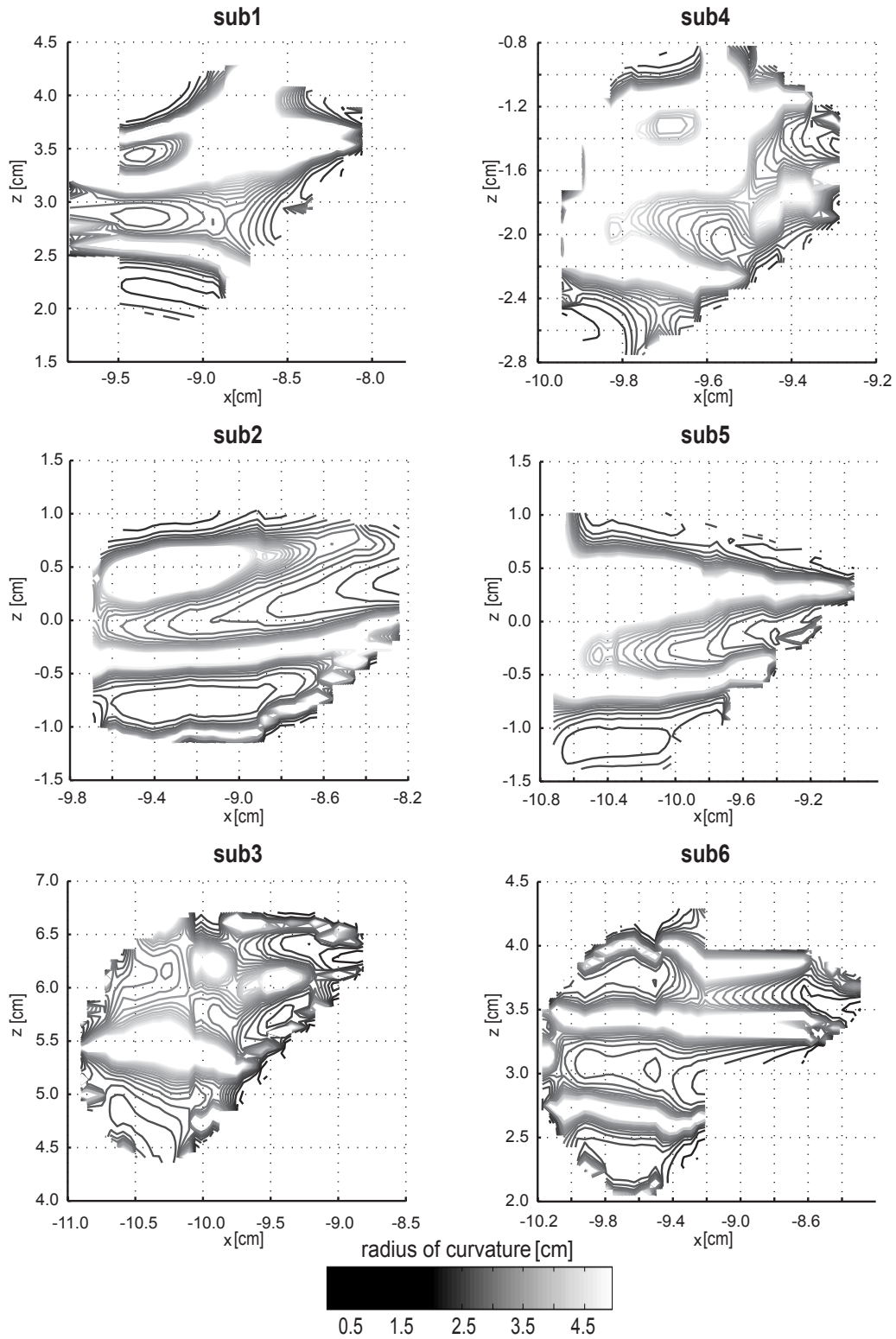


Fig. D-11 Projected radii of curvature of the cuboid surface articulating with the calcaneus. The curvature is determined in the frontal plane. No obvious differences between the 'normal' subjects (sub1-sub3) and the 'outlier' subjects (sub4-sub6) emerged.

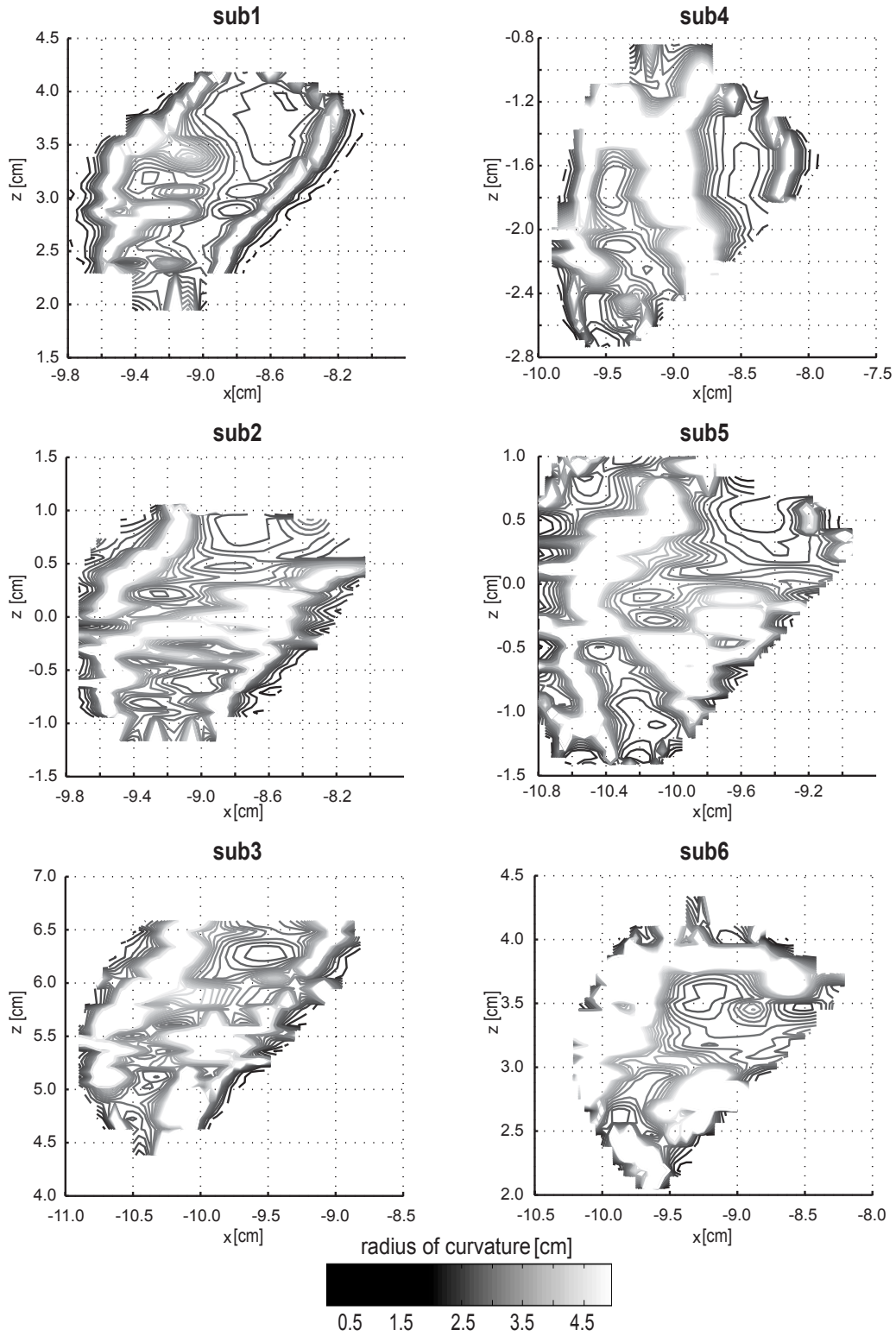


Fig. D-12 Projected radii of curvature of the cuboid surface articulating with the calcaneus. The curvature is determined in the transversal plane.

Acknowledgements

An dieser Stelle möchte ich mich von ganzem Herzen bei all denen bedanken, die wesentlich zur Durchführung dieser Doktorarbeit sowie zum Ausgleich zur selbigen beigetragen haben.

Mein Dank gilt zunächst Edgar Stüssi, der mir die Möglichkeit des Doktorats bot, dabei administrative Wogen glättete, mich meinen Kurs setzen liess und für den nötigen Rückenwind sorgte. *Merci viu mau, Edgar.*

Ich danke meinem unmittelbaren Betreuer Alex Stacoff, der mich fortlaufend unterstützte, seinen Fuss immer wieder hinhielt und Ausdauer bezüglich meines English for Runaways bewies. Nicht nur, dass er stets eine offene Tür hatte, sondern durch ihn öffneten sich auch andere. *Merci, Alex.*

Ich danke weiterhin Roger Luechinger für seine ständige, unkomplizierte und uneigennützigere Bereitschaft, dass Fuss-Innere abzubilden und dabei anfällige Probleme zu lösen. *Merci, Roger.*

Meinen Dank möchte ich auch an Sandra Keller Chandra richten, die meine vagen Vorstellungen einer Testapparatur präziserte und dank Peter Schwilch umsetzte, obwohl er nicht immer Zeit dafür gehabt hätte. *Merci Euch.*

Ich möchte mich ausserdem bei Jachen Denoth, der fachliches als auch soziales stets ins richtige Verhältnis brachte, und Hans Gerber, der sich rund um die rechnergestützte Auswertung einsetze, bedanken. *Grazcha fichI.*

I would like to express my deepest thanks to Arne Lundberg, Toni Arndt and Paul Lundgren for facilitating the intracortical pin study. *Många tack.* Further, I am truly grateful to Christoph Nester, Richard Jones, Anmin Liu, and Lee Murphy who collaborate in this study. *Cheers.* I would like to thank David Howard and Robert Riener for their patience, for their inspiration and for being referees of my thesis. *Thank you.*

Gedankt sei auch den WagiWagis: Der Nummer 1 und 2, Dominik Thomann und Claude Berney, die mich in Matlab ein-, ich jedoch bei Lupo vorführte. *Merci beaucoup.* Markus Dettwyler, insbesondere für Hilfen rund um extractionofT.m. *Engraziel fetg, Markus.* Benedicte Vanwanseele, für ihre administrative und bildgebende Pionierarbeit. *Hartelijk bedankt, Ben.* Und Mauro Foresti und Quang Thai, für ihre Unterstützung bei Hard- und Software. *Grazie mille.*

Acknowledgements

Mein Dank gilt auch den anderen vom Institut für Biomechanik für das angenehme Arbeiten mit Euch, wobei ich Urs Stöcker, für seine Ideen und seine Aufopferung, und Thomas Ukelo, für seine Mess- und Laufleistungen, hervorheben möchte.

Ich danke auch dem Institut für Biomedizinische Technik, Universität und ETH Zürich, unter Leitung von Peter Boesiger, ohne deren Einrichtungen diese Arbeit nicht möglich gewesen wäre. Weiterhin danke ich der Eidgenössischen Sportkommission, dem Barth Fond, sowie der International Society of Biomechanics für ihre finanzielle Unterstützung.

Mein besonderer Dank geht an Ivo Telley, für die manchmal auch philosophischen Diskussionen, und der zuletzt immens wichtigen Hilfe in Gestaltung, Word und Schrift. *Merci, Ivo*. Bleibt noch der Dank an die Ampelmännchen: Zum einen an Toru Fischbach, der mir neue Wege ausserhalb des Wagi-Areals aufzeigte, sei es am Fels, im Schnee, in der Dunkelkammer, in der Küche und und und. *Danke, Toru*. Zum anderen an Sven Knecht, der wohl über 55.000 Stunden mit mir da war, dem speziell zu danken aber die bisherigen Zeilen mehr als verdoppeln würde. Daher wünsche ich ihm lieber die notwendige Motivation für seinen Abschluss. *Hau rein, Sven*.

Ganz herzlich bedanken möchte ich mich abschliessend bei meinen Eltern Anja und Hans-Joachim Wolf und meinen Schwestern Bettina und Henrike, die mir diese wunderschöne Zeit überhaupt erst ermöglichten und mir stets Rückhalt gaben, und bei Lisa Fischer, für die Farbe, den Schwung und die Liebe, die sie mir fortwährend entgegenbrachte. *Danke*.

Curriculum vitae

ACADEMIC DEGREES AND EDUCATION

- 2002-2006 PhD Student, Institute for Biomechanics, Department of Mechanical and Process Engineering, ETH Zurich, Switzerland.
- 2002 M.A. in Sports-Engineering, TU Chemnitz, Germany.
- 1999-2002 Graduated studies in Sports-Engineering, TU Chemnitz, Germany.
- 1997-1999 Undergraduate studies in Sport-Science and Process Engineering, TU Chemnitz, Germany.
- 1987-1996 High School in Unna, Germany.

RESEARCH AND PROFESSIONAL EXPERIENCES

- 2005 Research Visit at the Department of Orthopaedics, Karolinska Institute at the Huddinge University Hospital, Stockholm, Sweden. Studies in walking and running with intracortical pins (financed by ISB dissertation grant 2005).
- 2002-2006 Tutor of diploma thesis and teaching assistant, Institute for Biomechanics, ETH Zurich, Switzerland.
- 2001 Master thesis at the adidas Test Center, Scheinfeld, Germany, entitled 'A material test to quantify material properties of running shoe soles at heel strike'.
- 2000 Employee at the adidas Test Center, Scheinfeld, Germany, focussing on dynamic material tests of midsoles of running shoes.
- 1999-2002 Research assistant at the Biomechanical Laboratory, TU Chemnitz, Germany.
- 1999-2000 Research assistant at the Institute of Mechanical and Plastic Engineering, TU Chemnitz, Germany.
- 1999 Internship at the Institut für Angewandte Trainingswissenschaften (IAT), Leipzig, Germany, focussing on a device measuring leg muscle forces.